THE GEOLOGICAL SOCIETY OF AMERICA®

Tectonic and magmatic construction of lower crust in the Southern California Batholith

Joshua J. Schwartz[1,†], Elena A. Miranda[1], Keith A. Klepeis[2], Gabriela Mora-Klepeis[2], Jade Star Lackey[3], Francine Robles[1], and Alina Tibaldi[4]

[1]*Department of Geology, California State University, Northridge, California 91330, USA*
[2]*Department of Geography and Geosciences, The University of Vermont, Burlington, Vermont 05405, USA*
[3]*Geology Department, Pomona College, Claremont, California 91711, USA*
[4]*Departamento de Geología, Universidad Nacional de Río Cuarto, Río Cuarto X5804BYA, Argentina*

ABSTRACT

We explore the growth of lower-continental crust by examining the root of the Southern California Batholith, an ~500-km-long, paleo-arc segment of the Mesozoic California arc that lies between the southern Sierra Nevada Batholith and northern Peninsular Ranges Batholith. We focus on the Cucamonga and San Antonio terranes located in the eastern San Gabriel Mountains where the deep root of the Mesozoic arc is exhumed by the Quaternary Cucamonga thrust fault. This lower- to mid-crustal cross section of the arc allows us to investigate (1) the timing and rates of Mesozoic arc construction, (2) mechanisms of sediment incorporation into the lower crust, and (3) the interplay between mantle input and crustal recycling during arc magmatic surges. We use U-Pb detrital zircon geochronology of four quartzites and one metatexite migmatite to investigate the origin of the lower-crustal Cucamonga metasedimentary sequence, and U-Pb zircon petrochronology of 26 orthogneisses to establish the timing of arc magmatism and granulite-facies metamorphism. We find that the Cucamonga metasedimentary sequence shares broad similarities to Sur Series metasedimentary rocks in the Salinia terrane, suggesting that both were deposited in a late Paleozoic to early Mesozoic forearc or intra-arc basin marginal to the Southern California Batholith. This basin was progressively underthrust beneath the arc during the Middle Jurassic to Late Cretaceous and was metamorphosed during two high-grade (>750 °C), metamorphic events at ca. 124 Ma and 89–75 Ma. These metamorphic events were associated with 100 m.y. of arc magmatism that lasted from 175 Ma to 75 Ma and culminated in a magmatic surge from ca. 90 Ma to 75 Ma. Field observations and petrochronology analyses indicate that partial melting of the underthrust Cucamonga metasedimentary rocks was triggered by the emplacement of voluminous, mid-crustal tonalites and granodiorites. Partial melting of the metasedimentary rocks played a subsidiary role relative to mantle input in driving the Late Cretaceous magmatic flare-up event.

INTRODUCTION

Cordilleran arcs are widely acknowledged as primary sites on Earth for the formation of new continental crust (Taylor and McLennan, 1985; Rudnick, 1995; Kemp et al., 2007; Ducea et al., 2015b; Cashman et al., 2017; Collins et al., 2020). In convergent margins, batholiths serve as expansive zones comprising intermediate to felsic, calc-alkalic plutons that originate above subduction zones (Hildreth and Moorbath, 1988; Petford and Gallagher, 2001; Annen et al., 2006). The petrological exploration of the origin and crustal architecture of Cordilleran batholiths has posed a longstanding problem, sparking intense debates on the rates of arc construction, the processes governing arc magma diversification, the mechanisms of sediment incorporation into the crust, and the interplay between mantle input and crustal recycling in generating arc magmas (Coleman et al., 2004; Samperton et al., 2017; Bucholz et al., 2017; Cashman et al., 2017; Sauer et al., 2017a; Ratschbacher et al., 2018; Collins et al., 2020; Hanson et al., 2022). Whereas these inquiries are pivotal for unraveling the architecture and processes underlying continental crust construction, a significant challenge in arc petrology is that we have limited comprehension of the processes occurring in the roots of arcs, where elevated temperatures resulting from advected mantle-derived heat foster intra-crustal melting, fractionation, and magma diversification within lower-crustal hot zones or MASH (melting, assimilation, storage and homogenization) zones.

A large portion of our knowledge about arc roots is derived indirectly from the geochemistry and petrochronology of whole rock and minerals in shallow- to mid-crustal rocks (Gromet and Silver, 1987; Petford and Atherton, 1996; Ducea, 2001, 2002; Saleeby et al., 2003; Lackey et al., 2006; Hollister and Andronicos, 2006; Ducea and Barton, 2007; Gehrels et al., 2009; Paterson et al., 2011; Girardi et al., 2012), xenolith studies (Ducea and Saleeby, 1996; Ducea, 2002; Chin et al., 2014), and experimental studies that replicate processes of deep-crustal partial melting and fractional crystallization (Rapp and Watson, 1995; Müntener et al., 2001; Alonso-Perez et al., 2009; Getsinger et al., 2009; Ulmer et al., 2018). Despite the pivotal role of arc roots in the construction of continental crust, our understanding is impeded by the scarcity of direct observations of exhumed deep-crustal exposures. Occurrences of arc roots are exceptionally rare in both active and ancient Cordilleran batholiths. For instance, in the North and South American Cordillera, exposures of Cordilleran arc rocks from depths exceeding 25 km are confined to a few locations, including the North Cascades crystalline block (Miller et al., 2009), the Salinian block in the Santa Lucia Mountains of central California (Kidder et al., 2003; Ducea et al., 2003), the Tehachapi Mountains in the southern Sierra Nevada Batholith (Sams and Saleeby, 1988; Saleeby, 1990; Klein and Jagoutz, 2021; Rezeau et al., 2021), the Cucamonga terrane in the eastern San Gabriel Mountains of Southern California (May and Walker, 1989; Barth and May, 1992), and the Sierra of Valle Fértil in Argentina (Tibaldi et al., 2013; Walker et al., 2015; Otamendi et al., 2020; Cornet et al., 2022). These rare instances are important to advancing

Joshua J. Schwartz https://orcid.org/0000-0002-8385-2705
[†]joshua.schwartz@csun.edu

GSA Bulletin; https://doi.org/10.1130/B37669.1.

our understanding of continental-crust construction because they offer crucial insights into the processes that govern deep arc magma construction that are otherwise inaccessible.

The importance of the lower crust in arcs is underscored by their role in arc flare-up events or episodic intervals of increased magma production (Ducea et al., 2015b, 2017; DeCelles and Graham, 2015; Schwartz et al., 2017; Decker et al., 2017; Klein and Jagoutz, 2021; Klein et al., 2021). These flare-up events occur at intervals of a few tens of millions of years to several hundreds of millions of years and can lead to rapid addition of magma to the crust up to thousands of kilometers along-strike (Ducea et al., 2015a; Paterson and Ducea, 2015; Kirsch et al., 2016; Ringwood et al., 2021). The cause of flare-ups is among the most fundamental questions in earth science, and there is considerable controversy about the mechanisms that drive them, including (1) the importance of tectonic and non-tectonic processes in the upper plate (contractional underthrusting, crustal thickening, extension, and arc-root delamination); (2) the geodynamics of the lower plate (slab breakoff, slab advance, and slab retreat); and (3) the relative contribution of mantle sources versus existing continental crustal sources (particularly melt fertile sediments) (Ducea, 2001; Ducea and Barton, 2007; Paterson and Ducea, 2015; Kirsch et al., 2016; Cope, 2017; Decker et al., 2017; Cecil et al., 2018; Martínez Ardila et al., 2019; Chapman and Ducea, 2019; Yang et al., 2020; Schwartz et al., 2021; Chapman et al., 2021b; Ringwood et al., 2021).

In this contribution, we address the thermal and temporal evolution of Cordilleran arc crust construction with new field and petrochronologic results from a lower- to mid-crustal exposure of Cretaceous continental arc crust in the Cucamonga terrane located in Southern California (Fig. 1). These exposures form the Mesozoic root of the Southern California Batholith (SCB), an ~500-km-wide, paleo-arc segment of the Mesozoic California arc that lies between the southern Sierra Nevada Batholith and northern Peninsular Ranges Batholith (Fig. 1A). Prior studies have demonstrated that the Southern California Batholith experienced a flare-up event from 90 Ma to 70 Ma, yet the processes that triggered this flare-up are unknown (Economos et al., 2021; Schwartz et al., 2023). Our new data highlight the interplay between contraction and intra-arc deformation, high-grade metamorphism, and non-steady-state arc magmatism in the petrogenesis of lower-continental crust in the Southern California Batholith during this critical interval. In addition, we explore the role of underthrusted sediments in the arc flare-up event and we provide a petrologic and chronological framework for understanding important tectonic events such as the Laramide Orogeny and the Baja–British Columbia (Baja-BC) controversy that is postulated to have affected Southern California in the Late Cretaceous (Livaccari et al., 1981; Henderson et al., 1984; Barth and Schneiderman, 1996; Maxson and Tikoff, 1996; Cowan et al., 1997; Butler et al., 2001; Liu et al., 2010; Tikoff et al., 2023; Schwartz et al., 2023).

GEOLOGIC BACKGROUND

Framework of the Southern California Batholith

Mesozoic Cordilleran arc magmatism in California was distributed along a once contiguous belt that spanned >2000 km and included, from north to south, the Sierra Nevada Batholith, the Southern California Batholith, and the Peninsular Ranges Batholith (Fig. 1A). The Southern California Batholith is the focus of this study and is presently disrupted by Tertiary faulting associated with development of the San Andreas transform plate boundary (Powell, 1993; Dickinson, 1996). Today, the Southern California Batholith consists of various fault-bounded structural

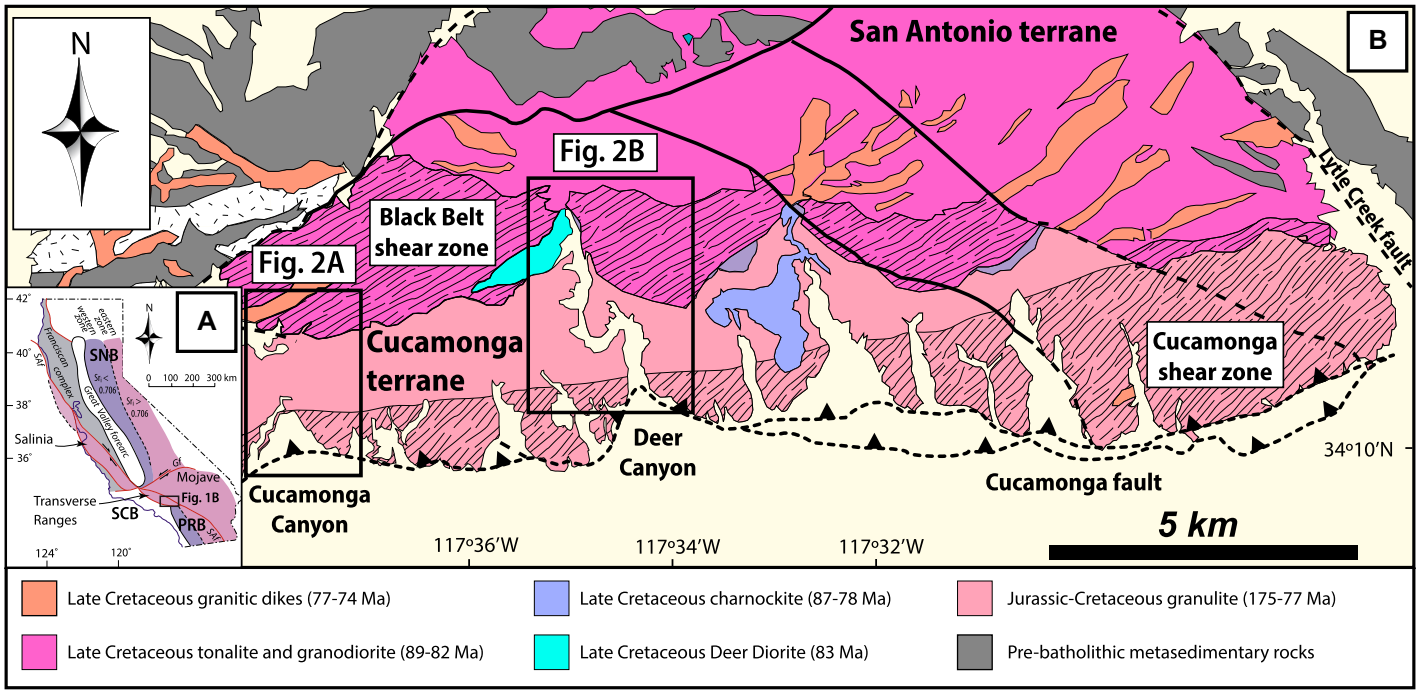

Figure 1. (A) Inset shows the location of the Cucamonga terrane in Southern California. The location of the Salina block is also indicated and has been displaced from Southern California by Tertiary dextral faulting. SCB—Southern California Batholith; SNB—Sierra Nevada Batholith; PRB—Peninsula Ranges Batholith; SAf—San Andreas fault; Gf—Garlock fault. (B) Simplified geologic map of the eastern San Gabriel Mountains showing the Cucamonga and San Antonio terranes. Diagonal lined pattern denotes the location of the Cucamonga and Black Belt shear zones. Boxes show the locations of two detailed studies in Cucamonga and Deer Canyons (Figs. 2A and 2B).

blocks that include the Salinia block, the Transverse Ranges, and the western Mojave province (Fig. 1A).

The Southern California Batholith is distinguished from other parts of the California Cordilleran arc by the presence of extensive Proterozoic basement gneisses that have U-Pb zircon ages that range from 1950 Ma to 660 Ma (Barth et al., 1997, 2001, 2008, 2009, 2016, 2017; Barth and Wooden, 2006; Needy et al., 2009; Nourse et al., 2020; Economos et al., 2021; Schwartz et al., 2023). Pre-batholithic basement rocks were intruded by calc-alkaline diorites, tonalites, granodiorites, and granites during three phases of arc magmatism at 260–210 Ma, 160–140 Ma, and 90–70 Ma. These Phanerozoic magmatic events culminated in a Late Cretaceous arc "flare-up" event, which peaked at 85–75 Ma and was associated with widespread, voluminous plutonism throughout the Southern California Batholith (Economos et al., 2021; Schwartz et al., 2023). This event occurred slightly later than similar magnitude flare-up events in the Sierra Nevada Batholith at ca. 98 Ma and in the Peninsular Ranges Batholith at ca. 93 Ma (Ducea et al., 2015a; Paterson and Ducea, 2015; Paterson et al., 2017).

In the Mojave region, Cretaceous magmatism consisted of peraluminous granitic rocks emplaced at middle crustal conditions from ca. 90 Ma to 73 Ma (Miller and Bradfish, 1980; Miller and Barton, 1990; Foster et al., 1992; Miller et al., 1996; Barth et al., 2008; Chapman et al., 2017, 2018, 2021a). Radiogenic isotopic studies of bulk rocks and zircons from these plutons demonstrate that they were sourced in part from Precambrian continental basement with contributions from juvenile mantle sources (Farmer and DePaolo, 1983; Miller and Barton, 1990; Patiño Douce et al., 1990; Wright and Wooden, 1991; Patiño Douce, 1999; Kapp et al., 2002; Barth et al., 2016; Chapman et al., 2018). In the Transverse Ranges, Late Cretaceous magmatism was widespread and voluminous. U-Pb zircon dating of shallow to mid-crustal Late Cretaceous plutons give 88–70 Ma ages, and some were emplaced at deeper levels in the Cucamonga terrane (Fig. 1; Barth, 1990; Barth and May, 1992; Barth et al., 2008, 2016; Needy et al., 2009). Geochemically, Late Cretaceous plutons are generally magnesian, metaluminous to weakly peraluminous, and calc-alkalic with strong crustal affinities that reflect assimilation of juvenile magmas with Proterozoic crust (Barth et al., 2008, 2016).

The Lower Crust of the Southern California Batholith

The lower crust of the Southern California Batholith is preserved in two locations: the Salinian block in the Santa Lucia Mountains of central California coast and the eastern San Gabriel Range Front Range of Southern California (Fig. 1B). These exposures offer rare insights into the composition and structure of the deep crust of the arc and present the opportunity to better understand the tempo of magmatism, melt sources, and the thermal conditions of the arc. In the Salinian block, arc magmatic activity occurred from 93 Ma to 81 Ma and involved the emplacement of meta-igneous rocks, including tonalites, diorites, and gabbros, into a metasedimentary sequence termed the Sur Series (Barth et al., 2003; Kidder et al., 2003; Barbeau et al., 2005). All of these rocks were deformed and metamorphosed at upper amphibolite- to granulite-facies conditions of 7.5 kbar and 800 °C (Kidder et al., 2003). Garnet Sm-Nd dating and microstructural analysis indicates that metamorphism occurred at ca. 75 Ma and overlapped with ductile deformation that is bracketed between 93 Ma and 76 Ma. These rocks were exhumed to the surface by ca. 68 Ma based on the presence of Maastrichtian sediments unconformably overlying the Salinian basement rocks (Saul, 1986; Seiders, 1986; Sliter, 1986).

In the eastern San Gabriel Mountains, lower-crustal rocks crop out in a belt 2–3 km wide and 20 km long (Figs. 1 and 2). Collectively, the rocks are referred to as the "Cucamonga terrane." They consist of heterogeneously distributed mafic and felsic granulite gneisses and amphibolite, interlayered with quartzofeldspathic gneisses and minor marble and calc-silicate rocks (Figs. 3A–3J; Hsu, 1955; May and Walker, 1989; Barth and May, 1992; Barth et al., 1992). These rocks contain a central core of well-preserved granulites, which is bounded to the north and south by two upper amphibolite-facies shear zones (Fig. 1; Alf, 1948). Alf (1948) mapped these rocks as the "pyroxene dioritic gneiss" unit and Hsu (1955) termed them the "Aurela Ridge group." In Hsu's (1955) detailed classification, he recognized four rock types in the Cucamonga granulites, including quartz-plagioclase granulites (which also include charnockites), pyroxene-plagioclase granulites, sillimanite-garnet granulites, and mar-

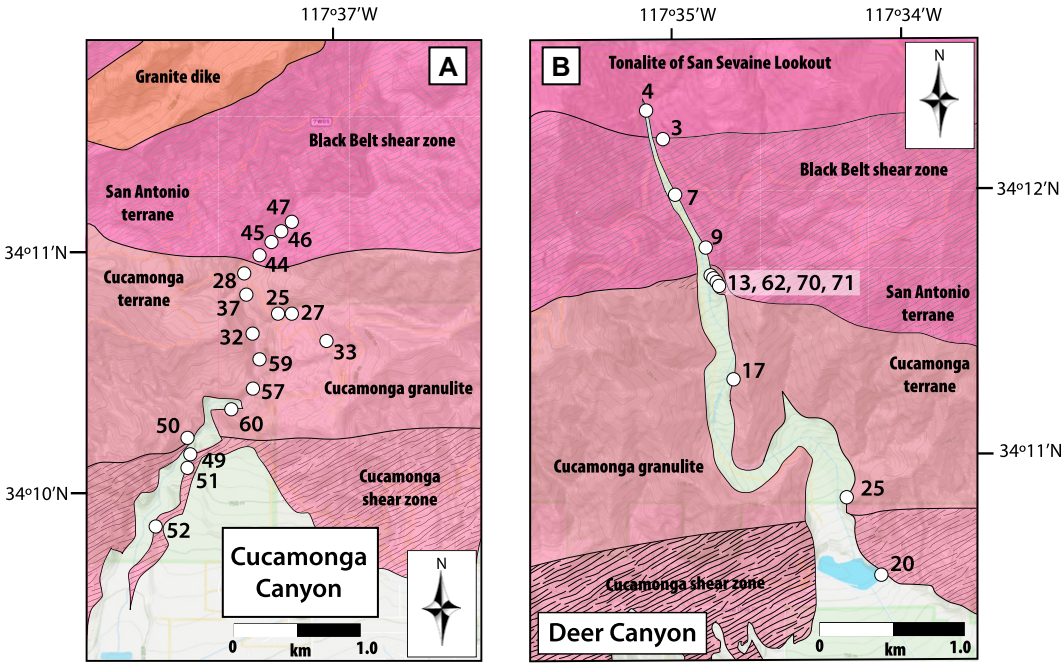

Figure 2. Simplified geologic maps of Cucamonga Canyon (A) and Deer Canyon (B). Locations of sample sites are shown with white circles. The Deer Diorite is not shown because we interpret it as a minor subphase of the Tonalite of San Sevaine Lookout. Sample locations correspond to last digit(s) of samples described in the text (e.g., 21CMXX for Cucamonga Canyon and 22DCXX for Deer Canyon).

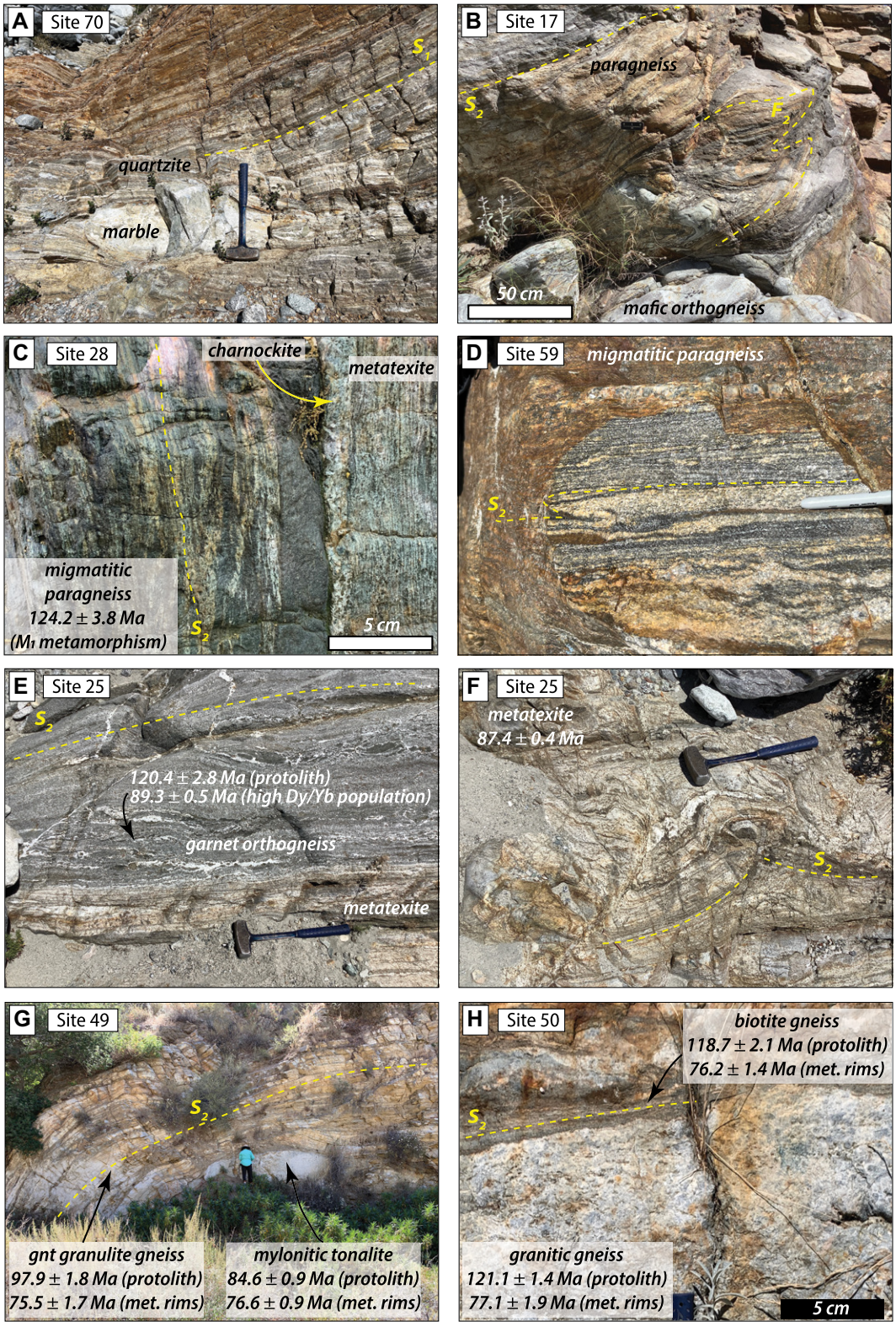

Figure 3. Representative field photographs for the lower crust in the Cucamonga terrane (A–J) and base of the middle crust in the San Antonio terrane (K–P). Zircon ages and 2σ uncertainties are indicated. (A) Foliated (S_1) metasedimentary sequence consisting of quartzite, quartzofeldspathic gneiss, schist, and marble; (B) tightly folded (F_2) S_1 foliation planes in mafic orthogneiss and paragneiss enveloped by an S_2 foliation; (C) foliated (S_2) migmatitic paragneiss interlayered with mafic granulite (black) metatexite and charnockite (leucocratic layer); (D) stromatic metatexite with folded granitic leucosomes; (E) granulite-facies mafic orthogneiss with diffuse leucosomes grading into metatexite; (F) metatexite with remnant metasedimentary layers and leucosomes segregation; (G) large fold of garnet granulite gneiss, mylonitic tonalite, and paragneiss in Cucamonga Canyon; (H) coarse-grained granitic orthogneiss and strongly foliated biotite gneiss; (I) garnet granulite-facies migmatitic orthogneiss interlayered within metasedimentary sequence; (J) close-up view of migmatitic orthogneiss from part I showing peritectic garnet associated with leucosomes; (K) weakly foliated biotite hornblende tonalite with mafic enclaves and thin centimeter-scale crosscutting veins (Cucamonga Canyon); (L) cataclastic and mylonitic biotite-hornblende tonalite from the Black Belt shear zone (Cucamonga Canyon); (M) massive outcrop of folded biotite hornblende tonalite orthogneiss in the Black Belt shear zone (Cucamonga Canyon); (N) strongly foliated and folded tonalite from the Black Belt shear zone (Cucamonga Canyon); (O) strongly foliated, biotite hornblende tonalite orthogneiss intruded by undeformed biotite granodiorite at the southern end of the Black Belt shear zone (Deer Canyon); (P) close-up view of biotite hornblende tonalite orthogneiss at same location as part O. Leucosome is folded into an F_3 M-fold. bt—biotite; hbl—hornblende.

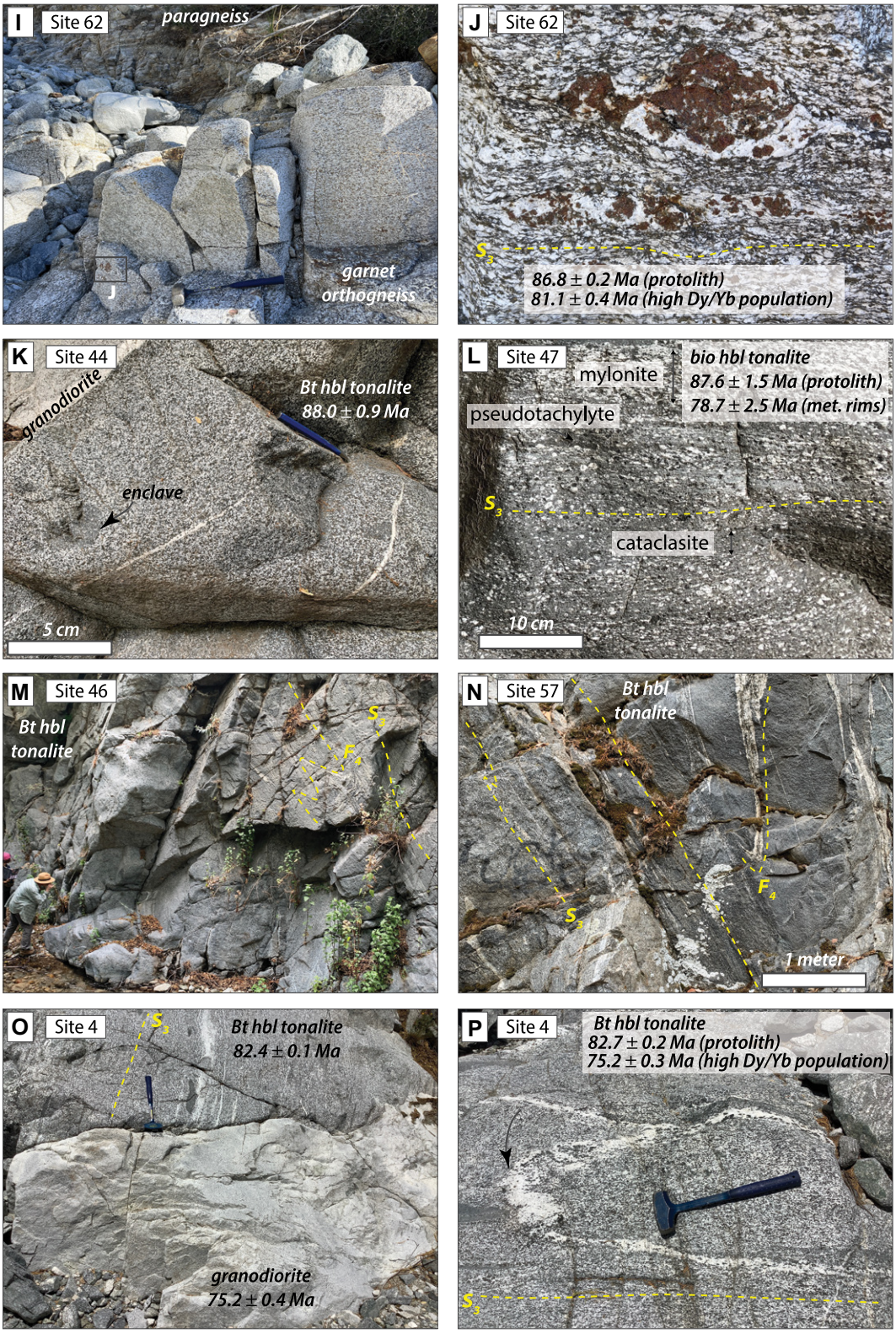

Figure 3. (*Continued*)

bles. Lesser amounts of calc-silicate, amphibolite, and quartzite are interlayered with these rocks. The granulitic belt lies structurally below Late Cretaceous tonalites and granodiorites of the San Antonio terrane (termed the Tonalite of San Sevaine Lookout by Morton et al., 2001; Figs. 2 and 3K–3P). Thermobarometry of lower crustal rocks indicates that metamorphism occurred at 7–9 kbar and 700–835 °C (Barth and May, 1992; Schwartz et al., 2023).

Previous zircon geochronology of the Cucamonga and San Antonio terranes is limited to multi-grain thermal ionization mass spectrometry dates (TIMS; May and Walker, 1989) and more recent ion probe and laser ablation

dates (Schwartz et al., 2023). May and Walker (1989) reported a multi-grain U-Pb zircon TIMS date of ca. 108 Ma for a granulite dike, which they interpret as approximating the upper limit of an earlier granulite-facies metamorphic event. Schwartz et al. (2023) reported several metamorphic titanite and zircon dates from the Cucamonga granulites, which gave ages ranging from 90 Ma to 82 Ma. These dates overlap the timing of the emplacement of a hypersthene tonalite orthogneiss and a granitic pluton both of which intruded migmatitic paragneisses in Deer Canyon at 88 Ma (May and Walker, 1989). May and Walker (1989) also report discordant age multi-grain TIMS date of ca. 85 Ma for the Tonalite of San Sevaine Lookout. Schwartz et al. (2023) report similar laser ablation–inductively coupled plasma mass spectrometry (LA-ICPMS) and sensitive high-resolution ion microprobe–reverse geometry (SHRIMP-RG) zircon dates for the Tonalite of San Sevaine Lookout ranging from 89 Ma to 85 Ma.

Late Cretaceous Shear Zones

Granulite-facies gneisses and migmatites in the Cucamonga terrane are overprinted by the Cucamonga Shear Zone (Figs. 1 and 2), which forms an ~1-km-thick zone of mylonite along the southern margin of the Cucamonga terrane in the hanging wall of the Quaternary Cucamonga Thrust Fault (dip = 25°–43°; McPhillips and Scharer, 2018; Morton and Miller, 2003; Morton and Matti, 1987). At the northern margin of the Cucamonga granulites, the Black Belt shear zone is marked by another ~1-km-thick zone composed of mylonitic and cataclastic fabrics that tectonically juxtaposes the granulites against mid-crustal tonalites (~5–7 kbar; May and Walker, 1989; Barth et al., 1995). This latter shear zone mainly deforms the Tonalites of San Sevaine Lookout (San Antonio terrane; Alf, 1948). May and Walker (1989) interpreted these features as a west-directed, synplutonic, ductile thrust system. The timing of this deformation is bracketed between the timing of emplacement of the Tonalite of San Sevaine Lookout at 89–85 Ma and crosscutting dikes at 74 Ma (Schwartz et al., 2023).

METHODS

Sampling Methods

We conducted two transects through Cucamonga Canyon and Deer Canyon to document the crustal architecture, thermal conditions, and temporal evolution of the arc root of the Southern California Batholith (Fig. 2). Both transects extend from the lower crust (Cucamonga terrane) into the base of the middle crust (San Antonio terrane). We collected 27 samples to document the variety of igneous and metamorphic rocks in the area. Samples consisted of four quartzites/metatexite and 23 igneous/meta-igneous rocks. Nine orthogneiss samples were reported in Schwartz et al. (2023) and are discussed in detail here. Except for a few undeformed, late-stage tonalites and granodiorites, most samples were variably metamorphosed at amphibolite- to granulite-facies conditions and are overprinted by subsolidus deformational fabrics, including those that form part of the Cucamonga and Black Belt shear zones. Consequently, most zircons have complex growth textures, including core, interior, and rim domains. Wherever possible we use zircon trace-element concentrations and ratios, particularly U (ppm), U/Th, Gd/Yb, and Dy/Yb, to distinguish metamorphic age populations (see "Orthogneisses in the Cucamonga Terrane").

Zircon and Titanite Petrochronology

Measurements were obtained at the California State University, Northridge (CSUN), Laser Lab and the University of California, Santa Barbara (UCSB). U-Pb ratios at UCSB were collected using a Nu Plasma multi-collector (MC)-ICPMS with a Photon Machines 193 ArF excimer laser with HelEx cell. Spot size and frequency were 35 microns and 4 Hz, respectively. Several standards, including 91500, Temora-2, and GJ-1, were analyzed throughout two analytical sessions to ensure the quality of the data. The methods for U-Pb ratio analysis closely follow the methods outlined in Kylander-Clark et al. (2013).

The U-Pb analyses were collected at CSUN using a ThermoScientific Element2 sector field (SF)-ICPMS coupled with a Teledyne Cetec Analyte G2 Excimer Laser (operating at a wavelength of 193 nm). Before analysis, the Element2 was tuned using the NIST-612 glass standard to optimize signal intensity and stability. The laser beam diameter was ~25 microns for zircon at 10 Hz and 75%–100% power. Ablation was performed in a HelEx II Active 2-Volume Cell™ and sample aerosol was transported with He carrier gas through Teflon-lined tubing, where it was mixed with Ar gas before introduction to the plasma torch. Flow rates for Ar and He gases were as follows: Ar cooling gas (16.0 NL/min); Ar auxiliary gas (1.0 NL/min); He carrier gas (~0.3–0.5 NL/min); and Ar sample gas (1.1–1.3 NL/min). Isotope data were collected in E-scan mode with magnet set at mass 202, and RF Power at 1245 W. Isotopes measured include ^{202}Hg, ^{204}(Pb + Hg), ^{206}Pb, ^{207}Pb, ^{208}Pb, ^{232}Th, and ^{238}U. All isotopes were collected in counting mode, except ^{232}Th and ^{238}U, which were collected in analogue mode. Analyses were conducted in an ~40 min time-resolved analysis mode. Each zircon and titanite analysis consisted of a 20-second integration with the laser firing on the sample, and a 20-second delay to purge the previous sample and move to the next sample. The approximate depth of ablation pit was ~20–30 microns.

For analyses in both laboratories, the primary standard 91500, was analyzed every 10 analyses to correct for in-run fractionation of Pb/U and Pb isotopes. The secondary zircon standard (Temora-2) was also analyzed every ~10 analyses to assess the reproducibility of the data. In the CSUN laboratory, U-Pb analysis of Temora-2 during all analytical sessions yielded concordant results and error-weighted average ages of 411 ± 0.4 Ma (n = 280), which is within ~1%–2% uncertainty of the accepted ages of 416.78 ± 0.33 Ma and 418.37 ± 0.14 Ma (Black et al., 2004; Mattinson, 2010). The quoted uncertainties in the text, figures, and Tables S1–S4[1] are reported as 2SE internal calculated from Iolite and IsoplotR (Paton et al., 2010; Vermeesch, 2018); however, when compared to data from other laboratories, we assign a 2% uncertainty to all dates to account for reproducibility of standards during analyses.

Zircon dates are reported using the ^{206}Pb/^{238}U date for analyses younger than 1100 Ma, and the ^{207}Pb/^{206}Pb date for those older than 1100 Ma. For zircons younger than 1100 Ma, the ^{207}Pb/^{206}Pb date is an unreliable indicator of discordance due to low abundances of measured ^{207}Pb. For these zircons, discordance is calculated as the percent difference between the ^{207}Pb/^{235}U date and the ^{206}Pb/^{238}U date. Analyses with greater than 10% uncertainty in ^{207}Pb/^{206}Pb date (1-sigma) or 5% uncertainty in ^{206}Pb/^{238}U date (1-sigma), 20% discordance, and/or 5% reverse discordance are excluded.

Corrections for minor amounts of common Pb in zircon were made on ^{206}Pb/^{238}U dates following the methods of Tera and Wasserburg (1972) using measured ^{207}Pb/^{206}Pb and ^{238}U/^{206}Pb ratios and an age-appropriate Pb isotopic composition of Stacey and Kramers (1975). Zircons with large common Pb corrections (e.g., analyses interpreted as having ~20% or greater contribution from common Pb) were discarded from further consideration. No corrections were made

[1]Supplemental Material. The supplemental material contains U-Pb isotope data for zircons from the Cucamonga and San Antonio terranes. Please visit https://doi.org/10.1130/GSAB.S.26218589 to access the supplemental material; contact editing@geosociety.org with any questions.

on $^{207}Pb/^{206}Pb$ dates due to large uncertainties in measured ^{204}Pb.

Cathodoluminescence (CL) images were obtained using an FEI Quanta scanning electron microscope before and after ablation to correlate the locations of analyzed domains with growth textures (Fig. 4). Wherever possible, we targeted all growth domains and report $^{207}Pb/^{206}Pb$-corrected $^{206}Pb/^{238}U$ ages of texturally homogeneous populations in the results below. In some cases, post-ablation CL imaging showed that laser spot analyses overlapped multiple domains. We report these data in tables; however, they are not considered in weighted mean calculations. Concordia plots and error-weighted average ages are shown in Figures 5–8, and data are summarized in Table 1.

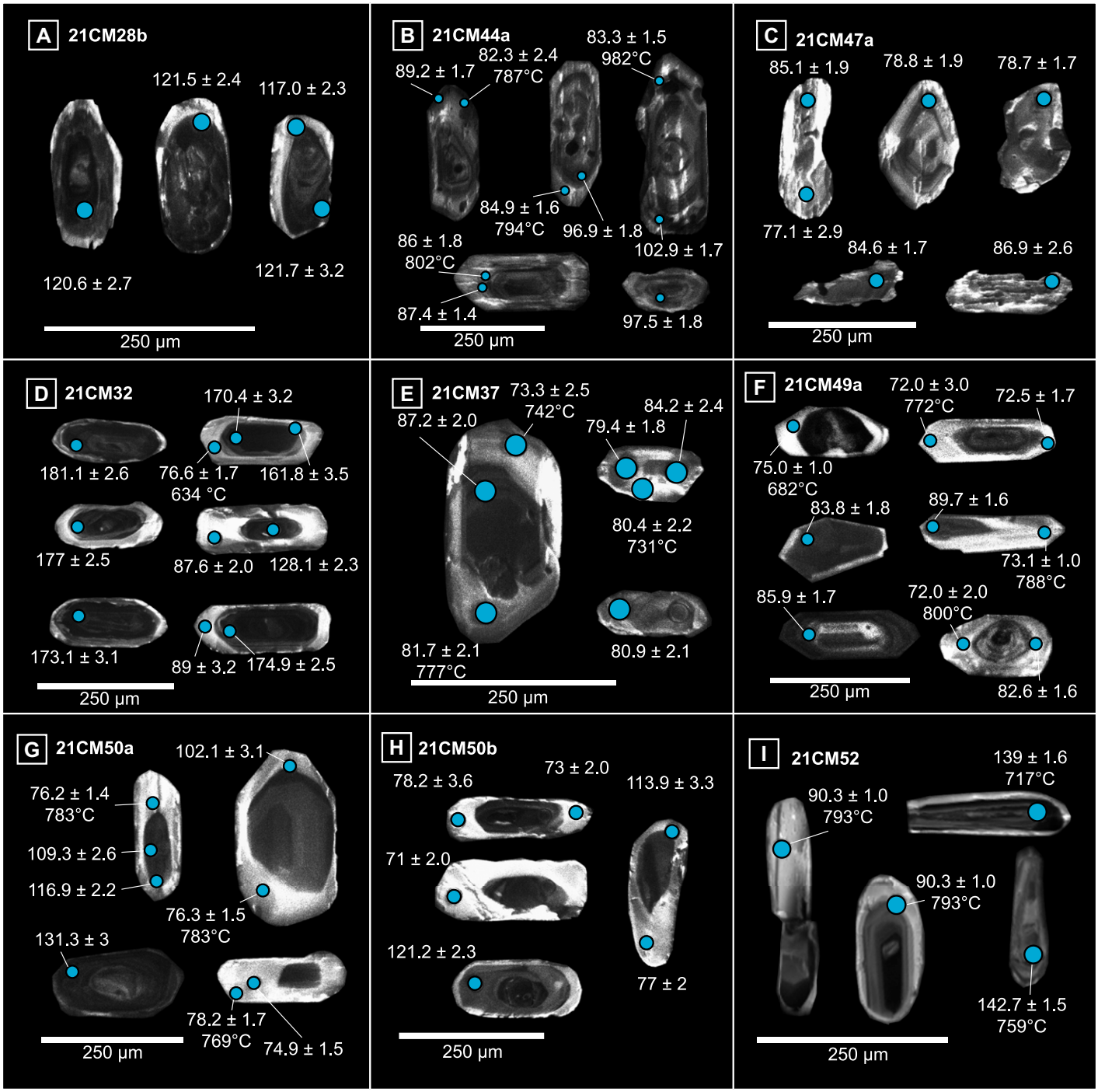

Figure 4. Cathodoluminescence images of representative zircons from the Cucamonga (A, D–I) and San Antonio terranes (B, C). Solid blue circles indicate location of laser ablation spots where U-Pb isotopes and trace-element concentrations were collected simultaneously. Quoted uncertainties are 1σ. Scale bars are 250 µm.

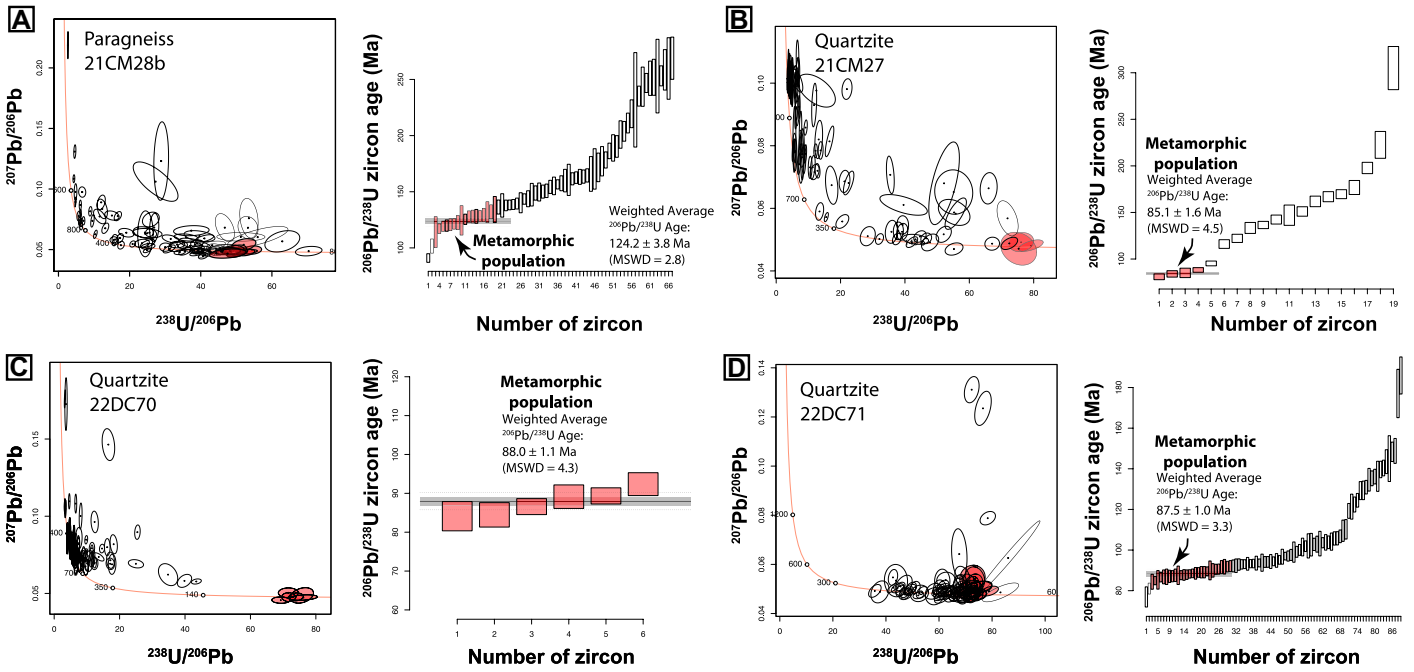

Figure 5. Tera-Wasserburg concordia diagrams and weighted average age plots for zircons from quartzites and metatexite in the Cucamonga terrane. The youngest statistically significant metamorphic population is shown in red and is interpreted to represent the timing of Early Cretaceous (A) and Late Cretaceous (B–D) high-grade metamorphism in the metasedimentary sequence. MSWD—mean square of weighted deviates.

Zircon LA-SF-ICPMS Trace-Element Geochemistry

Trace elements were measured simultaneously with U-Pb isotopes by LA-SF-ICPMS as described above using Zr as the internal standard. For zircon, we use nominal values of 43.14% Zr. Trace-element data were reduced using Iolite (Paton et al., 2010, 2011) and concentrations were calculated relative to NIST-612 as a primary standard. BHVO-2G was analyzed as a secondary standard to assess reproducibility of the data. For zircon, model Ti-in-zircon temperatures were calculated using the Ferry and Watson (2007) calibration. All samples contain quartz fixing the $a\mathrm{SiO_2}$ at unity. Samples from the Cucamonga granulites are associated with granulite-facies mineral assemblages containing rutile. For these samples, we estimate the activity of $\mathrm{TiO_2}$ at unity. For samples with ilmenite, $a\mathrm{TiO_2}$ likely ranges between 0.8 and 0.5 based on studies of igneous plutons (Schiller and Finger, 2019). For these samples, we assume an intermediate value of 0.6.

In the Cucamonga granulites, zircons commonly display rounded shapes and complex zonation patterns, commonly consisting of thin luminescent overgrowths (e.g., Figs. 4D–4I). These overgrowths are similar to those observed in other high-grade metamorphic terranes (e.g., Corfu et al., 2003; Schwartz et al., 2016). In granulite terranes, Gd/Yb and Dy/Yb values are particularly useful in distinguishing metamorphic populations because zircons that grow in equilibrium with garnet display elevated ratios associated with flattened chondrite-normalized middle to heavy rare earth element patterns due to the competition between garnet and zircon for the heavy rare earth elements during co-crystallization. In detrital samples, we also used changes in U (ppm) and U/Th values to identify possible metamorphic effects and to distinguish metamorphic zircons from detrital populations.

RESULTS

Field and Petrological Observations

Lower-crustal rocks in the Cucamonga terrane consist of heterogeneous, granulite-facies paragneisses, orthogneisses, and migmatites with subordinate marble and felsic dikes (Figs. 3A–3J). Paragneisses in Cucamonga and Deer Canyons occur as thick sequences of thinly layered quartzite, amphibolite, quartzofeldspathic gneiss (quartz + plagioclase + biotite + potassium feldspar + garnet), and occasional lenses of boudinaged marble and calc-silicate rock (Fig. 3A). In many outcrops, an early gneissic foliation (S_1), which is folded into tight, north-verging recumbent F_2 folds is observed. Where paragneisses are biotite-rich, stromatic migmatites are common and display centimeter- to meter-scale folds (Figs. 3C and 3D). Melanosomes in the metatexite consist of plagioclase + quartz + orthopyroxene + clinopyroxene + biotite ± garnet; whereas, leucosomes contain biotite + quartz + plagioclase + potassium feldspar ± orthopyroxene. Zircon and rutile are ubiquitous accessory phases in nearly all rock types.

Mafic gneisses in both Deer and Cucamonga Canyons are characterized by mineral assemblages containing plagioclase + orthopyroxene + clinopyroxene + biotite ± garnet (Hsu, 1955; Figs. 3E and 3F). Given the degree of metamorphism and deformation, it is unclear whether their protoliths were mafic volcanic rocks, volcanogenic sediments, or fine-grained mafic intrusive rocks. Felsic granulites are less common and occur as medium- to coarse-grained orthopyroxene-bearing gneissic granites (charnockites) and mylonitic tonalites often with conspicuous metamorphic garnet associated with diffuse leucosomes (Figs. 3G–3J). In high-grade gneisses of all compositions, intense metamorphism resulted in local development of leucosomes and stromatitic migmatites. The latter often grade into irregular bodies of metatexite where gneissic layering is progressively replaced by coarse leucosomes containing biotite + quartz + plagioclase ± garnet ± orthopyroxene (Figs. 3C, 3E, and 3F).

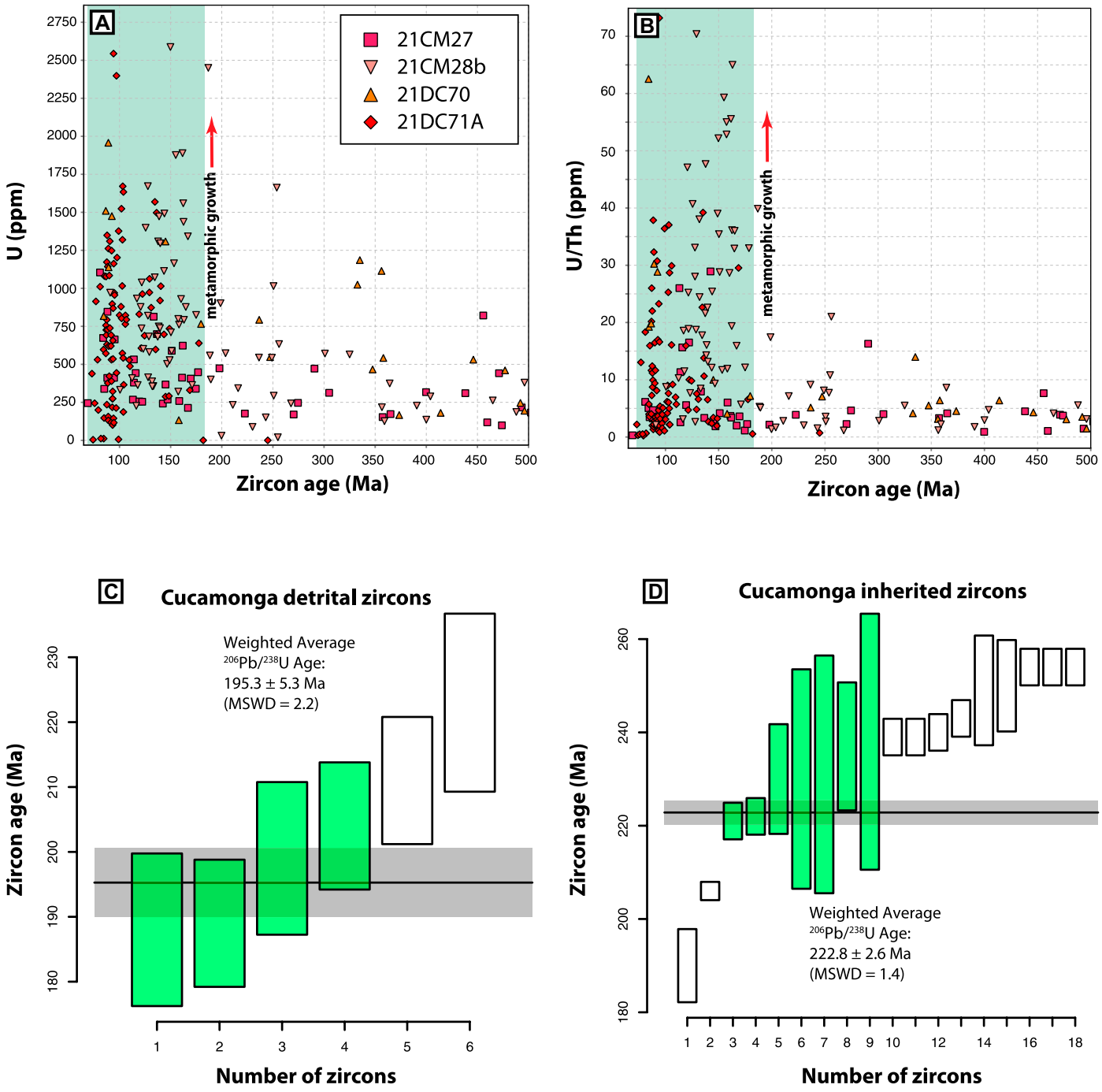

Figure 6. Detrital zircon age versus U (ppm) (A) and U/Th (B) for four metasedimentary rocks in the Cucamonga terrane. Zircons younger than ca. 180 Ma show an uptick in U (ppm) and U/Th, which signals that they have been affected by new metamorphic growth, recrystallization, and/or Pb loss. Therefore, we consider all zircons younger than 180 Ma suspect even if they have low U/Th and U (ppm) because they may be affected by Pb-loss. (C) Maximum depositional age calculation for the youngest zircon mode in the four combined Cucamonga metasedimentary rocks, excluding obvious metamorphic analyses. (D) Youngest age population calculated for inherited zircons in orthogneisses that intruded the Cucamonga paragneiss sequence. This age is consistent with the maximum depositional age calculated in part C from zircons in the Cucamonga metasedimentary rocks. Data are from this study and Schwartz et al. (2023). MSWD—mean square of weighted deviates.

Late-stage biotite granodiorites and biotite granites cut paragneisses and orthogneisses and are weakly to moderately deformed. The granodiorite and granites exhibit protomylonitic fabrics, with quartz and plagioclase accommodating crystal-plastic deformation. Late-stage dikes generally lack granulite-facies mineral assemblages but have amphibolite-facies assemblages, suggesting that they formed during the

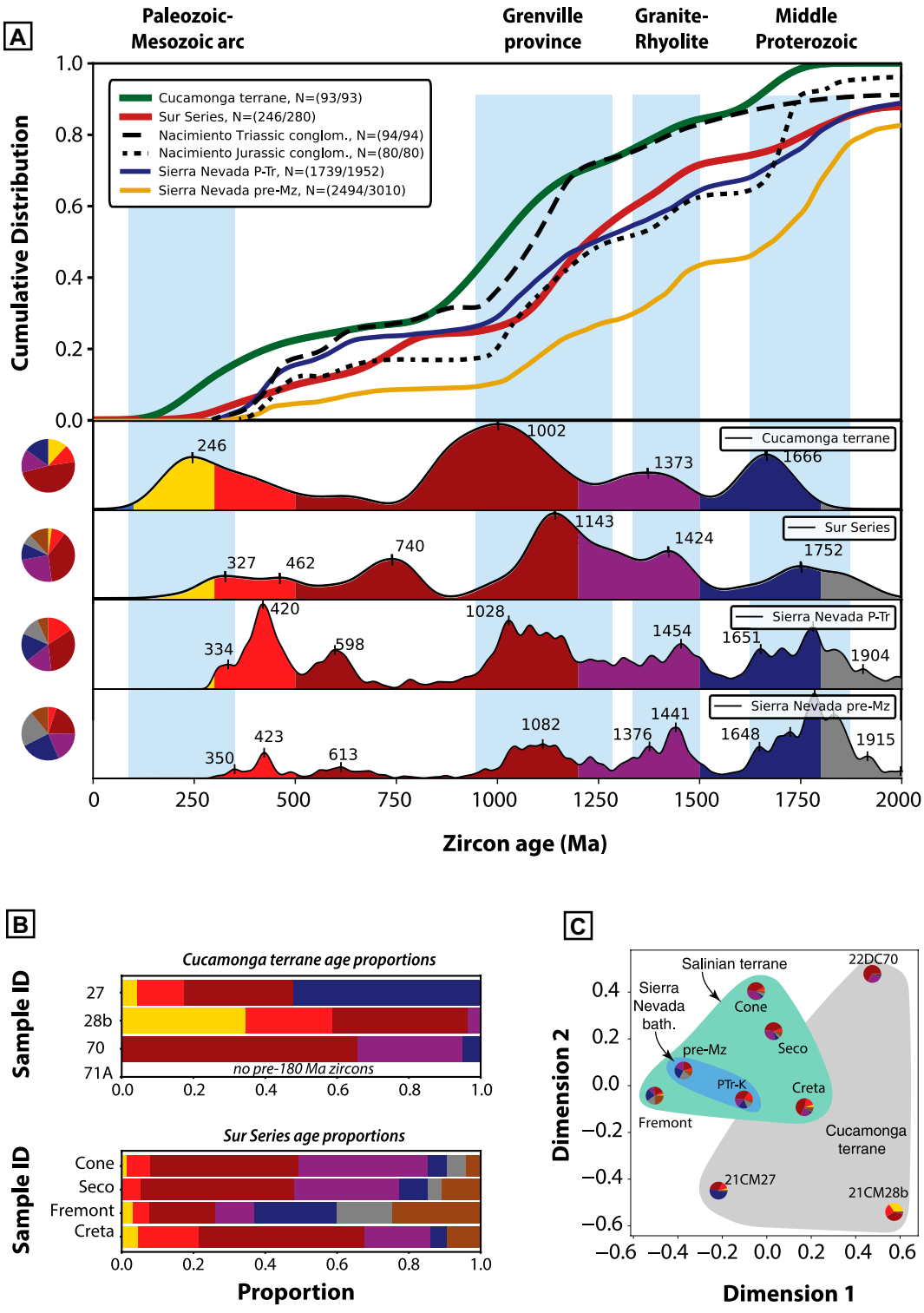

Figure 7. Detrital zircon data from the Cucamonga terrane compared to data from the Sur Series (Salinia block; Barbeau et al., 2005), Triassic to Jurassic conglomerates in the Nacimiento block (Johnston et al., 2018), and intra-arc strata in the Sierra Nevada Batholith (Attia et al., 2021). Cucamonga and Sur Series data are filtered to exclude metamorphic populations. (A) Cumulate distribution plots and kernel density estimate plots with peak modal populations indicated. Pie charts to the left of kernel density estimates show relative proportions of zircon populations colored by age. (B) Relative proportion of zircon ages in the four Cucamonga metasedimentary samples compared to those in the Sur Series. The presence of Mesozoic zircons and similar populations is consistent with a shared depositional history between the two high-grade sequences. (C) Multidimensional scaling plot comparing Cucamonga, Sur Series, and intra-arc sediments in the Sierra Nevada Batholith. Plots generated in detritalPy (Sharman et al., 2018). PTr—Permo-Triassic; Mz—Mesozoic; K, Creta—Cretaceous.

final stages of metamorphism and ductile shearing in the lower crust.

Structurally above the lower-crustal granulites in the Cucamonga terrane is a sequence of mylonitic to gneissic tonalites and granodiorites that comprise the Tonalite of San Sevaine Lookout in the San Antonio terrane (Figs. 3K–3P; Morton et al., 2001). Outside the Black Belt shear zone, these rocks are predominantly medium- to coarse-grained, generally equigranular, hornblende-biotite tonalites with lesser hornblende biotite granodiorite and quartz diorite (Fig. 3K). Locally, large septa of marble, gneiss, and schist are present and likely assimilated from structurally overlying schists and paragneiss. Within the Black Belt shear zone, gneissic and mylonitic foliations are defined by oriented hornblende, biotite, and flattened mafic enclaves (Fig. 3L). Cataclastic fabrics alternate with mylonites and layer-parallel pseudotachylytes, all of which

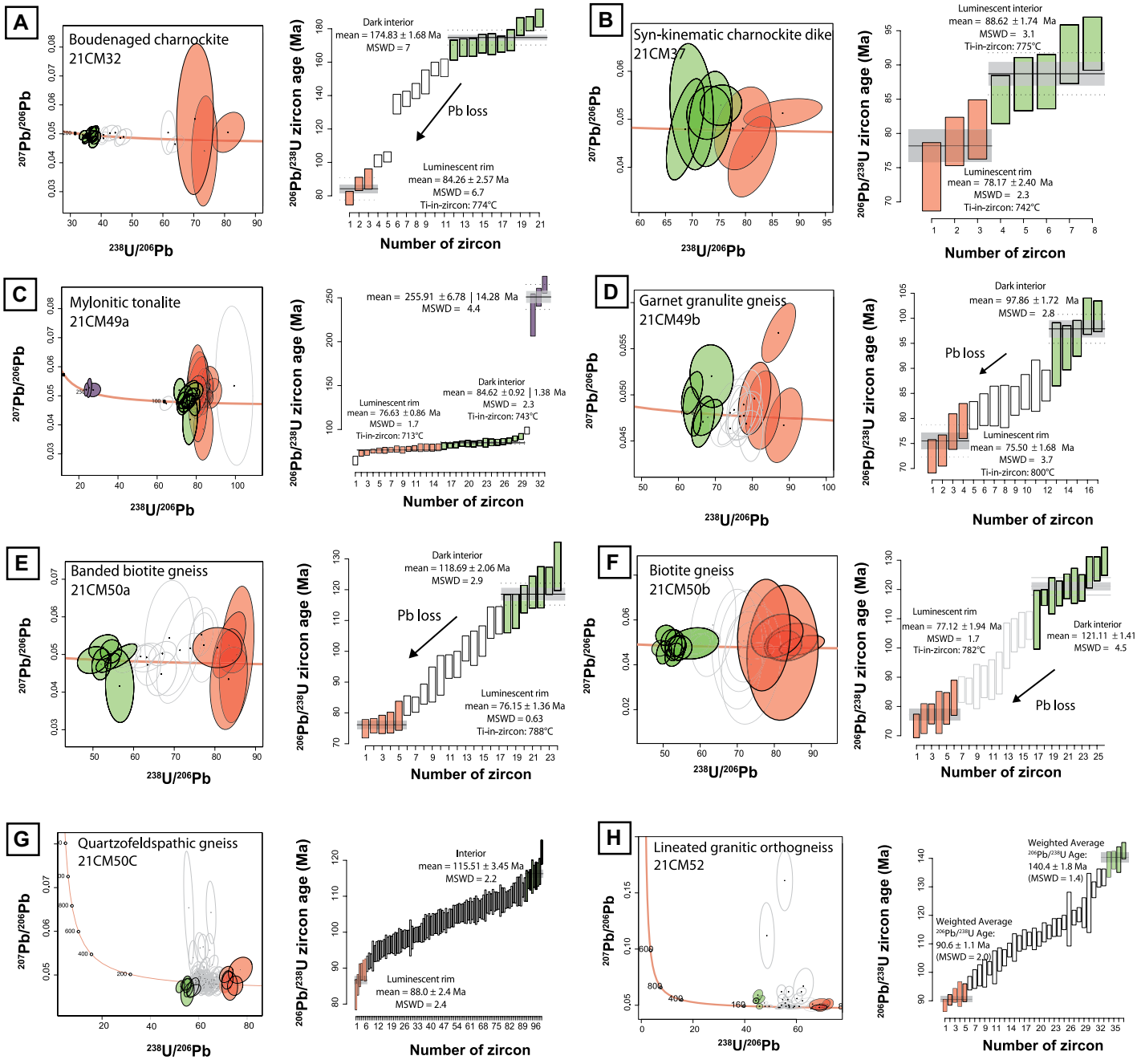

Figure 8. Tera-Wasserburg concordia diagrams and weighted average age plots for zircons from meta-igneous rocks from Cucamonga and Deer Canyons. Concordia and weighted average diagrams show all analyzed spots (including rejected spots in open circles). Green filled error ellipses and error bars indicate igneous population whereas those in red are interpreted to be metamorphic based on texture and/or geochemistry. Error ellipses show 2σ total uncertainty for individual spot analyses. MSWD—mean square of weighted deviates.

are mylonitically deformed at amphibolite-facies conditions (Fig. 3L). Within the Black Belt shear zone, gneissic and mylonitic foliations generally strike to the NW-SE and dip moderately to the northeast. Mineral lineations composed of biotite, hornblende, plagioclase, and quartz plunge variably to the northeast on foliation planes. The foliations are folded into tight, recumbent folds (e.g., Figs. 3M and 3N).

At the top of Deer Canyon, gneissic tonalites contain diffuse plagioclase-rich leucosomes with peritectic garnet up to 1 cm in diameter. Locally, leucosomes coalesce into diatexitic migmatites, which form channels through the tonalitic orthogneiss (Figs. 3O and 3P). Leucosomes are sometimes folded (Fig. 3P) and are cut by late-stage, unstrained, and unmetamorphosed granodiorites (Fig. 3O).

Structural Observations

Foliations within the Cucamonga granulites generally strike NW-SE and dip moderately to the northeast. The oldest gneissic fabrics (a composite S_1/S_2 foliation) in these rocks record top-to-the-S and top-to-the-SE (present-day reference frame) reverse-sense motion. These structures define an early D_1/D_2 thrust system that

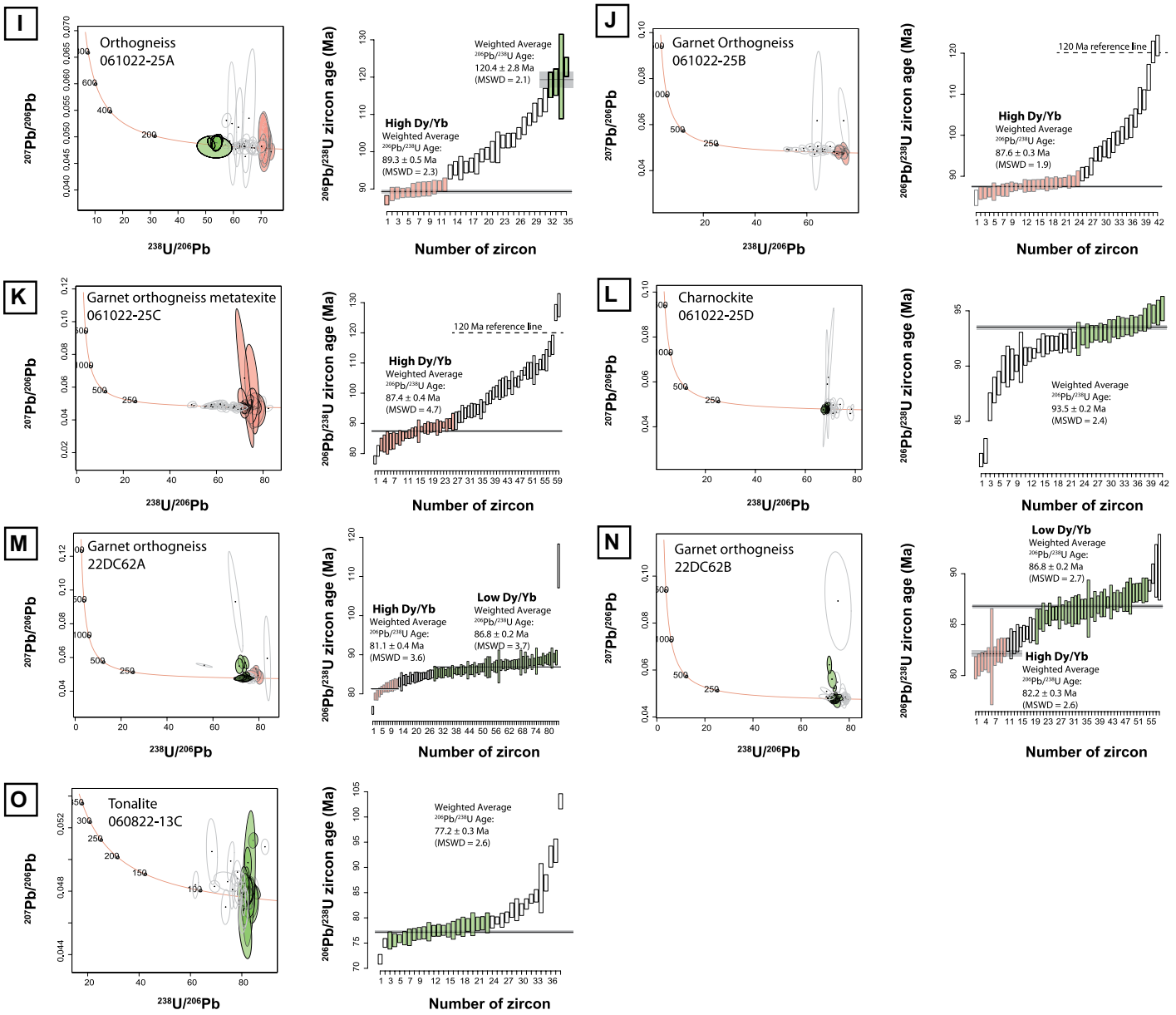

Figure 8. (***Continued***)

only occurs in the Cucamonga granulites and is absent in the tonalites (Baskin et al., 2023; Klepeis et al., 2023). Superimposed on this thrust system is a penetrative, N- and NW-dipping, S_3 foliation and shallowly plunging lineations, which record sinistral-reverse displacements. This transpressional fabric occurs throughout the Cucamonga and San Antonio terranes and defines the Black Belt and Cucamonga shear zones (e.g., May and Walker, 1989; Baskin et al., 2023; Klepeis et al., 2023). The S_3 fabrics are folded into a series of south-vergent, overturned folds (F_4), some of which are syn-kinematic with granodioritic dikes suggesting that they formed during the latest stages of D_3 transpression and magmatism. Superimposed on all these structures are a series of ductile-to-brittle thrust faults and folds, some of which are related to the formation of the late Quaternary Cucamonga thrust fault system (Baskin et al., 2023; Klepeis et al., 2023).

Zircon Petrochronology

Detrital Zircons in the Cucamonga Terrane

We collected two quartzites from Deer Canyon and one metatexite and one quartzite from Cucamonga Canyon to establish sediment provenance and maximum depositional age (MDA) of the high-grade metasedimentary sequence in the Cucamonga terrane. A complicating factor in this approach is that all samples were metamorphosed at upper-amphibolite to granulite-facies conditions, and consequently zircons show textural, chemical, and age evidence for metamorphic growth. While we primarily targeted zircon cores, results from all samples show the presence of ubiquitous Cretaceous metamorphic populations (Fig. 5). For example, the metatexite (sample 21CM28b) yielded evidence for an Early Cretaceous, M_1 metamorphic event and gave a weighted average of the youngest statistical population at 124.2 ± 3.8 Ma (Figs. 3C and 5A). Zircon CL imaging shows that this population includes both luminescent rims

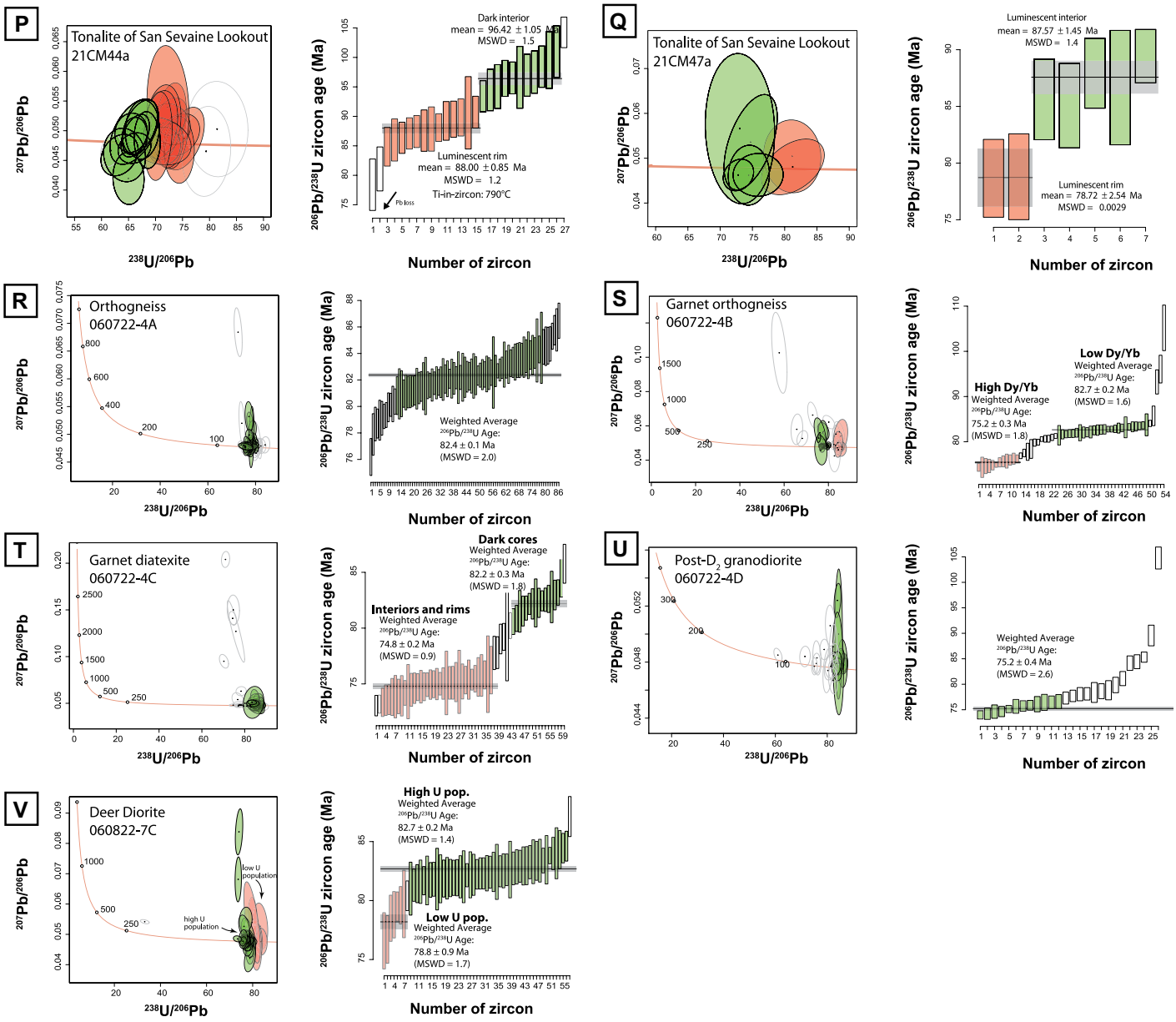

Figure 8. (*Continued*)

and dark cores, which formed during a previously unrecognized, Early Cretaceous metamorphic event (Fig. 4). In contrast, the three quartzites yielded Late Cretaceous, M_2 metamorphic populations at 85.1 ± 1.6 Ma (sample 21CM27), 87.5 ± 1.1 Ma (sample 22DC71), and 88.0 ± 1.1 Ma (sample 22DC70; Fig. 5). These zircon populations are generally characterized by high U and U/Th values (Figs. 6A and 6B), and they overlap in age with metamorphic overgrowth in zircons from granulite-facies orthogneisses discussed below.

To discriminate between detrital and metamorphic zircon grains, we apply a cut-off for zircon populations with pronounced increases in U (ppm) and U/Th, both of which are useful indicators in identifying metamorphic zircons (Figs. 6A and 6B). In the Cucamonga zircons, we observe that many zircons younger than ca. 180 Ma display high U (ppm) and U/Th, suggesting that they are metamorphic in origin. We note that not all zircons in this age group have elevated U (ppm) and U/Th values; however, we view all grains younger than 180 Ma as potentially suspect due to the possibility that they may have experienced new metamorphic growth, recrystallization, and/or Pb loss. After removing these grains from our dataset, 93 non-metamorphic, detrital cores remain out of 394 total analyses. They are characterized by a mixture of Precambrian and Mesozoic modes (Figs. 5, 7A, and 7B). Zircons in the quartzite sample (21CM27) in Cucamonga Canyon include Precambrian modes with ages at 1170–1000 Ma and 1698–1600 Ma, and a Mesozoic mode at 223–180 Ma. The metatexite in Cucamonga Canyon (21CM28b) yielded predominantly Phanerozoic zircons with Mesozoic modes at 230–180 Ma and Paleozoic modes at 477–250 Ma. Lesser abundant Mesoproterozoic ages range from 1034 Ma to 943 Ma. The quartzite sample (22DC70) in Deer Canyon also yielded predominantly Precambrian zircon ages with modes at 1187–851 Ma, 1449–1260 Ma, and 1739–1709 Ma.

TABLE 1. SUMMARY OF ZIRCON GEOCHRONOLOGY IN THE CUCMAONGA AND SAN ANTONIO TERRANES

Sample	Unit	Location	Rock type	Latitude (°N)	Longitude (°W)	Chronometer	Age cal.	Date (Ma)	Error (2SE) Internal	Error (2SE) Total	MSWD	Number analyzed*	Analytical instrument	Laboratory	Interpretation
San Antonio terrane															
SGM12-19†	Granodiorite dike	Road 1N34	Post-D2 aplite dikelette	34.19770	117.47066	Zircon	WM	74.0	0.7	1.5	0.8	4	SHRIMP-RG	USGS-Stanford	Igneous
060722-4c (rims/ interiors)	Tonalite of San Sevaine Lookout	Deer Canyon	Garnet diatexite	34.20453	117.58684	Zircon	WM	74.8	0.2	1.5	0.9	34	LA-SF-ICPMS	UCSB	M_2 metamorphism
060722-4b (high Dy/Yb pop)	Tonalite of San Sevaine Lookout	Deer Canyon	Garnet orthogneiss	34.20453	117.58684	Zircon	WM	75.2	0.3	1.5	1.8	12	LA-SF-ICPMS	UCSB	M_2 metamorphism
060722-4d	Tonalite of San Sevaine Lookout	Deer Canyon	Post-D2 granodiorite	34.20453	117.58684	Zircon	WM	75.2	0.4	1.5	2.6	12	LA-SF-ICPMS	UCSB	Igneous
SGM12-13 (rims)†	Tonalite of San Sevaine Lookout	Road 1N34	Biotite hornblende tonalite	34.20023	117.48246	Zircon	WM	75.5	5.3	1.5	4.3	9	SHRIMP-RG	USGS-Stanford	M_2 metamorphism
SGM12-12†	Granodiorite dike	Road 1N34	Granite dike	34.19799	117.48012	Zircon	WM	76.2	0.5	1.5	1.1	6	SHRIMP-RG	USGS-Stanford	Igneous
21CM47a (rims)†	Tonalite of San Sevaine Lookout	Cucamonga Canyon	Mylonitic tonalite	34.18464	117.62659	Zircon	WM	78.7	2.5	1.6	0	2	LA-SF-ICPMS	CSUN	M_2 metamorphism
060822-7c (low U pop)	Deer Diorite	Deer Canyon	Diorite	34.19931	117.58429	Zircon	WM	78.8	0.9	1.6	1.7	7	LA-SF-ICPMS	UCSB	M_2 metamorphism
17SGM48†	Tonalite of San Sevaine Lookout	Road 1N34	Mylonitic tonalite	34.1955	117.471	Zircon	WM	79.8	0.6	1.6	2.2	60	LA-SF-ICPMS	CSUN	Igneous
17SGM47†	Tonalite of San Sevaine Lookout	Road 1N34	Mylonitic tonalite	34.1962	117.47084	Zircon	WM	80.4	0.8	1.6	3.1	34	LA-SF-ICPMS	CSUN	Igneous
060722-4c (dark cores)	Tonalite of San Sevaine Lookout	Deer Canyon	Garnet diatexite	34.20453	117.58684	Zircon	WM	82.2	0.3	1.6	1.8	16	LA-SF-ICPMS	UCSB	Igneous
060722-4a	Tonalite of San Sevaine Lookout	Deer Canyon	Orthogneiss (no garnet)	34.20453	117.58684	Zircon	WM	82.4	0.1	1.6	2	67	LA-SF-ICPMS	UCSB	Igneous
060722-4b (low Dy/Yb pop)	Tonalite of San Sevaine Lookout	Deer Canyon	Garnet orthogneiss	34.20453	117.58684	Zircon	WM	82.7	0.2	1.7	1.6	26	LA-SF-ICPMS	UCSB	Igneous
060822-7c (high U pop)	Deer Diorite	Deer Canyon	Diorite	34.19931	117.58429	Zircon	WM	82.7	0.2	1.7	1.4	48	LA-SF-ICPMS	UCSB	Igneous
SGM12-13 (cores)†	Tonalite of San Sevaine Lookout	Road 1N34	Biotite hornblende tonalite	34.20023	117.48246	Zircon	WM	85.8	0.6	1.7	1.5	4	SHRIMP-RG	USGS-Stanford	Igneous
21CM47a (cores)†	Tonalite of San Sevaine Lookout	Cucamonga Canyon	Mylonitic tonalite	34.18464	117.62659	Zircon	WM	87.6	1.5	1.8	1.4	5	LA-SF-ICPMS	CSUN	Igneous
SGM12-27†	Tonalite of San Sevaine Lookout	Road 1N34	Biotite hornblende tonalite	34.21267	117.52972	Zircon	WM	87.7	0.6	1.8	1.5	31	LA-SF-ICPMS	CSUN	Igneous
21CM44a (rims)†	Tonalite of San Sevaine Lookout	Cucamonga Canyon	Biotite hornblende tonalite	34.18227	117.62837	Zircon	WM	88.0	0.9	1.8	1.2	13	LA-SF-ICPMS	CSUN	Igneous
SGM12-25†	Tonalite of San Sevaine Lookout	Road 1N34	Biotite hornblende tonalite	34.21410	117.50070	Zircon	WM	89.4	0.5	1.8	2.6	57	LA-SF-ICPMS	CSUN	Igneous
21CM44a (cores)†	Tonalite of San Sevaine Lookout	Cucamonga Canyon	Biotite hornblende tonalite	34.18227	117.62837	Zircon	WM	96.4	1.1	1.9	1.5	11	LA-SF-ICPMS	CSUN	Xenocrystic cores

(*Continued*)

TABLE 1. (*Continued*)

Sample	Unit	Location	Rock type	Latitude (°N)	Longitude (°W)	Chronometer	Age cal.	Date (Ma)	Error (2SE) Internal	Error (2SE) Total	MSWD	Number analyzed*	Analytical instrument	Laboratory	Interpretation
Cucamonga terrane															
13EC17†	Cucamonga granulite	Etiwanda Canyon	Mafic orthogneiss	34.179	117.52039	Zircon	WM	72.0	1.3	1.4	7.1	5	LA-SF-ICPMS	CSUN	M_2 metamorphism
21CM49b (rims)†	Cucamonga granulite	Cucamonga Canyon	Garnet orthogneiss	34.17185	117.63259	Zircon	WM	75.5	1.7	1.5	3.7	4	LA-SF-ICPMS	CSUN	M_2 metamorphism
21CM50a (rims)†	Cucamonga granulite	Cucamonga Canyon	Megacrystic granite	34.17178	117.63268	Zircon	WM	76.2	1.4	1.5	0.6	5	LA-SF-ICPMS	CSUN	M_2 metamorphism
21CM49a (rims)†	Cucamonga granulite	Cucamonga Canyon	Mylonitic tonalite	34.17185	117.63259	Zircon	WM	76.6	0.9	1.5	1.7	14	LA-SF-ICPMS	CSUN	M_2 metamorphism
21CM50b (rims)†	Cucamonga granulite	Cucamonga Canyon	Banded gneiss	34.17178	117.63268	Zircon	WM	77.1	1.9	1.5	1.7	6	LA-SF-ICPMS	CSUN	M_2 metamorphism
060822-13c	Cucamonga granulite	Deer Canyon	Tonalite sill	34.19353	117.58152	Zircon	WM	77.2	0.3	1.5	2.6	21	LA-SF-ICPMS	UCSB	Igneous
17SGM51†	Cucamonga granulite	Road 1N34	Lineated orthogneiss	34.19355	117.46256	Zircon	WM	77.7	1.2	1.6	2.4	19	LA-SF-ICPMS	CSUN	Igneous
13SGM38†	Charnockite pluton	Day Canyon	Charnockite	34.18444	117.54724	Zircon	WM	77.8	1.2	1.6	1.1	25	LA-SF-ICPMS	CSUN	Igneous
13SGM34†	Cucamonga granulite	Day Canyon	Migmatitic garnet granulite	34.18282	117.54411	Zircon	WM	77.9	0.6	1.6	3.1	26	LA-SF-ICPMS	CSUN	M_2 metamorphism
21CM37 (rims)†	Cucamonga granulite	Cucamonga Canyon	Syndeformational dike	34.18107	117.62919	Zircon	WM	78.2	2.4	2.4	2.3	3	LA-SF-ICPMS	CSUN	M_2 metamorphism
LCVIA†	Cucamonga granulite	Cucamonga Canyon	Skarn	34.21285	117.45696	Titanite	LI	78.8	0.6	1.6	3.5	29	LA-SF-ICPMS	CSUN	M_2 metamorphism
22DC62a (high Dy/Yb pop)	Cucamonga granulite	Deer Canyon	Garnet orthogneiss	34.19263	117.58138	Zircon	WM	81.1	0.4	1.6	3.6	11	LA-SF-ICPMS	UCSB	M_2 metamorphism
17SGM50†	Cucamonga granulite	Road 1N34	Biotite orthogneiss	34.19308	117.46279	Zircon	WM	82.2	1.0	1.6	2.6	25	LA-SF-ICPMS	CSUN	Igneous
22DC62b (high Dy/Yb pop)	Cucamonga granulite	Deer Canyon	Garnet orthogneiss	34.19263	117.58138	Zircon	WM	82.2	0.3	1.6	2.6	13	LA-SF-ICPMS	UCSB	M_2 metamorphism
17SGM49†	Cucamonga granulite	Road 1N34	Garnet orthogneiss	34.19300	117.46288	Zircon	WM	82.5	0.6	1.7	1.5	46	LA-SF-ICPMS	CSUN	Igneous
LCVI†	Cucamonga granulite	Cucamonga Canyon	Skarn	34.21285	117.45696	Titanite	LI	82.5	0.8	1.7	3.1	57	LA-SF-ICPMS	CSUN	M_2 metamorphism
SGM12-20 (rims)†	Cucamonga granulite	Road 1N34	Garnet orthogneiss	34.1958	117.46338	Zircon	WM	83.8	1.5	1.7	1.2	7	SHRIMP-RG	USGS-Stanford	M_2 metamorphism
12EC8†	Cucamonga granulite	Etiwanda Canyon	Quartzofeldspathic gneiss	34.1862	117.52305	Zircon	WM	84.0	1.2	1.7	2.4	11	LA-SF-ICPMS	CSUN	M_2 metamorphism
21CM32 (rims)†	Cucamonga granulite	Cucamonga Canyon	Boudinaged charnockite dike	34.17879	117.62931	Zircon	WM	84.3	2.6	2.6	6.7	3	LA-SF-ICPMS	CSUN	M_2 metamorphism
21CM49a (cores)†	Cucamonga granulite	Cucamonga Canyon	Mylonitic tonalite	34.17185	117.63259	Zircon	WM	84.6	0.9	1.7	2.3	13	LA-SF-ICPMS	CSUN	Igneous
21CM27	Cucamonga granulite	Cucamonga Canyon	Quartzofeldspathic paragneiss	34.179	117.6271	Zircon	WM	85.1	1.6	1.7	4.5	4	LA-SF-ICPMS	CSUN	M_2 metamorphism
12EC2A†	Cucamonga granulite	Etiwanda Canyon	Garnet orthogneiss	34.1852	117.53036	Zircon	WM	85.6	1.3	1.7	1.8	11	LA-SF-ICPMS	CSUN	Igneous
21CM2†5	Cucamonga granulite	Cucamonga Canyon	Post-kinematic dike	34.17895	117.62736	Zircon	WM	85.6	0.7	1.7	2	35	LA-SF-ICPMS	CSUN	Igneous
12EC7†	Cucamonga granulite	Etiwanda Canyon	Quartzofeldspathic gneiss	34.1862	117.52305	Zircon	WM	85.9	1.6	1.7	1.9	8	LA-SF-ICPMS	CSUN	M_2 metamorphism
12EC6†	Cucamonga granulite	Etiwanda Canyon	Calc-silicate	34.1782	117.52237	Zircon	WM	86.1	2.5	2.5	1.6	5	SHRIMP-RG	USGS-Stanford	M_2 metamorphism
SGM12-20 (cores)†	Cucamonga granulite	Road 1N34	Garnet orthogneiss	34.1958	117.46338	Zircon	WM	86.1	0.7	1.7	1.8	7	SHRIMP-RG	USGS-Stanford	M_2 metamorphism
22DC62a (low Dy/Yb pop)	Cucamonga granulite	Deer Canyon	Garnet orthogneiss	34.19263	117.58138	Zircon	WM	86.8	0.2	1.7	3.7	56	LA-SF-ICPMS	UCSB	Igneous

(*Continued*)

TABLE 1. (*Continued*)

Sample	Unit	Location	Rock type	Latitude (°N)	Longitude (°W)	Chronometer	Age cal.	Date (Ma)	Error (2SE) Internal	Error (2SE) Total	MSWD	Number analyzed*	Analytical instrument	Laboratory	Interpretation
22DC62b (low Dy/Yb pop)	Cucamonga granulite	Deer Canyon	Garnet orthogneiss	34.19263	117.58138	Zircon	WM	86.8	0.2	1.7	2.7	35	LA-SF-ICPMS	UCSB	Igneous
13SGM37†	Charnockite pluton	Day Canyon	Charnockite	34.1831	117.54479	Zircon	WM	87.1	0.6	1.7	3.5	40	LA-SF-ICPMS	CSUN	Igneous
061022-25c (high Dy/Yb pop)	Cucamonga granulite	Deer Canyon	Migmatitic orthogneiss	34.18036	117.57105	Zircon	WM	87.4	0.4	1.7	4.7	24	LA-SF-ICPMS	UCSB	M_2 metamorphism
22DC71	Cucamonga granulite	Deer Canyon	Quartzofeldspathic paragneiss	34.19353	117.58152	Zircon	WM	87.5	1.0	1.8	3.3	30	LA-SF-ICPMS	CSUN	M_2 metamorphism
GREG-6†	Cucamonga granulite	Etiwanda Canyon	Charnockite dike	34.1782	117.52237	Zircon	WM	87.5	2.7	2.7	5.8	5	SHRIMP-RG	USGS-Stanford	Igneous
061022-25b (high Dy/Yb pop)	Cucamonga granulite	Deer Canyon	Garnet orthogneiss	34.18036	117.57105	Zircon	WM	87.6	0.3	1.8	1.9	23	LA-SF-ICPMS	UCSB	M_2 metamorphism
21CM50c (rims)	Cucamonga granulite	Cucamonga Canyon	Quartzofeldspathic gneiss	34.17178	117.63268	Zircon	WM	88.0	2.4	2.4	2.4	6	LA-SF-ICPMS	CSUN	M_2 metamorphism
22DC70	Cucamonga granulite	Deer Canyon	Quartzofeldspathic paragneiss	34.19353	117.58146	Zircon	WM	88.0	1.1	1.8	4.3	6	LA-SF-ICPMS	CSUN	M_2 metamorphism
21CM37 (interiors)†	Cucamonga granulite	Cucamonga Canyon	Syndeformational dike	34.18107	117.62919	Zircon	WM	88.6	1.7	1.8	3.1	5	LA-SF-ICPMS	CSUN	Igneous
061022-25a (high Dy/Yb pop)	Cucamonga granulite	Deer Canyon	Orthogneiss with minor garnet	34.18036	117.57105	Zircon	WM	89.3	0.5	1.8	2.3	12	LA-SF-ICPMS	UCSB	M_2 metamorphism
21CM33†	Cucamonga granulite	Cucamonga Canyon	Skarn	34.17727	117.62473	Titanite	LI	90.0	2.3	2.3	1.8	86	LA-SF-ICPMS	CSUN	M_2 metamorphism
21CM52 (rims)	Cucamonga granulite	Cucamonga Canyon	Lineated granitic tectonite	34.16738	117.63572	Zircon	WM	90.6	1.1	1.8	2	5	LA-SF-ICPMS	UCSB	M_2 metamorphism
12EC6†	Cucamonga granulite	Etiwanda Canyon	Calc-silicate	34.1782	117.52237	Zircon	WM	90.6	0.9	1.8	1	21	LA-SF-ICPMS	CSUN	M_2 metamorphism
061022-25d	Cucamonga granulite	Deer Canyon	Leucogranite	34.18036	117.57105	Zircon	WM	93.5	0.2	1.9	2.4	20	LA-SF-ICPMS	UCSB	Igneous
21CM49b (cores/ interiors)†	Cucamonga granulite	Cucamonga Canyon	Garnet orthogneiss	34.17185	117.63259	Zircon	WM	97.9	1.7	2.0	2.8	5	LA-SF-ICPMS	CSUN	Igneous
21CM50c (cores)	Cucamonga granulite	Cucamonga Canyon	Quartzofeldspathic gneiss	34.17178	117.63268	Zircon	WM	115.5	3.5	3.5	2.2	9	LA-SF-ICPMS	CSUN	Igneous
21CM50a (cores)†	Cucamonga granulite	Cucamonga Canyon	Megacrystic granite	34.17178	117.63268	Zircon	WM	118.7	2.1	2.4	2.9	7	LA-SF-ICPMS	CSUN	Igneous
061022-25a (cores)	Cucamonga granulite	Deer Canyon	Orthogneiss with minor garnet	34.18036	117.57105	Zircon	WM	120.4	2.8	2.8	2.1	4	LA-SF-ICPMS	UCSB	Igneous
21CM50b (cores)†	Cucamonga granulite	Cucamonga Canyon	Banded gneiss	34.17178	117.63268	Zircon	WM	121.1	1.4	2.4	4.5	10	LA-SF-ICPMS	CSUN	Igneous
21CM28b	Cucamonga granulite	Cucamonga Canyon	Quartzofeldspathic paragneiss	34.1812	117.62984	Zircon	WM	124.2	3.8	3.8	2.8	19	LA-SF-ICPMS	CSUN	M_1 metamorphism
21CM52 (cores)	Cucamonga granulite	Cucamonga Canyon	Lineated granitic tectonite	34.16738	117.63572	Zircon	WM	140.4	1.8	2.8	1.4	4	LA-SF-ICPMS	UCSB	Igneous
21CM32 (cores/ interiors)†	Cucamonga granulite	Cucamonga Canyon	Boudinaged charnockite dike	34.17879	117.62931	Zircon	WM	174.8	1.7	3.5	7	10	LA-SF-ICPMS	CSUN	Igneous

Note: Primary standard for zircon and titanite is 91500 and MKED, respectively; pop—population(s); cal.–calculation; WM–weighted mean age; LI–lower intercept age; MSWD—mean square of weighted deviates; SHRIMP-RG—sensitive high-resolution ion microprobe–reverse geometry; LA-SF-ICPMS—laser ablation–sector field–inductively coupled plasma mass spectrometry; UCSB—University of California at Santa Barbara; CSUN—California State University, Northridge; USGS–U.S. Geological Survey.

*Zircons used in age calculations.

†Data from Schwartz et al. (2023).

A significant portion of detrital grains have Triassic to Early Jurassic ages, which is suggestive of an early Mesozoic MDA (Fig. 7A). To calculate the MDA for these rocks, we pool all samples and treat them as a single unit due to the low number of non-discordant and non-metamorphic zircons in our dataset. This approach will obscure temporal variations within the Cucamonga sequence. However, the approach is justified based on the high degree of metamorphism, folding, and presence of small-scale thrust faults that disrupts the original stratigraphy of the unit. We use two conservative calculations for computing the MDA for these rocks because of the likelihood of potential Pb-loss in the zircons (youngest grain cluster [YGC] 1σ and YGC 2σ; Dickinson and Gehrels, 2009). Using the weighted average of the youngest two or more dates that overlap within the 1σ level (YGC 1σ), we calculate an MDA of 191.6 ± 6.3 Ma (n = 4; not shown). Alternatively, the youngest grain cluster of 3 or more dates that overlap at the 2σ level (YGC 2σ) yields a weighted average age of 195.3 ± 5.4 Ma (n = 4; Fig. 6C). While we prefer the latter because it is a more conservative interpretation for these high-grade rocks, we note that both MDA calculations indicate that at least some portions of the Cucamonga sequence were deposited in the Early Jurassic.

Orthogneisses in the Cucamonga Terrane

Sample 32 is a boudinaged charnockite dike that intruded high-grade migmatitic paragneisses in Cucamonga Canyon. Ten magmatic cores yielded an average age of 174.8 ± 1.7 Ma, which we interpret as the protolith crystallization age of the rock (Figs. 4D and 8A). This sample also places a lower limit on the depositional age of the Cucamonga paragneisses described above. Three luminescent metamorphic rims yielded an average age of 84.3 ± 2.6 Ma.

Sample 37 is a metamorphosed charnockite dikelette that intruded the boundary between the Cucamonga granulites and the San Antonio tonalites in Cucamonga Canyon synchronously with the D_3 transpressional deformation that accompanied the intrusion of the tonalites. Five luminescent interior domains yielded an average age of 88.6 ± 1.7 Ma with an average temperature condition of 775 °C (Fig. 8B). Three thick luminescent metamorphic rims gave an average age of 78.2 ± 2.4 Ma and an average temperature of 742 °C.

Sample 49a is a mylonitic biotite tonalite similar in composition to the Tonalite of San Sevaine Lookout in the San Antonio terrane (Figs. 3G and 8C). Fourteen interior analyses yielded an average age of 84.6 ± 0.9 Ma with an average temperature condition of 743 °C. We interpret this age as the protolith age of the rock. Fourteen metamorphic luminescent rim analyses yielded an average age of 76.6 ± 0.9 Ma with average temperature conditions of 713 °C. Sample 49a contained three xenocrystic cores that yielded an average age of 255.9 ± 6.8 Ma. Sample 49b is a garnet-bearing mafic gneiss from the same location (Figs. 3G and 8D). Five core analyses yielded an average age of 97.9 ± 1.7 Ma, while four metamorphic luminescent rims yielded an average age of 75.5 ± 1.7 Ma with an average temperature of 800 °C.

Sample 50a is a garnet-bearing metatonalite in Cucamonga Canyon (Fig. 3H). Seven dark interior dates yielded an average age of 118.7 ± 2.1 Ma, which we interpret as the protolith age of the rock (Fig. 8E). Five metamorphic luminescent rim analyses yielded an average age of 76.2 ± 1.4 Ma with average temperature conditions of 788 °C. Sample 50b is a folded biotite gneiss in the same location. Ten dark interior analyses yielded an average age of 121.1 ± 1.4 Ma, which we interpret as the protolith age of the rock (Fig. 8F). Six analyses from the metamorphic luminescent rims yielded an average age of 77.1 ± 1.9 Ma and an average temperature of 782 °C. Sample 50c is a deformed quartzofeldspathic gneiss. One hundred zircon interior analyses gave dates ranging from 121.9 Ma to 83.0 Ma. The oldest population of nine spots yielded an average age of 115.5 ± 3.5 Ma, which we interpret as the most likely protolith age of the rock (Fig. 8G). Six young spots gave an average age of 88.0 ± 2.4 Ma, which we interpret as the timing of metamorphism.

Sample 52 is a lineated granitic orthogneiss from Cucamonga Canyon. Four core ages yielded an average age of 140.4 ± 1.8 Ma with an average temperature of 757 °C (Fig. 8H). Five spots gave an average age of 90.6 ± 1.1 Ma and an average temperature of 765 °C, which likely records the timing and conditions of metamorphism.

Samples 25A–25D were collected near the base of Deer Canyon and represent a suite of high-grade orthogneisses, migmatites, and charnockite. Sample 25A is a garnet-bearing mafic orthogneiss (Figs. 3E and 8I). It contains an older protolith population with an average age of 120.4 ± 2.8 Ma and a younger, higher Dy/Yb (>0.2) and low U (<100 ppm) metamorphic population at 89.3 ± 0.5 Ma. The Ti-in-zircon temperature of the younger, high Dy/Yb population is 776 °C. Sample 25B is a higher-grade, garnet-bearing orthogneiss. It also contains a range of dates and two Dy/Yb populations (Fig. 8J). The older protolith population of low Dy/Yb grains shows a scattering of ages, the oldest of which gives dates at 122–120 Ma. The high Dy/Yb metamorphic population typically has values >0.5 and consists of 23 grains that give an average age of 87.6 ± 0.3 Ma and a Ti-in-zircon temperature of 767 °C. Sample 25C is a garnet-bearing metatexite (Figs. 3F and 8K) with two populations. The older population has low average Dy/Yb values (typically <1.0) and higher average Y values (typically <100 ppm). This population contains a range of dates from 129 Ma to 91 Ma with no statistically meaningful age population. The younger population is defined by low U, light gray rims, and light gray interiors domains. These domains typically have higher average Dy/Yb values (>1.0) and lower Y (<100 ppm). These zircons yielded an average age of 87.4 ± 0.4 Ma and a temperature of 747 °C, which we interpret to be the timing and conditions of metamorphism in this sample. Finally, a late-stage, foliated charnockite (25D) yielded zircon spots ranging in age from 95.2 Ma to 81.5 Ma. The zircon ages define a population with an average age of 93.5 ± 0.2 Ma and a temperature of 749 °C (Fig. 8L), which we interpret to be the timing and conditions of magmatism. Younger zircons in this sample are likely affected by Late Cretaceous Pb loss and/or recrystallization with the youngest two grains yielding dates of 82.3–81.5 Ma, respectively. While these dates are somewhat younger than the metamorphic dates at this sample location, they overlap with other metamorphic dates nearby (e.g., see site 62 in the following paragraph).

We sampled two dioritic to tonalitic orthogneisses in Deer Canyon interlayered within a deformed paragneiss sequence close to the contact with the San Antonio terrane (62A-B). The orthogneisses display strong migmatitic/garnet-granulite facies metamorphic overprints with local development of garnet-bearing leucosomes (Figs. 3I and 3J). Sample 62A is a garnet-bearing orthogneiss from this sequence. The oldest population in this rock contains slow Dy/Yb zircons and yielded an average age for the protolith population of 86.8 ± 0.2 Ma (Fig. 8M). The younger population consists of higher Dy/Yb and low U metamorphic rims, which gave an average age of 81.1 ± 0.4 Ma and a temperature of 734 °C. Sample 62B was collected from the same location and is also a garnet-bearing orthogneiss. It also contains two Dy/Yb populations. The older, low Dy/Yb population gave an average age of 86.8 ± 0.2 Ma, while the younger, high Dy/Yb, metamorphic population gave an average age of 82.2 ± 0.3 Ma (Fig. 8N). The temperature of this population is 741 °C.

Sample 13C is a metatonalite sill that was collected north of site 62, also in the transition zone between the Cucamonga granulite and the San Antonio terrane tonalites/granodiorites. It has

an S_3 foliation that is concordant with the foliation in host metasedimentary rocks (Fig. 3B). Zircons in this sample do not have metamorphic rims, and they give a dominant Late Cretaceous age population with some scattered xenocrystic, Permo-Triassic and Early Proterozoic core ages. The average age of the Late Cretaceous group is 77.2 ± 0.3 Ma with a Ti-in-zircon temperature of 723 °C (Fig. 8O). We consider this to be the crystallization age.

Tonalites and Granodiorites in the San Antonio Terrane

Sample 44A is a weakly foliated, coarse-grained biotite-hornblende tonalite from the Tonalite of San Sevaine Lookout immediately north of the Cucamonga terrane in Cucamonga Canyon (Fig. 3K). Eleven xenocrystic cores from this sample yielded an average age of 96.4 ± 1.1 Ma (Fig. 8P). Thirteen magmatic rims yielded an average age of 88.0 ± 0.9 Ma with an average temperature of 790 °C (Fig. 4B).

Sample 47A is a coarse-grained biotite-hornblende tonalite also from the Tonalite of San Sevaine Lookout within the Black Belt shear zone in Cucamonga Canyon. Locally, the sample displays alternating cataclastic and mylonitic fabrics (Fig. 3L). Seven luminescent interiors yield an average age of 87.6 ± 1.5 Ma and two luminescent metamorphic rims yielded an average age of 78.7 ± 2.5 Ma (Figs. 4C and 8Q).

Samples 4A–4D were collected at the northernmost end of the Black Belt shear zone in the Tonalite of San Sevaine Lookout. These rocks record various phases of metamorphism within the unit. We sampled a gneissic host (sample 4A), a garnet-bearing gneissic host (sample 4B), a diatexite migmatite (sample 4C), and post-kinematic granodiorite (sample 4D). Sample 4A represents a hornblende-bearing tonalite gneiss. We analyzed 87 zircons in this sample and dates range from 86.5 Ma to 76.2 Ma (Fig. 8R). The weighted average age of the majority of zircons is 82.4 ± 0.1 Ma (MWSD = 2.0) with an average temperature of 727 °C. Several zircons younger than 80 Ma were excluded in this calculation and likely represent Pb-loss or metamorphic growth at 80–76 Ma as documented in samples 4B and 4C. Sample 4B is a garnet-bearing gneissic tonalite from the same outcrop. It contains two populations defined by a chemically distinct, older population defined by oscillatory zoned grains with low average Dy/Yb values (<0.3) and a weighted average age of 82.7 ± 0.2 Ma. The younger population is primarily defined by low U, metamorphic rims that display an uptick in Dy/Yb (>0.3) at 75.2 ± 0.3 Ma (Fig. 8S). We note that there is overlap in Dy/Yb between these two groups, which likely reflects a combination of new metamorphic growth producing high Dy/Yb domains and intracrystalline Pb diffusion within older, low Dy/Yb domains. Therefore, we interpret the 82.7 Ma populations as reflecting the timing of igneous intrusion and the 75.2 Ma populations as the timing of metamorphism and garnet growth. The temperatures of the older and younger populations are 737 °C and 723 °C, respectively. Sample 4C is a diatexitic migmatite layer from the same outcrop. Cathodoluminescence imaging shows that zircons in this sample contain dark cores that are truncated by light gray, oscillatory zone interiors and rims. The weighted average age of the rim and interior population is 74.8 ± 0.2 Ma and the average temperature is 758 °C (Fig. 8T). We interpret this to record the timing of migmatization in the rock. The dark gray cores give a weighted average age of 82.2 ± 0.3 Ma, which statistically overlaps with the weighted average age of the two host samples (samples 4A and 4B). We interpret these to be xenocrysts derived from the gneissic host. Finally, we dated a post-deformational, granodiorite (sample 4D), which cuts all other rocks. Zircons from this sample range from 1809 Ma to 74 Ma (Fig. 8U). The weighted average age of the youngest population is 75.2 ± 0.4 Ma and the average temperature is 742 °C. We interpret these features to record the timing of magmatic emplacement. The older analyses represent dark core domains, and they are interpreted as xenocrysts. We note that magmatic emplacement of the granodiorite occurred simultaneously with migmatization as documented in the diatexite, sample 4C.

In Deer Canyon, we collected a tonalite from the unit mapped by Alf (1948) as the Deer Diorite (sample 7C). This sample is located north of the Cucamonga terrane and within the Black Belt shear zone. It is a relatively undeformed example of the Deer Diorite, and based on similarities with nearby tonalites, we interpret it as a minor subunit of the Tonalite of San Sevaine Lookout. Locally, these rocks are cut by alternating cataclasite, mylonite and pseudotachylyte similar to fabrics observed in the Black Belt shear zone in Cucamonga Canyon. Some zircons in this sample contain bright luminescent rims likely of metamorphic origin. Rims typically have low U concentrations (23–58 ppm) whereas interiors and core domains have moderate U concentrations (40–647 ppm). The cores and interior domains with higher U concentrations yielded an average age of 82.7 ± 0.2 Ma, which we interpret as the protolith age of the rock (Fig. 8V). The younger population gave an age of 78.8 ± 0.9 Ma, which we interpret as reflecting the timing of metamorphism.

DISCUSSION

The Origin of the Cucamonga Paragneisses: A Mesozoic Forearc Basin

The high-grade metasedimentary rocks of the Cucamonga terrane are an enigma in Southern California. Their high-grade metamorphic overprint is unlike other metasedimentary rocks in the area except for the Morongo migmatites (Paterson et al., 2017) and the high-grade paragneisses in the Sur Series in central California (Barth et al., 2003; Kidder et al., 2003; Barbeau et al., 2005). In addition, they are compositionally characterized by lesser volumes of quartzite compared to nearby metasedimentary rocks in the San Antonio terrane and in the San Bernardino Mountains, both of which are interpreted to be passive sedimentary sequences (Brown, 1991; Stewart, 2005; Barth et al., 2009; Wooden et al., 2013; Nourse and Thompson, 2022). A complicating factor in interpreting the Cucamonga metasedimentary rocks is that their depositional age is unknown, which precludes understanding their depositional setting and their possible correlations with other sedimentary sequences.

Our detrital zircon petrochronology data bear on this problem. Our MDA calculations from the four integrated samples indicate the Cucamonga sequence was deposited in the Early Jurassic at ca. 195–191 Ma and prior to the intrusion of the oldest charnockite dike at 175 Ma (sample 32; Fig. 8A). Analysis of inherited zircons in Cucamonga orthogneisses that intruded the paragneisses also provides support for an early Mesozoic MDA. We compiled all xenocrystic zircons from this study and those reported in Schwartz et al. (2023) and found that a sizable portion of grains (n = 27) range from 273 Ma to 190 Ma. The youngest population of seven grains from this population gives a weighted average age of 222.8 ± 2.6 Ma (MWSD = 1.4; Fig. 6D). Two grains not included in this calculation have younger ages at 190 Ma and 206 Ma, respectively, the youngest of which overlaps the MDA calculated from the Cucamonga metasedimentary rocks. While there are assumptions associated with interpreting inherited grains as an MDA, we note that both the detrital and inherited plutonic datasets give similar results and are both consistent with the deposition of zircon-bearing siliciclastic rocks in a Late Triassic to Early Jurassic basin.

Detrital zircon cores also provide information about potential sources of detritus during deposition. Zircon cores have ages in the Phanerozoic (ca. 465–188 Ma), Mesoproterozoic (1.5–0.8 Ga) and late Paleoproterozoic (1.7–1.6 Ga), and peak modes that occur at ca. 246 Ma, 1002 Ma,

1373 Ma, and 1666 Ma (Fig. 7A). While some Archean grains are present in our dataset, they are few and are strongly discordant. Consequently, they are not shown in Figure 7. In general, all samples contain abundant Mesoproterozoic to Neoproterozoic sources (Figs. 7A and 7B), whereas other populations are more variable between samples, which likely reflects the low number of non-metamorphic zircons analyzed in the samples.

Sources for the observed age populations in our dataset can be found in nearby basement rocks of the Southern California Batholith, the Mojave province, and sandstones in the southwestern United States. For example, Permo-Triassic plutons ranging from 298 Ma to 211 Ma are recognized in the eastern San Gabriel Mountains, throughout the Southern California Batholith, and in the northern Mojave Desert and northern Sonora Mexico (Barth and Wooden, 2006; Riggs et al., 2013; Cecil et al., 2019; Nourse and Thompson, 2022; Schwartz et al., 2023). These rocks record the establishment of a Permo-Triassic arc along the truncated western coast of Laurentia. Older Paleozoic zircons were likely sourced from accreted terranes along the western US Cordillera and in associated outboard terranes (Dickinson, 2000; Dickinson and Lawton, 2001; DeCelles, 2004).

Mesoproterozoic zircons in the Cucamonga terrane were potentially sourced from local plutons in the San Gabriel Mountains, which have ages ranging from 1.21 Ga to 1.11 Ga (anorthosite-mangerite-charnockite-granite suite), 1.43–1.40 Ga (syenites and granites), and 1.94–1.63 Ga (basement gneisses; Barth et al., 2001; Wooden et al., 2013; Nourse et al., 2020; Schwartz et al., 2023). Zircons of this age are also common in sandstones and quartzites from southern North America and eolian quartzarenites from the Colorado Plateau (Gehrels, 2000; Dickinson and Gehrels, 2009). Thus, the majority of Phanerozoic to Mesoproterozoic zircons in the Cucamonga siliciclastic rocks were likely sourced from a combination of proximal plutons in the Southern California Batholith and from recycling of older Proterozoic to Paleozoic strata present across the southwestern United States and northern Mexican Cordillera.

In contrast to the proximal sources described above, the source(s) of the minor Early Jurassic zircon population in our dataset are more enigmatic, as they are not well represented in the Southern California or the Mojave province. In the adjacent Sierra Nevada Batholith, preserved Early Jurassic igneous rocks are restricted to minor volcanic layers in the Mount Morrison and Mineral King pendants as well as intrusive and volcanic rocks in the central belt of the Western Metamorphic Belt (Saleeby, 1982, 2011; Edelman and Sharp, 1989; Bateman, 1992; Klemetti et al., 2014; Barth et al., 2018). Despite the lack of exposed sources, Early Jurassic zircons are abundant in Jurassic age intra-arc strata in the Sierra Nevada (Attia et al., 2021) and in the Mojave Desert (Barth et al., 2004; Stone et al., 2013; Riggs et al., 2013). These sediments were deposited during an Early Jurassic magmatic lull in the Sierra Nevada Batholith, which coincided with the establishment of shallow- and deep-marine basins across the northern and southern Sierran Nevada (Behrman and Parkison, 1978; Saleeby and Busby, 1993; Attia et al., 2018, 2020, 2021). The Early Jurassic is proposed to be a time of significant regional extension across the southwestern Cordilleran margin (Busby-Spera, 1988; Saleeby and Busby, 1993; Saleeby and Dunne, 2015), which may have resulted in the development of extensional sedimentary basins in the Cucamonga sector of the Southern California Batholith.

Common Sedimentary Basins for Cucamonga and Salinia Metasedimentary Rocks

The Sur Series located in the Salinia block bears strong similarities to the Cucamonga metasedimentary rocks and was once part of the northern Southern California Batholith prior to northward translation along sinistral and dextral strike-slip faults in the Late Cretaceous and Tertiary, respectively (see reconstruction in Fig. 9; Singleton and Cloos, 2013; Chapman et al., 2016; Johnston et al., 2018, 2019). The Sur Series consists of heterolithic gneisses, schists, marbles, and quartzites, which were metamorphosed at upper amphibolite- to granulite-facies conditions ca. 81–76 Ma (Kidder et al., 2003). Based on detrital zircon analysis, Barbeau et al. (2005) proposed a late Paleozoic (360–280 Ma) MDA for the Sur Series, although they note that the presence of early Mesozoic peaks might indicate an early Mesozoic depositional age. They proposed that Sur Series rocks were

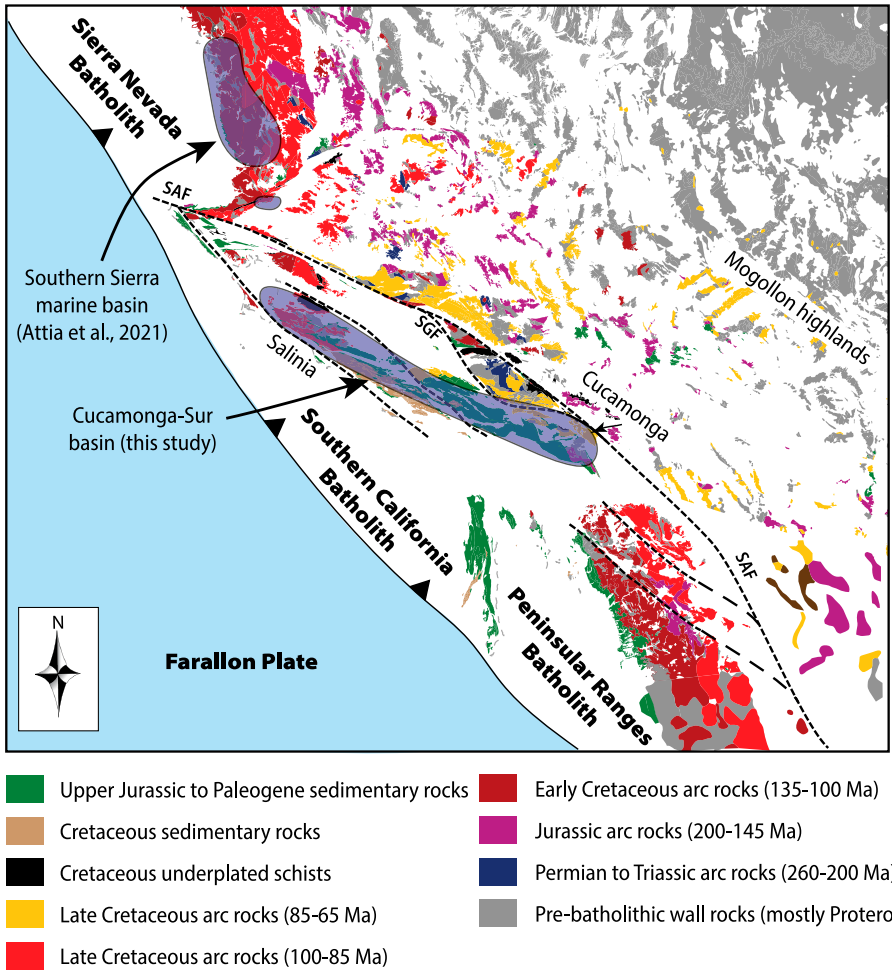

Figure 9. Tectonic reconstruction of the Cordilleran arc in Southern California in the early Mesozoic (Triassic to Early Jurassic after Sharman et al., 2015). The Cucamonga-Sur basin is proposed to have been the Mesozoic forearc to the Southern California Batholith (SCB). SAF—San Andreas fault; SGF—San Gabriel fault.

sourced from proximal rocks in the Mojave Desert region (El Paso Mountains) and recycling of passive margin sediments during Phanerozoic orogenic events.

To test possible linkages between the Sur Series and Cucamonga metasedimentary rocks, we plotted cumulative distributions and modes of non-metamorphic detrital zircon ages in four samples from the Sur Series (n = 280) and three samples from the Cucamonga terrane (n = 93; Figs. 7A and 7B). The plots show that both sequences are dominated by Paleozoic, Mesoproterozoic, and late Paleoproterozoic age populations. The Sur Series differs in that it also contains Archean and Neoproterozoic populations that are absent in the Cucamonga samples (Fig. 7B). Barbeau et al. (2005) interpreted these age populations to reflect contributions from recycled passive margin rocks for the Neoproterozoic samples and erosion of Archean rocks from the Mojave province. Given the low number of zircons in our study, it is unclear if the differences between our datasets reflect different sources, variations in sediment dispersal, and/or sampling artifacts due to low numbers of non-metamorphic zircons. Both the Cucamonga and Sur Series rocks also bear strong similarities to detrital zircons from intra-arc sediments in the Sierra Nevada Batholith and Triassic to Jurassic conglomerates in the Nacimiento forearc (Figs. 7A and 7C; Johnston et al., 2018; Attia et al., 2021).

We use multidimensional scaling (MDS) to further assess the similarity and/or dissimilarity between Cucamonga and Sur Series metasedimentary samples. In MDS space, samples are plotted as distance in Cartesian coordinates based on the maximum separation between cumulative distribution functions (Kolgomorov–Smirnov D_{max}) following methods in Vermeesch (2013) and Saylor and Sundell (2016). Samples that have similar age distributions plot closer together, whereas those that are more dissimilar plot farther apart. For the Cucamonga and Sur Series rocks, the seven samples from both terranes plot closely together, and in some cases, they overlap in MDS space (Fig. 7C). Both the Cucamonga and Sur Series rocks also plot close to intra-arc sediments in the Sierra Nevada Batholith. Given these similarities, we propose that the Sur Series and Cucamonga metasedimentary rocks were formerly adjacent parts of a late Paleozoic to early Mesozoic, intra-arc basin or forearc basin that extended along the western North American margin from the northern Sierra Nevada to Southern California (Fig. 9). This basin was subsequently buried during Jurassic to Early Cretaceous D_1/D_2 thrusting and metamorphosed at least twice during the Early and Late Cretaceous, respectively (see next section).

Early Mesozoic Arc Magmatism and Metamorphism

Our zircon dates and trace-element data from the Cucamonga terrane allow us to establish the timing of igneous and metamorphic activity in the lower crust of the Southern California Batholith. Existing studies have shown that Mesozoic magmatism in the Southern California Batholith was expressed as three flare-ups of increased magma addition rates at ca. 260–210 Ma, 160–140 Ma, and 90–70 Ma, which were separated by magmatic lulls (Schwartz et al., 2023). In the Cucamonga terrane, the initiation of magmatism in the lower crust occurred at 175 Ma and is represented by the intrusion of charnockitic dikes into the paragneiss sequence. Emplacement of these dikes occurred during the beginning of the second Mesozoic flare-up event in the Jurassic and signals the termination of sedimentation in the Cucamonga basin.

Similar age Jurassic plutonic rocks are widely exposed in the eastern Mojave Desert and Transverse Ranges of the Southern California Batholith and record a pulse of magmatism lasting ~35–40 m.y. in duration from ca. 180–140 Ma (e.g., Fox and Miller, 1990; Barth et al., 2017). In the eastern Mojave, this phase of magmatism is associated with explosive silicic volcanism and the emplacement of shallow plutons at 181–175 Ma (Barth et al., 2017). The presence of abundant caldera structures associated with eolian quartz-rich sand from the continental interior suggest that the Jurassic arc was a low-elevation feature, which may have persisted until early Middle Jurassic time (Busby-Spera, 1988; Barth et al., 2017). The low-standing arc was associated with a phase of regional extension; however, by the Middle to Late Jurassic, contractional structures were active in the region (Dunne and Walker, 2004).

In the Cucamonga terrane, magmatism renewed at ca. 140 Ma and from 120 Ma to 98 Ma. Zircons in plutons in this interval have moderate U/Yb values (0.5–10), and low Th/U and Dy/Yb values (Figs. 10A–10C). The latter values indicate that zircons in Early Cretaceous plutons did not crystallize with igneous or metamorphic garnet, and we see no evidence that they were yet buried to lower-crustal depths. While Late Jurassic to Early Cretaceous plutons are widely recognized in the Southern California Batholith, the middle Cretaceous pulse represents a previously unrecognized phase of magmatism in the Southern California Batholith. Although Early Cretaceous rocks are common in the Sierra Nevada and Peninsular Ranges Batholiths (e.g., Saleeby and Sharp, 1980; Stern et al., 1981; Lackey et al., 2012; Premo et al., 2014; Paterson and Ducea, 2015), they are scarce in this sector of the Mesozoic California arc system. This observation was noted by Jacobson et al. (2011), who proposed that their absence in Southern California may have been caused by Late Cretaceous to Early Cenozoic truncation of the arc by sinistral strike-slip movement along the Nacimiento fault. In their model, Early Cretaceous rocks that once were part of the Southern California Batholith were displaced northward and are now located in the displaced Salinia block. The small remnants of Early Cretaceous arc rocks in the Cucamonga terrane may represent a sliver of the truncated arc, which correlates with similar lithologies in the Salinia block.

Early Cretaceous arc magmatism in the Cucamonga terrane is also associated with a cryptic M_1 migmatization event at ca. 124 Ma (sample 28b), which resulted in development of stromatic migmatites throughout the paragneiss sequence. The Early Cretaceous migmatites are considered cryptic because they are overprinted by a second generation of Late Cretaceous, high-grade metamorphism and partial melting (M_2 event; see next section) at granulite-facies conditions. The Early Cretaceous migmatites are also strongly deformed by Late Cretaceous D_3, sinistral transpressional deformation, which makes it difficult to distinguish them from M_2 migmatites in the field. Because of these factors, the extent of M_1 melting and the pressure conditions for the event are currently unclear. Nonetheless, our data indicate that the paragneiss sequence reached high-grade thermal conditions (>650 °C) in the Early Cretaceous during a period of regional contraction, arc magmatism, and underthrusting of the Cucamonga basin into the middle crust. Plutons emplaced during this interval record Ti-in-zircon temperatures ranging from ~700 °C to 850 °C, which may have provided heat to partially melt the Cucamonga paragneisses during their emplacement (Fig. 10D).

Late Cretaceous Flare-Up Magmatism and Metamorphism

Late Cretaceous magmatism and metamorphism occurred in both the Cucamonga and San Antonio terranes during a period of widespread arc magmatism throughout the Southern California Batholith (Schwartz et al., 2023). Figure 11 shows a compilation of metamorphic and igneous dates from this study and Schwartz et al. (2023) for the lower and middle crust. The data show that in the lower crust, Late Cretaceous meta-igneous rocks were emplaced over ~16 m.y. from 93 Ma to 77 Ma. They consist of strongly deformed and metamorphosed tonalites, granodiorites, charnockites and late-stage dikes/veins that are volumetrically minor compared to Early Cretaceous orthogneisses and the

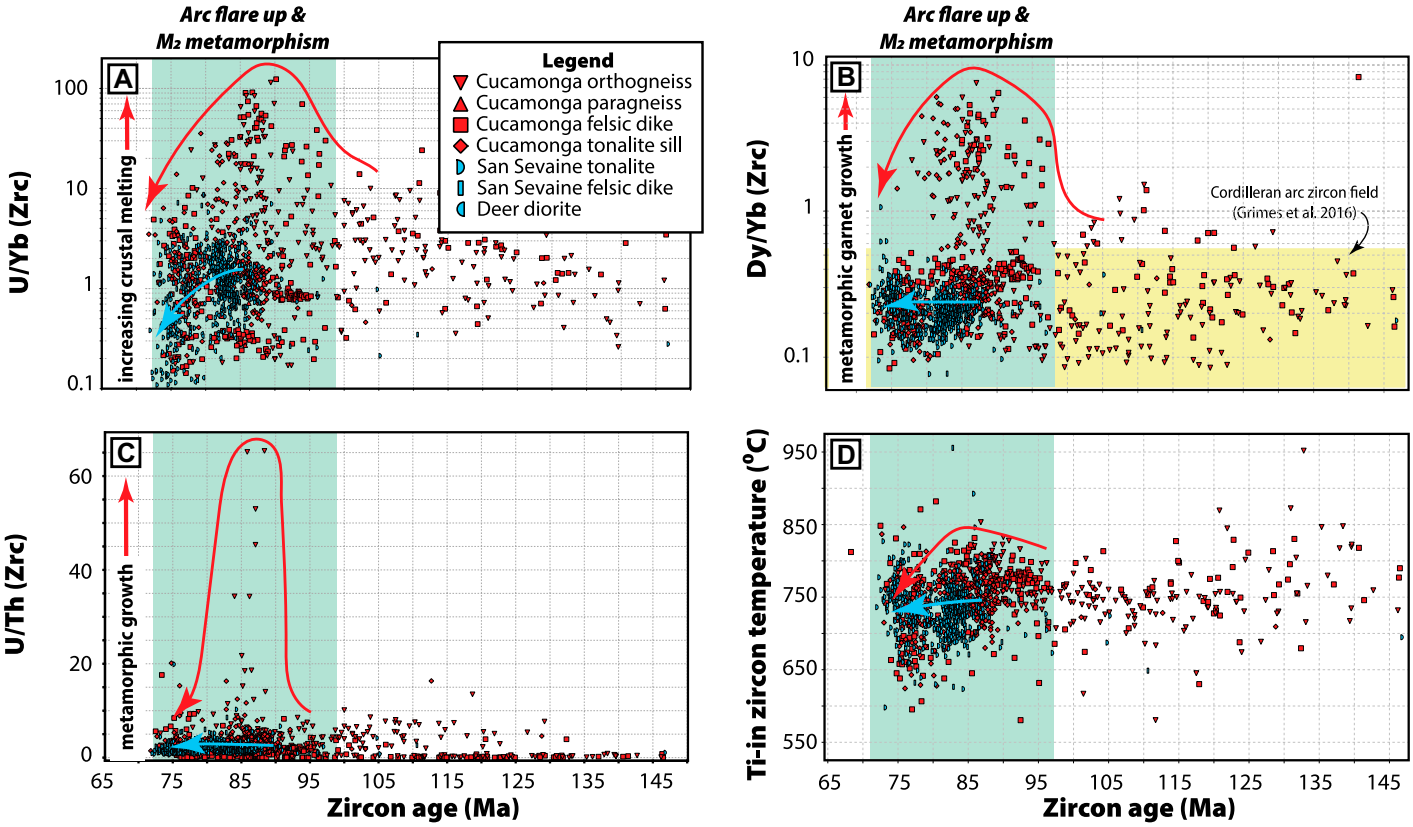

Figure 10. Zircon trace-element plots for igneous and meta-igneous zircons in the Cucamonga and San Antonio terranes. (A) U/Yb versus zircon age. (B) Dy/Yb versus zircon age. (C) U/Th versus zircon age. (D) Ti-in-zircon temperature versus zircon age. Red trend line is for the Cucamonga terrane, and blue trend line is for the San Antonio terrane. Results show that Late Cretaceous partial melting and granulite-facies metamorphism in the lower crust of the Cucamonga terrane generated high U/Yb and Dy/Yb melts (red symbols) primarily at 90–80 Ma. Zircons from the mid-crustal San Antonio terrane do not show the influence of these garnet-granulite melts implying that they were not directly sourced from partial melting of the Cucamonga terrane granulites. Instead, they most likely reflect mantle melting during the Late Cretaceous arc flare-up event in the Southern California Batholith.

host metasedimentary sequence. In contrast, the structurally overlying Tonalite of San Sevaine Lookout occupies 90 km^2 and was emplaced during the same interval from 89 Ma to 74 Ma. The emplacement of the large tonalite body (the Tonalite of San Sevaine Lookout) into the base of the middle crust introduced significant mass and heat to the arc and functioned to load the lower crust and heat it from above.

The emplacement of arc plutons into the lower and middle crust occurred simultaneously with M_2 metamorphism. In the Cucamonga terrane, granulite-facies metamorphism is recorded in metamorphic zircons from 91 Ma to 72 Ma, and at the base of the middle crust, it is expressed in migmatitic and mylonitic gneisses that give metamorphic ages of 83–74 Ma (Schwartz et al., 2023; this study). During this interval, the metasedimentary sequence experienced widespread partial melting at 7–9 kbar and temperatures of 730–800 °C based on Ti-in-zircon thermometry in this study. These temperatures agree with existing garnet-quartz oxygen isotope thermometry (777–835 °C; Schwartz et al., 2023) and garnet + orthopyroxene + plagioclase + quartz thermometry (700–800 °C; Barth et al., 1992). At the base of the middle crust and near the Black Belt shear zone, gneissic tonalites were migmatized at 723–758 °C. Although the cause of the high-temperature heating event in the lower and middle crust is not well understood, we speculate that magma emplacement and loading was a likely cause and explains the distribution of migmatites and granulites near the intrusive contact with the Tonalite of San Sevaine Lookout. We explore this possibility below in terms of triggering mechanisms for the Late Cretaceous arc flare-up event.

Triggering the Late Cretaceous Arc Flare-Up in the Southern California Batholith

Studies of long-lived continental arcs have shown that episodic magmatic surges of 10–30 m.y. duration are a common feature in Cordilleran arcs (Ducea and Barton, 2007; DeCelles et al., 2009; Kirsch et al., 2016; Ratschbacher et al., 2018; Chapman et al., 2021b; Ringwood et al., 2021). These episodic and relatively short-lived, high magma addition rate (MAR) events are significant because they contribute to the overall budget of new crust added to the Cordilleran batholiths, and they can lead to widespread thermal and mass transfer from the mantle to the crust, vertical uplift and exhumation, and erosion at the surface (e.g., Armstrong, 1988; Kimbrough et al., 2001; Ducea, 2002; Ducea and Barton, 2007; DeCelles et al., 2009; de Silva et al., 2015; DeCelles and Graham, 2015). A key problem in understanding high-MAR events in Cordilleran arcs is that there is no consensus about the cause of these events, including whether they represent partial melting of fertile continental crust underthrust beneath the arc (Ducea, 2001; DeCelles et al., 2009), elevated geothermal gradients resulting from increasing mantle melt influx to the base of the crust (de Silva et al., 2015; Schwartz et al.,

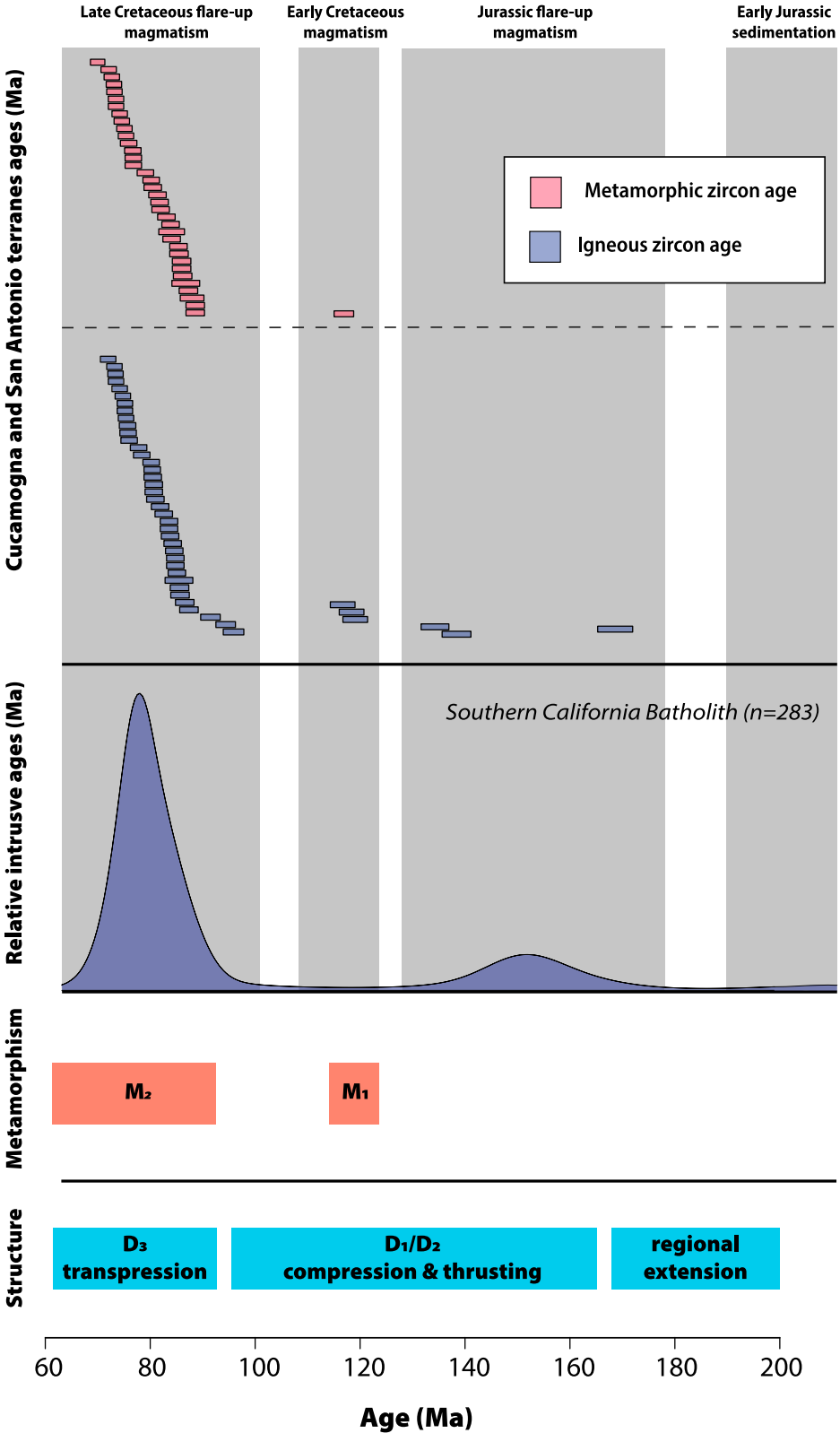

Figure 11. Summary plot of all zircon age determinations for igneous and meta-igneous rocks in the Cucamonga and San Antonio terranes. Relative intrusive flux curve for the Southern California Batholith is after Schwartz et al. (2023). Structural observations for the Southern California Batholith (including the Mojave region) after Barth et al. (2017) and Klepeis et al. (2023).

2017; Decker et al., 2017; Ardill et al., 2018; Cecil et al., 2018; Ringwood et al., 2021), and/or migration of the arc into melt-fertile, metasomatized, subcontinental lithosphere (Chapman and Ducea, 2019).

In the case of the Late Cretaceous high-MAR events in California, prior studies in adjacent sectors of the arc have documented magmatic surges in the central and southern Sierra Nevada Batholith at 110–87 Ma and in the northern Peninsular Ranges Batholith at 99–91 Ma (Ducea, 2001; Ducea and Barton, 2007; Grove et al., 2008; Paterson et al., 2011; Paterson and Ducea, 2015; Chapman and Ducea, 2019). In both adjacent sectors, there is strong disagreement about the cause of the Cretaceous flare-up events. For example, Grove et al. (2008) and Chapman et al. (2013) suggested that the Late Cretaceous high-MAR events resulted from shallowing of the Farallon plate and widespread devolatilization of schistose rocks. In contrast, Martínez-Ardila et al. (2019) postulated that the high-MAR event in the western Peninsular Ranges Batholith was driven by mantle-melting processes. Klein and Jagoutz (2021) and Klein et al. (2021) arrived at a similar conclusion based on analysis of the root of the southern Sierra Nevada Batholith. In the central Sierra Nevada Batholith, Attia et al. (2020) examined zircon trace elements and isotope compositions in metavolcanic rocks and concluded that the temporal record of arc flare-ups also represents periods of increased mantle magma input generating significant volumes of new continental crust. Finally, Chapman and Ducea (2019) argued that continentward arc migration into metasomatized, subcontinental lithospheric melt source regions could have sparked the high-flux event in the Sierra Nevada Batholith.

The unique lower-crustal exposures in the Cucamonga terrane bear on this controversy and allow us to investigate the tectonic and petrologic processes associated with the Late Cretaceous high-MAR event in the root of the Southern California Batholith. A key finding in this study is that the emplacement of voluminous intermediate magmas into the base of the middle crust was temporally and spatially associated with widespread partial melting of the Cucamonga paragneiss sequence. Biotite-rich paragneisses commonly display significant development of in situ partial-melting textures manifested by the development of layer-parallel, stromatic migmatites and diffuse leucosomes that coalesce into diatexites (Figs. 3A–3H). The close temporal association of anatexis in the lower crust and voluminous emplacement of intermediate magmas without any discernable lag time strongly suggests that advection of magmas triggered partial melting of the metasedimentary sequence

beginning at ca. 90 Ma. An outstanding question is what role partial melting of this sequence had on triggering the arc flare-up and its duration.

Zircon trace-element data provide insights to this question and show a pronounced increase in Dy/Yb values in the lower-crustal orthogneisses in the Cucamonga terrane starting at ca. 90 Ma. The increase in Dy/Yb also correlates with increasing U/Yb values and a subtle increase in Ti-in-zircon temperatures in lower-crustal orthogneisses reflecting the increasing anatexis of the Cucamonga metasedimentary rocks in the production of lower-crust melts (Figs. 10A–10D). We interpret these increases to record the generation of lower-crustal melts in equilibrium with metamorphic or peritectic garnet at 750–850 °C. Zircon trace-element data also show that crustal anatexis and granulite-facies metamorphism primarily peaked at 90–80 Ma, during emplacement of the Tonalite of San Sevaine Lookout, whereas from 80 Ma to 70 Ma, there is marked decrease in zircon growth in equilibrium with garnet (e.g., Fig. 10B). This pattern likely reflects heating of the lower crust from 90 Ma to 80 Ma due to advection of heat from the overlying mid-crustal tonalites, followed by cooling and lower temperature metamorphism at upper amphibolite-facies conditions from 80 Ma to 70 Ma (Figs. 10A–10C).

In contrast to the lower crustal rocks, middle crustal tonalites and granodiorites do not show the same magnitude of increase in U/Yb or Dy/Yb (Figs. 10A and 10B). Instead, they display modest U/Yb values and have Dy/Yb values that plot within the Cordilleran arc field as defined by Mesozoic and Cenozoic arc zircons in western North America (Grimes et al., 2015). A likely explanation for the difference in zircon chemistry is that the intermediate magmas in the middle crust are dominantly mixtures of mantle-derived melts with a limited component of partial melts derived from the Cucamonga metasedimentary rocks. Although limited in scope, existing bulk-rock radiogenic isotope data from mid-crustal tonalites indicates that they can be modeled as binary mixtures of a mantle-derived source and a limited component of radiogenic aluminous gneisses (e.g., Barth et al., 1992).

The close temporal and spatial association of tonalitic to granodioritic magmatism and partial melting of the Cucamonga granulites implies that lower-crustal anatexis was driven by the advection of heat to the base of the middle crust and possibly below it as well, though deeper parts of the arc are not currently exposed. High-grade metamorphism also lasted 15 m.y. and overlapped entirely with the surge of magmatism in the San Antonio terrane and the greater Southern California Batholith. These results indicate that heating was not likely driven by the relaxation of geothermal gradients due to crustal thickening, but instead, our results point to an external, mantle trigger for the arc flare-up and lower-crustal partial melting event in the Late Cretaceous. Our interpretations are supported by modeling results of the Cretaceous Sierra Nevada Batholith by Yang et al. (2020) who concluded that partial melting of underthrust lower crust plays a partial or subsidiary role in driving magmatic flare-up events. They determined that advection of mantle-derived heat was required to achieve sustained magmatic output during flare-up events. These results agree with our observations, and we conclude that partial melting of the Cucamonga granulites was a response to the Late Cretaceous arc flare-up event and not a trigger for it.

Tectonic Evolution of the Southern California Batholith Root

Our geochronologic results allow us to construct a new model for the magmatic and tectonic development of the lower crust of the Southern California Batholith. Based on detrital zircon analysis in this study and Barbeau et al. (2005), we propose that the high-grade metasedimentary rocks in the Cucamonga terrane and Salina block were once part of a contiguous late Paleozoic to early Mesozoic forearc basin along the margin of the Southern California Batholith (Figs. 9 and 12A). This interpretation for the Cucamonga-Sur basin is based on similarities between the two metasedimentary sequences and the presence of detrital zircon age distributions, which point to proximal detrital sources from the Transverse Ranges and Mojave province along with more distal sources from the southern Sierra Nevada Batholith and the southwestern United States. This basin likely formed adjacent to a low-standing arc during a phase of regional extension documented in the Mojave province (Barth et al., 2017). We note that the substrate upon which the Cucamonga-Sur basin was deposited is not currently exposed, and Proterozoic basement gneisses are notably absent in both deep-crustal arc sections in the Salinia block and the Cucamonga terrane. This observation is consistent with the hypothesis that the Cucamonga-Sur basin was originally located trenchward of its current position relative to the cratonic margin, possibly in a paleo-forearc depositional setting (see hypothesized location in Fig. 9). Our hypothesis also explains the apparent absence of the Triassic to Jurassic forearc in this sector of Southern California.

Sedimentation in the Cucamonga-Sur basin ceased by 175 Ma as indicated by the intrusion of the oldest charnockitic dikes in the Cucamonga terrane (Fig. 12A). By the Middle Jurassic to Early Cretaceous, the Cucamonga-Sur basin was progressively underthrust beneath the Southern California Batholith during a phase of regional contraction (Fig. 12B). This period of intra-arc deformation coincides with east-dipping subduction beneath the Sierra Nevada–Southern California–Peninsular Ranges Batholiths (Dunne et al., 1998; Paterson and Ducea, 2015; Barth et al., 2017; Attia et al., 2020). In the Cucamonga terrane, deformation is recorded by early S_1/S_2 foliations with down-dip lineations that indicate a predominantly thrust sense of shear (Baskin et al., 2023; Klepeis et al., 2023). Restoration of Miocene and younger rotation of the San Gabriel block along the San Andreas fault indicates that Mesozoic thrusting was directed toward the paleo trench. Early Cretaceous M_1 migmatization also occurred during this interval (sample 28b) and is temporally associated with intrusion of bimodal mafic and felsic plutons (Fig. 12B).

The Late Cretaceous surge of magmatism in the lower and middle crust triggered widespread granulite-facies metamorphism and partial melting of the lower crust (Fig. 12C). This event is observed in the Cucamonga region and in the Salinian block where lower-crustal rocks were metamorphosed at upper amphibolite- to granulite-facies conditions (7.5 kbar and 800 °C) at ca. 75 Ma (Kidder et al., 2003). In the Cucamonga region, arc magmatism and metamorphism were synchronous with sinistral-oblique, intra-arc shearing in the Black Belt and Cucamonga shear zones (Alf, 1948; May and Walker, 1989; May, 1989; Baskin et al., 2023; Klepeis et al., 2023). Following the arc flare-up, the Cucamonga block was rapidly exhumed to upper crustal levels by 60 Ma, and both blocks were exhumed to the surface or near it by ca. 70–60 Ma likely due to underthrusting of an oceanic plateau (e.g., Schwartz et al., 2023).

Implications for the Incorporation of Sediments into the Deep Crust of the Southern California Batholith

The incorporation of sediments into the deep crust of continental arcs plays an important role in modifying the architecture, composition, and rheology of continental crust (Rudnick, 1995; Miller and Paterson, 2001; Miller and Snoke, 2009; Hacker et al., 2011; Chin et al., 2014; Hanson et al., 2022). Metasedimentary rocks are found in continental arcs worldwide, including the North Cascades (Gordon et al., 2017; Sauer et al., 2017a, 2017b, 2018, 2019), the Central Gneiss Complex, the Coast Mountains batholith (Pearson et al., 2017), the Sierra Nevada Batholith (Grove et al., 2003; Chin et al., 2013; Cao et al., 2015), the Famatinian arc, Argentina (Otamendi et al., 2020), and the Median Batholith, New Zea-

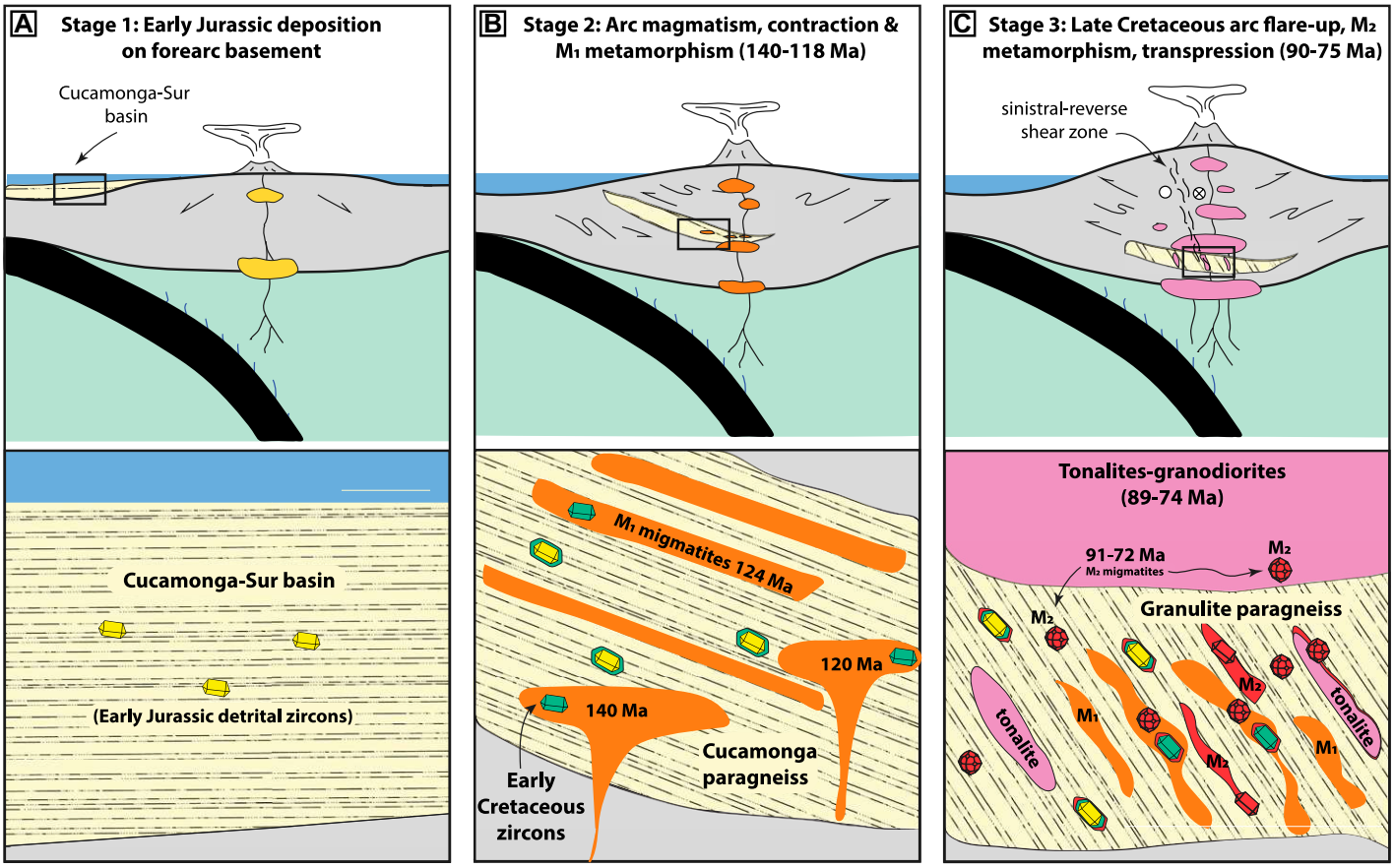

Figure 12. Schematic cartoon cross sections and insets showing our preferred model for the tectonic and magmatic development of the Mesozoic Southern California Batholith. (A) We postulate that the Cucamonga and Sur Series metasedimentary rocks once formed a contiguous Mesozoic forearc basin the Late Triassic to Early Jurassic. (B) The Cucamonga-Sur basin was underthrust beneath the arc by thrusting in the forearc resulting in burial, intrusion by Early Cretaceous plutons, and M_1 metamorphism at 124 Ma. (C) By the Late Cretaceous, the Cucamonga basin was buried to 7–9 kbar and metamorphosed at 700–800 °C during M_2 metamorphism. This metamorphic event corresponded with an arc magmatic flare-up from 90 Ma to 70 Ma in the Southern California Batholith. Magma loading at the base of the lower crust by arc tonalites and granodiorites resulted in widespread anatexis and granulite-facies metamorphism of the Cucamonga (and Sur Series) metasedimentary rocks.

land (Irel and Gibson, 1998; Hollis et al., 2004; Daczko et al., 2009; Jongens et al., 2023). Prior studies have demonstrated that sediments can be introduced into the deep-crust of arcs by multiple mechanisms, including underthrusting of forearc, accretionary complex, and/or backarc basins and/or relamination from the subducting slab (Haxel et al., 2002; Matzel et al., 2004; Currie et al., 2007; Ducea and Barton, 2007; DeCelles et al., 2009; Behn et al., 2011; Gordon et al., 2017; Strickland et al., 2018; Hanson et al., 2022). The deep burial of sediments into arcs is an important process because it introduces rheological heterogeneities, which can form weak layers into which strain is preferentially partitioned particularly if melt and fluids are present (Miller and Paterson, 2001; Klepeis et al., 2022).

In the root of the Southern California Batholith, we postulate that sediment incorporation occurred via trench-direct underthrusting of the Cucamonga-Sur forearc basin beneath the arc (i.e., the D_1/D_2 thrust system in the Cucamonga terrane). Reconstruction of Miocene and younger faults related to the San Andreas plate boundary shows that the Cucamonga-Sur basin would have extended over 500 km from the northern end of the Southern California Batholith (Salina) to the southern end (Fig. 9; Jacobson et al., 2011; Sharman et al., 2015; Schwartz et al., 2023). Given this distribution, these underthrust metasedimentary rocks constitute a significant volume of metasedimentary material incorporated in the lower crust of the Southern California Batholith in the Mesozoic.

We postulate that the incorporation of sediments into the deep crust of the Southern California Batholith occurred over a protracted period from the Middle Jurassic to Late Cretaceous. This period of time overlapped with two Mesozoic flare-up events involving both magmatic and tectonic thickening of the crust in Southern California (Figs. 12B and 12C). During the Late Cretaceous, heat from the 90–70 Ma magmatic flux event occurred at all structural levels in the Southern California Batholith. Heating functioned to weaken the crust and facilitated burial along intra-arc, transpressional shear zones, including the Black Belt and Cucamonga shear zones. In the lower crust of the Cucamonga terrane, strain was in part localized near the lower boundary between the granulites and the partially molten tonalites and granodiorites (Klepeis et al., 2023). In this region, rheological contrasts and the presence of partial melts functioned to localize strain during repeated magmatic injection and crystallization. The presence of pseudotachylytes and cataclasites in this region also

record evidence for high strain rates and possibly repeated seismogenic events that occurred synchronously with high rates of magma addition within the arc. Collectively, these features demonstrate that sediment incorporation into the lower crust of the Southern California Batholith was associated with major structural and rheological changes in the architecture of the arc.

CONCLUSIONS

U-Pb zircon petrochronology results from the Cucamonga and San Antonio terranes document the tempo of lower continental arc construction in the Southern California Batholith. The lower crust consisted of granulite-facies paragneisses that were deposited in a forearc or intra-arc basin. These paragneisses bear strong similarities to high-grade metasedimentary rocks in the basement of the Salinia block, and they were likely deposited together in adjacent basins receiving detritus from similar sources. The rocks in the Cucamonga terrane were metamorphosed during two high-temperature events: ca. 124 Ma and 89–75 Ma. The latter event resulted in widespread granulite-facies metamorphism and anatexis of metasedimentary rocks in the lower crust during a 15- to 20-m.y.-long magmatic surge event that affected the entire Southern California Batholith. The arc magmatic surge marked the termination of a prolonged period of magmatism (∼100 m.y.) in the Cucamonga terrane that lasted from ca. 175 Ma to 75 Ma. The Late Cretaceous arc magmatic surge was also associated with major changes within the arc and was linked to (1) sinistral transpression, accommodated by the Black Belt and Cucamonga shear zones; (2) crustal thickening via underthrusting of metasedimentary rocks from the forearc; (3) intrusion of voluminous arc-related tonalites and granodiorites into the middle and upper crust resulting in magma loading; and (4) widespread granulite-facies metamorphism of first generation metasedimentary rocks. We conclude that partial melting of these rocks was limited in its contribution to the budget of the flare-up magmas with melts remaining relatively localized. In contrast, substantial mantle input was essential to trigger and sustain the Late Cretaceous magmatic flare-up.

ACKNOWLEDGMENTS

This research was supported by US National Science Foundation grants EAR-2138733 (Schwartz and Miranda), EAR 1655152 (Cecil and Schwartz), EAR-0948706 and OCE-1338842 (Lackey), and NSF-EAR 2138734 (Klepeis), and Southern California Earthquake Center grants #21140 and #19023 (Miranda and Schwartz). Robles thanks the Geological Society of America for financial assistance. Justin Okin is thanked for assistance with fieldwork, and Zhan Peng and Andrew Kylander-Clark are thanked for petrochronology assistance. Xiaowei Li is thanked for assistance with mineral separation. John Banacky and Ron Goodman from the Cucamonga Foothill Preservation Alliance provided tremendous assistance with field logistics. We thank the science editor, Mihai Ducea, and the associate editor, Jay Chapman, for editorial handling, and George Bergantz, Maddie Lewis, and Manuel Contreras-López for constructive and helpful reviews.

REFERENCES CITED

Alf, R.M., 1948, A mylonite belt in the southeastern San Gabriel Mountains, California: Geological Society of America Bulletin, v. 59, p. 1101–1120, https://doi.org/10.1130/0016-7606(1948)59[1101:AMBITS]2.0.CO;2.

Alonso-Perez, R., Müntener, O., and Ulmer, P., 2009, Igneous garnet and amphibole fractionation in the roots of island arcs: Experimental constraints on andesitic liquids: Contributions to Mineralogy and Petrology, v. 157, p. 541–558, https://doi.org/10.1007/s00410-008-0351-8.

Annen, C., Blundy, J.D., and Sparks, R.S.J., 2006, The genesis of intermediate and silicic magmas in deep crustal hot zones: Journal of Petrology, v. 47, p. 505–539, https://doi.org/10.1093/petrology/egi084.

Ardill, K., Paterson, S., and Memeti, V., 2018, Spatiotemporal magmatic focusing in upper-mid crustal plutons of the Sierra Nevada arc: Earth and Planetary Science Letters, v. 498, p. 88–100, https://doi.org/10.1016/j.epsl.2018.06.023.

Armstrong, R.L., 1988, Mesozoic and early Cenozoic magmatic evolution of the Canadian Cordillera, *in* Clark, S.P., Jr., Burchfiel, B.C., and Suppe, J., eds., Processes in Continental Lithospheric Deformation: Geological Society of America Special Paper 218, p. 55–92, https://doi.org/10.1130/SPE218-p55.

Attia, S., Paterson, S.R., Cao, W., Chapman, A.D., Saleeby, J., Dunne, G.C., Stevens, C.H., and Memeti, V., 2018, Late Paleozoic tectonic assembly of the Sierra Nevada prebatholithic framework and western Laurentian provenance links based on synthesized detrital zircon geochronology, *in* Ingersoll, R.V., Lawton, T.F., and Graham, S.A., eds., Tectonics, Sedimentary Basins, and Provenance: A Celebration of the Career of William R. Dickinson: Geological Society of America Special Paper 540, p. 267–296, https://doi.org/10.1130/2018.2540(12).

Attia, S., Cottle, J.M., and Paterson, S.R., 2020, Erupted zircon record of continental crust formation during mantle driven arc flare-ups: Geology, v. 48, p. 446–451, https://doi.org/10.1130/G46991.1.

Attia, S., Paterson, S.R., Saleeby, J., and Cao, W., 2021, Detrital zircon provenance and depositional links of Mesozoic Sierra Nevada intra-arc strata: Geosphere, v. 17, p. 1422–1453, https://doi.org/10.1130/GES02296.1.

Barbeau, D.L., Ducea, M.N., Gehrels, G.E., Kidder, S., Wetmore, P.H., and Saleeby, J.B., 2005, U-Pb detrital-zircon geochronology of northern Salinian basement and cover rocks: Geological Society of America Bulletin, v. 117, p. 466–481, https://doi.org/10.1130/B25496.1.

Barth, A.P., 1990, Mid-crustal emplacement of Mesozoic plutons, San Gabriel Mountains, California, and implications for the geologic history of the San Gabriel terrane, *in* Anderson, J.L., ed., The Nature and Origin of Cordilleran Magmatism: Geological Society of America Memoir 174, p. 33–46, https://doi.org/10.1130/MEM174-p33.

Barth, A.P., and May, D.J., 1992, Mineralogy and pressure–temperature–time path of Cretaceous granulite gneisses, south-eastern San Gabriel Mountains, southern California: Journal of Metamorphic Geology, v. 10, p. 529–544, https://doi.org/10.1111/j.1525-1314.1992.tb00103.x.

Barth, A.P., and Schneiderman, J.S., 1996, A comparison of structures in the Andean orogen of northern Chile and exhumed mid-crustal structures in southern California, USA: An analogy in tectonic style?: International Geology Review, v. 38, p. 1075–1085, https://doi.org/10.1080/00206819709465383.

Barth, A.P., and Wooden, J.L., 2006, Timing of magmatism following initial convergence at a passive margin, southwestern U.S. Cordillera, and ages of lower crustal magma sources: The Journal of Geology, v. 114, p. 231–245, https://doi.org/10.1086/499573.

Barth, A.P., Wooden, Z.J.L., and May, D.J., 1992, Small scale heterogeneity of Phanerozoic lower crust: Evidence from isotopic and geochemical systematics of mid-Cretaceous granulite gneisses, San Gabriel Mountains, southern California: Contributions to Mineralogy and Petrology, v. 109, p. 394–407, https://doi.org/10.1007/BF00283327.

Barth, A.P., Wooden, J.L., Tosdal, R.M., and Morrison, J., 1995, Crustal contamination in the petrogenesis of a calc-alkalic rock series: Josephine Mountain intrusion, California: Geological Society of America Bulletin, v. 107, p. 201–212, https://doi.org/10.1130/0016-7606(1995)107<0201:CCITPO>2.3.CO;2.

Barth, A.P., Tosdal, R.M., Wooden, J.L., and Howard, K.A., 1997, Triassic plutonism in southern California: Southward younging of arc initiation along a truncated continental margin: Tectonics, v. 16, p. 290–304, https://doi.org/10.1029/96TC03596.

Barth, A.P., Wooden, J.L., and Coleman, D.S., 2001, Shrimp-RG-U-Pb zircon geochronology of Mesoproterozoic metamorphism and plutonism in the southwesternmost United States: The Journal of Geology, v. 109, p. 319–327, https://doi.org/10.1086/319975.

Barth, A.P., Wooden, J.L., Grove, M., Jacobson, C.E., and Pedrick, J.N., 2003, U-Pb zircon geochronology of rocks in the Salinas Valley region of California: A reevaluation of the crustal structure and origin of the Salinian block: Geology, v. 31, p. 517–520, https://doi.org/10.1130/0091-7613(2003)031<0517:UZGORI>2.0.CO;2.

Barth, A.P., Wooden, J.L., Jacobson, C.E., and Probst, K., 2004, U-Pb geochronology and geochemistry of the McCoy Mountains Formation, southeastern California: A Cretaceous retroarc foreland basin: Geological Society of America Bulletin, v. 116, p. 142–153, https://doi.org/10.1130/B25288.1.

Barth, A.P., Wooden, J.L., Howard, K.A., and Richards, J.L., 2008, Late Jurassic plutonism in the southwest U.S. Cordillera, *in* Wright, J.E., and Shervais, J.W., eds., Ophiolites, Arcs, and Batholiths: A Tribute to Cliff Hopson: Geological Society of America Special Paper 438, p. 379–396, https://doi.org/10.1130/2008.2438(13).

Barth, A.P., Wooden, J.L., Coleman, D.S., and Vogel, M.B., 2009, Assembling and disassembling California: A zircon and monazite geochronologic framework for Proterozoic crustal evolution in Southern California: The Journal of Geology, v. 117, p. 221–239, https://doi.org/10.1086/597515.

Barth, A.P., Wooden, J.L., Mueller, P.A., and Economos, R.C., 2016, Granite provenance and intrusion in arcs: Evidence from diverse zircon types in Big Bear Lake Intrusive Suite, USA: Lithos, v. 246–247, p. 261–278, https://doi.org/10.1016/j.lithos.2015.12.009.

Barth, A.P., Wooden, J.L., Miller, D.M., Howard, K.A., Fox, L.K., Schermer, E.R., and Jacobson, C.E., 2017, Regional and temporal variability of melts during a Cordilleran magma pulse: Age and chemical evolution of the Jurassic arc, eastern Mojave Desert, California: Geological Society of America Bulletin, v. 129, p. 429–448, https://doi.org/10.1130/B31550.1.

Barth, A.P., Wooden, J.L., Riggs, N.R., Walker, J.D., Tani, K., Penniston-Dorland, S.C., Jacobson, C.E., Laughlin, J.A., and Hiramatsu, R., 2018, Marine volcaniclastic record of early arc evolution in the eastern Ritter Range Pendant, Central Sierra Nevada, California: Geochemistry, Geophysics, Geosystems, v. 19, p. 2543–2559, https://doi.org/10.1029/2018GC007456.

Baskin, J., Klepeis, K., Schwartz, J., Miranda, E., Robles, F., and Mora-Klepeis, G., 2023, Styles and history of convergent margin deformation in the Southern California Batholith during the Late Cretaceous beginning of the Laramide Orogeny: Geological Society of America Abstracts with Programs, v. 55, no. 6, https://doi.org/10.1130/abs/2023AM-394531.

Bateman, P.C., 1992, Plutonism in the central part of the Sierra Nevada Batholith, California: U.S. Geological Survey Professional Paper 1483, 186 p., https://doi.org/10.3133/pp1483.

Behn, M.D., Kelemen, P.B., Hirth, G., Hacker, B.R., and Massonne, H.-J., 2011, Diapirs as the source of the sediment signature in arc lavas: Nature Geoscience, v. 4, p. 641–646, https://doi.org/10.1038/ngeo1214.

Behrman, P.S., and Parkison, G.A., 1978, Pre-Callovian rocks, west of the Melones fault, central Sierra Nevada Foothills, *in* Howell, D.G., and McDougall, K.A., eds., Mesozoic Paleogeography of the Western United States: Pacific Section, Society of Economic Paleontologists and Mineralogists, Pacific Coast Paleogeography Symposium 2, Sacramento, California, p. 337–348.

Black, L.P., et al., 2004, Improved $^{206}Pb/^{238}U$ microprobe geochronology by the monitoring of a trace-element-related matrix effect; SHRIMP, ID-TIMS, ELA-ICP-MS and oxygen isotope documentation for a series of zircon standards: Chemical Geology, v. 205, p. 115–140, https://doi.org/10.1016/j.chemgeo.2004.01.003.

Brown, H.J., 1991, Stratigraphy and paleogeographic setting of Paleozoic rocks in the San Bernardino Mountains, California, *in* Cooper, J.D., and Stevens, C.H., eds., Paleozoic Paleogeography of the Western United States: Pacific Section, Society of Economic Paleontologists and Mineralogists, Paleozoic Paleogeography Symposium, 2nd, Bakersfield, California, v. 67, p. 193–207.

Bucholz, C.E., Eddy, M.P., Jagoutz, O., Bowring, S.A., Schmidt, M.W., and Sambuu, O., 2017, Constraining the time scales of magmatic differentiation with U-Pb zircon geochronology: Geology, v. 45, p. 11–14, https://doi.org/10.1130/G38505.1.

Busby-Spera, C.J., 1988, Speculative tectonic model for the early Mesozoic arc of the southwest Cordilleran United States: Geology, v. 16, p. 1121–1125, https://doi.org/10.1130/0091-7613(1988)016<1121:STMFTE>2.3.CO;2.

Butler, R.F., Gehrels, G.E., and Kodama, K.P., 2001, A Moderate translation alternative to the Baja British Columbia hypothesis: GSA Today, v. 11, no. 6, p. 4–10, https://doi.org/10.1130/1052-5173(2001)011<0004:AMTATT>2.0.CO;2.

Cao, W., Paterson, S., Memeti, V., Mundil, R., Anderson, J.L., and Schmidt, K., 2015, Tracking paleodeformation fields in the Mesozoic central Sierra Nevada arc: Implications for intra-arc cyclic deformation and arc tempos: Lithosphere, v. 7, p. 296–320, https://doi.org/10.1130/L389.1.

Cashman, K.V., Sparks, R.S.J., and Blundy, J.D., 2017, Vertically extensive and unstable magmatic systems: A unified view of igneous processes: Science, v. 355, https://doi.org/10.1126/science.aag3055.

Cecil, M.R., Rusmore, M.E., Gehrels, G.E., Woodsworth, G.J., Stowell, H.H., Yokelson, I.N., Chisom, C., Trautman, M., and Homan, E., 2018, Along-strike variation in the magmatic tempo of the Coast Mountains Batholith, British Columbia, and implications for processes controlling episodicity in arcs: Geochemistry, Geophysics, Geosystems, v. 19, p. 4274–4289, https://doi.org/10.1029/2018GC007874.

Cecil, M.R., Ferrer, M.A., Riggs, N.R., Marsaglia, K., Kylander-Clark, A., Ducea, M.N., and Stone, P., 2019, Early arc development recorded in Permian–Triassic plutons of the northern Mojave Desert region, California, USA: Geological Society of America Bulletin, v. 131, p. 749–765, https://doi.org/10.1130/B31963.1.

Chapman, A.D., Saleeby, J.B., and Eiler, J., 2013, Slab flattening trigger for isotopic disturbance and magmatic flareup in the southernmost Sierra Nevada batholith, California: Geology, v. 41, p. 1007–1010, https://doi.org/10.1130/G34445.1.

Chapman, A.D., Jacobson, C.E., Ernst, W.G., Grove, M., Dumitru, T., Hourigan, J., and Ducea, M.N., 2016, Assembling the world's type shallow subduction complex: Detrital zircon geochronologic constraints on the origin of the Nacimiento block, central California Coast Ranges: Geosphere, v. 12, p. 533–557, https://doi.org/10.1130/GES01257.1.

Chapman, J.B., and Ducea, M.N., 2019, The role of arc migration in Cordilleran orogenic cyclicity: Geology, v. 47, p. 627–631, https://doi.org/10.1130/G46117.1.

Chapman, J.B., Ducea, M.N., Kapp, P., Gehrels, G.E., and DeCelles, P.G., 2017, Spatial and temporal radiogenic isotopic trends of magmatism in Cordilleran orogens: Gondwana Research, v. 48, p. 189–204, https://doi.org/10.1016/j.gr.2017.04.019.

Chapman, J.B., Dafov, M.N., Gehrels, G., Ducea, M.N., Valley, J.W., and Ishida, A., 2018, Lithospheric architecture and tectonic evolution of the southwestern U.S. Cordillera: Constraints from zircon Hf and O isotopic data: Geological Society of America Bulletin, v. 130, p. 2031–2046, https://doi.org/10.1130/B31937.1.

Chapman, J.B., et al., 2021a, The North American Cordilleran Anatectic Belt: Earth-Science Reviews, v. 215, https://doi.org/10.1016/j.earscirev.2021.103576.

Chapman, J.B., Shields, J.E., Ducea, M.N., Paterson, S.R., Attia, S., and Ardill, K.E., 2021b, The causes of continental arc flare ups and drivers of episodic magmatic activity in Cordilleran orogenic systems: Lithos, v. 398–399, https://doi.org/10.1016/j.lithos.2021.106307.

Chin, E.J., Lee, C.-T.A., Tollstrup, D.L., Xie, L., Wimpenny, J.B., and Yin, Q.-Z., 2013, On the origin of hot metasedimentary quartzites in the lower crust of continental arcs: Earth and Planetary Science Letters, v. 361, p. 120–133, https://doi.org/10.1016/j.epsl.2012.11.031.

Chin, E.J., Lee, C.T.A., and Barnes, J.D., 2014, Thickening, refertilization, and the deep lithosphere filter in continental arcs: Constraints from major and trace elements and oxygen isotopes: Earth and Planetary Science Letters, v. 397, p. 184–200, https://doi.org/10.1016/j.epsl.2014.04.022.

Coleman, D.S., Gray, W., and Glazner, A.F., 2004, Rethinking the emplacement and evolution of zoned plutons: Geochronologic evidence for incremental assembly of the Tuolumne Intrusive Suite, California: Geology, v. 32, p. 433–436, https://doi.org/10.1130/G20220.1.

Collins, W.J., Murphy, J.B., Johnson, T.E., and Huang, H.-Q., 2020, Critical role of water in the formation of continental crust: Nature Geoscience, v. 13, p. 331–338, https://doi.org/10.1038/s41561-020-0573-6.

Cope, T., 2017, Phanerozoic magmatic tempos of North China: Earth and Planetary Science Letters, v. 468, p. 1–10, https://doi.org/10.1016/j.epsl.2017.03.022.

Corfu, F., Hanchar, J.M., Hoskin, P.W.O., and Kinny, P., 2003, Atlas of Zircon Textures: Reviews in Mineralogy and Geochemistry, v. 53, p. 469–500, https://doi.org/10.2113/0530469.

Cornet, J., Laurent, O., Wotzlaw, J.-F., Antonelli, M.A., Otamendi, J., Bergantz, G.W., and Bachmann, O., 2022, Reworking subducted sediments in arc magmas and the isotopic diversity of the continental crust: The case of the Ordovician Famatinian crustal section, Argentina: Earth and Planetary Science Letters, v. 595, https://doi.org/10.1016/j.epsl.2022.117706.

Cowan, D.S., Brandon, M.T., and Garver, J.I., 1997, Geological tests of hypotheses for large coastwise displacements; a critique illustrated by the Baja British Columbia controversy: American Journal of Science, v. 297, p. 117–173, https://doi.org/10.2475/ajs.297.2.117.

Currie, C.A., Beaumont, C., and Huismans, R.S., 2007, The fate of subducted sediments: A case for backarc intrusion and underplating: Geology, v. 35, p. 1111–1114, https://doi.org/10.1130/G24098A.1.

Daczko, N.R., Milan, L.A., and Halpin, J.A., 2009, Metastable persistence of pelitic metamorphic assemblages at the root of a Cretaceous magmatic arc—Fiordland, New Zealand: Journal of Metamorphic Geology, v. 27, p. 233–247, https://doi.org/10.1111/j.1525-1314.2009.00815.x.

DeCelles, P.G., 2004, Late Jurassic to Eocene evolution of the Cordilleran thrust belt and foreland basin system, western U.S.A.: American Journal of Science, v. 304, https://doi.org/10.2475/ajs.304.2.105.

DeCelles, P.G., and Graham, S.A., 2015, Cyclical processes in the North American Cordilleran orogenic system: Geology, v. 43, p. 499–502 https://doi.org/10.1130/G36482.1.

DeCelles, P.G., Ducea, M.N., Kapp, P., and Zandt, G., 2009, Cyclicity in Cordilleran orogenic systems: Nature Geoscience, v. 2, p. 251–257 https://doi.org/10.1038/ngeo469.

Decker, M., Schwartz, J.J., Stowell, H.H., Klepeis, K.A., Tulloch, A.J., Kitajima, K., Valley, J.W., and Kylander-Clark, A., 2017, Slab-triggered arc flare-up in the Cretaceous Median Batholith and the growth of lower arc crust, Fiordland, New Zealand: Journal of Petrology, https://doi.org/10.1093/petrology/egx049.

de Silva, S.L., Riggs, N.R., and Barth, A.P., 2015, Quickening the pulse: Fractal tempos in continental arc magmatism: Elements, v. 11, p. 113–118, https://doi.org/10.2113/gselements.11.2.113.

Dickinson, W.R., 1996, Kinematics of Transrotational Tectonism in the California Transverse Ranges and Its Contribution to Cumulative Slip along the San Andreas Transform Fault System: Geological Society of America Special Paper 305, 46 p., https://doi.org/10.1130/0-8137-2305-1.1.

Dickinson, W.R., 2000, Geodynamic interpretation of Paleozoic tectonic trends oriented oblique to the Mesozoic Klamath-Sierran continental margin in California, *in* Soreghan, M.J., and Gehrels, G.E., eds., Paleozoic and Triassic Paleogeography and Tectonics of Western Nevada and Northern California: Geological Society of America Special Paper 347, p. 209–246, https://doi.org/10.1130/0-8137-2347-7.209.

Dickinson, W.R., and Lawton, T.F., 2001, Carboniferous to Cretaceous assembly and fragmentation of Mexico: Geological Society of America Bulletin, v. 113, p. 1142–1160, https://doi.org/10.1130/0016-7606(2001)113<1142:CTCAAF>2.0.CO;2.

Dickinson, W.R., and Gehrels, G.E., 2009, Use of U–Pb ages of detrital zircons to infer maximum depositional ages of strata: A test against a Colorado Plateau Mesozoic database: Earth and Planetary Science Letters, v. 288, p. 115–125, https://doi.org/10.1016/j.epsl.2009.09.013.

Ducea, M., 2001, The California arc: Thick granitic batholiths, eclogitic residues, lithospheric-scale thrusting, and magmatic flare-ups: GSA Today, v. 11, no. 11, p. 4–10, https://doi.org/10.1130/1052-5173(2001)011<0004:TCATGB>2.0.CO;2.

Ducea, M.N., 2002, Constraints on the bulk composition and root foundering rates of continental arcs: A California arc perspective: Journal of Geophysical Research: Solid Earth, v. 107, p. 1–13, https://doi.org/10.1029/2001JB000643.

Ducea, M.N., and Barton, M.D., 2007, Igniting flare-up events in Cordilleran arcs: Geology, v. 35, p. 1047–1050, https://doi.org/10.1130/G23898A.1.

Ducea, M.N., and Saleeby, J.B., 1996, Buoyancy sources for a large, unrooted mountain range, the Sierra Nevada, California: Evidence from xenolith thermobarometry: Journal of Geophysical Research: Solid Earth, v. 101, p. 8229–8244, https://doi.org/10.1029/95JB03452.

Ducea, M.N., Kidder, S., and Zandt, G., 2003, Arc composition at mid-crustal depths: Insights from the Coast Ridge Belt, Santa Lucia Mountains, California: Geophysical Research Letters, v. 30, https://doi.org/10.1029/2002GL016297.

Ducea, M.N., Paterson, S.R., and DeCelles, P.G., 2015a, High-volume magmatic events in subduction systems: Elements, v. 11, p. 99–104, https://doi.org/10.2113/gselements.11.2.99.

Ducea, M.N., Saleeby, J.B., and Bergantz, G., 2015b, The architecture, chemistry, and evolution of continental magmatic arcs: Annual Review of Earth and Planetary Sciences, v. 43, p. 299–331, https://doi.org/10.1146/annurev-earth-060614-105049.

Ducea, M.N., Bergantz, G.W., Crowley, J.L., and Otamendi, J., 2017, Ultrafast magmatic buildup and diversification to produce continental crust during subduction: Geology, v. 45, p. 235–238, https://doi.org/10.1130/G38726.1.

Dunne, G.C., and Walker, J.D., 2004, Structure and evolution of the East Sierran thrust system, east central California: Tectonics, v. 23, https://doi.org/10.1029/2002TC001478.

Dunne, G.C., Garvey, T.P., Oborne, M., Schneidereit, D., Fritsche, A.E., and Walker, J.D., 1998, Geology of the Inyo Mountains Volcanic Complex: Implications for Jurassic paleogeography of the Sierran magmatic arc in eastern California: Geological Society of America Bulletin, v. 110, p. 1376–1397, https://doi.org/10.1130/0016-7606(1998)110<1376:GOTIMV>2.3.CO;2.

Economos, R.C., et al., 2021, Testing models of Laramide orogenic initiation by investigation of Late Cretaceous magmatic-tectonic evolution of the central Mojave sector of the California arc: Geosphere, v. 17, p. 2042–2061, https://doi.org/10.1130/GES02225.1.

Edelman, S.H., and Sharp, W.D., 1989, Terranes, early faults, and pre-Late Jurassic amalgamation of the western Sierra Nevada metamorphic belt, Cali-

fornia: Geological Society of America Bulletin, v. 101, p. 1420–1433, https://doi.org/10.1130/0016-7606(1989)101<1420:TEFAPL>2.3.CO;2.

Farmer, G.L., and DePaolo, D.J., 1983, Origin of Mesozoic and Tertiary granite in the western United States and implications for Pre-Mesozoic crustal structure: 1. Nd and Sr isotopic studies in the geocline of the Northern Great Basin: Journal of Geophysical Research: Solid Earth, v. 88, p. 3379–3401, https://doi.org/10.1029/JB088iB04p03379.

Ferry, J.M., and Watson, E.B., 2007, New thermodynamic models and revised calibrations for the Ti-in-zircon and Zr-in-rutile thermometers: Contributions to Mineralogy and Petrology, v. 154, p. 429–437, https://doi.org/10.1007/s00410-007-0201-0.

Foster, D.A., Miller, C.F., Harrison, T.M., and Hoisch, T.D., 1992, $^{40}Ar/^{39}Ar$ thermochronology and thermobarometry of metamorphism, plutonism, and tectonic denudation in the Old Woman Mountains area, California: Geological Society of America Bulletin, v. 104, p. 176–191, https://doi.org/10.1130/0016-7606(1992)104<0176:AATATO>2.3.CO;2.

Fox, L.K., and Miller, D.M., 1990, Jurassic granitoids and related rocks of the southern Bristol Mountains, southern Providence Mountains, and Colton Hills, Mojave Desert, California, *in* Anderson, J.L., ed., The Nature and Origin of Cordilleran Magmatism: Geological Society of America Memoir 174, p. 111–132, https://doi.org/10.1130/MEM174-p111.

Gehrels, G., et al., 2009, U-Th-Pb geochronology of the Coast Mountains batholith in north-coastal British Columbia: Constraints on age and tectonic evolution: Geological Society of America Bulletin, v. 121, p. 1341–1361, https://doi.org/10.1130/B26404.1.

Gehrels, G.E., 2000, Introduction to detrital zircon studies of Paleozoic and Triassic strata in western Nevada and northern California, *in* Soreghan, M.J., and Gehrels, G.E., eds., Paleozoic and Triassic Paleogeography and Tectonics of Western Nevada and Northern California: Geological Society of America Special Paper 347, p. 1–18, https://doi.org/10.1130/0-8137-2347-7.1.

Getsinger, A., Rushmer, T., Jackson, M.D., and Baker, D., 2009, Generating high Mg-numbers and chemical diversity in tonalite-trondhjemite-granodiorite (TTG) magmas during melting and melt segregation in the continental crust: Journal of Petrology, v. 50, p. 1935–1954, https://doi.org/10.1093/petrology/egp060.

Girardi, J.D., Patchett, P.J., Ducea, M.N., Gehrels, G.E., Cecil, M.R., Rusmore, M.E., Woodsworth, G.J., Pearson, D.M., Manthei, C., and Wetmore, P., 2012, Elemental and isotopic evidence for granitoid genesis from deep-seated sources in the Coast Mountains Batholith, British Columbia: Journal of Petrology, v. 53, p. 1505–1536, https://doi.org/10.1093/petrology/egs024.

Gordon, S.M., Miller, R.B., and Sauer, K.B., 2017, Incorporation of sedimentary rocks into the deep levels of continental magmatic arcs: Links between the North Cascades arc and surrounding sedimentary terranes, *in* Haugerud, R.A., and Kelsey, H.M., eds., From the Puget Lowland to East of the Cascade Range: Geologic Excursions in the Pacific Northwest: Geological Society of America Field Guide 49, p. 101–142, https://doi.org/10.1130/2017.0049(06).

Grimes, C.B., Wooden, J.L., Cheadle, M.J., and John, B.E., 2015, "Fingerprinting" tectono-magmatic provenance using trace elements in igneous zircon: Contributions to Mineralogy and Petrology, v. 170, p. 1–26, https://doi.org/10.1007/s00410-015-1199-3.

Gromet, P., and Silver, L.T., 1987, REE variations across the Peninsular Ranges Batholith: Implications for batholithic petrogenesis and crustal growth in magmatic arcs: Journal of Petrology, v. 28, p. 75–125, https://doi.org/10.1093/petrology/28.1.75.

Grove, M., Jacobson, C.E., Barth, A.P., and Vucic, A., 2003, Temporal and spatial trends of Late Cretaceous–early Tertiary underplating Pelona and related schist beneath southern California and southwestern Arizona, *in* Johnson, S.E., Paterson, S.E., Fletcher, J.M., Girty, G.H., Kimbrough, D.L., and Martin-Barajas, A., eds., Tectonic Evolution of Northwestern Mexico and the Southwestern USA: Geological Society of America Special Paper 374, p. 1–26, https://doi.org/10.1130/0-8137-2374-4.381.

Grove, M., Bebout, G.E., Jacobson, C.E., Barth, A.P., Kimbrough, D.L., King, R.L., Zou, H., Lovera, O.M., Mahoney, B.J., and Gehrels, G.E., 2008, The Catalina Schist: Evidence for middle Cretaceous subduction erosion of southwestern North America, *in* Draut, A.E., et al., eds., Formation and Applications of the Sedimentary Record in Arc Collision Zones: Geological Society of America Special Paper 436, p. 335–361, https://doi.org/10.1130/2008.2436(15).

Hacker, B.R., Kelemen, P.B., and Behn, M.D., 2011, Differentiation of the continental crust by relamination: Earth and Planetary Science Letters, v. 307, p. 501–516, https://doi.org/10.1016/j.epsl.2011.05.024.

Hanson, A.E.H., Gordon, S.M., Ashley, K.T., Miller, R.B., and Langdon-Lassagne, E., 2022, Multiple sediment incorporation events in a continental magmatic arc: Insight from the metasedimentary rocks of the northern North Cascades, Washington (USA): Geosphere, v. 18, p. 298–326, https://doi.org/10.1130/GES02425.1.

Haxel, G.B., Jacobson, C.E., Richard, S.M., Tosdal, R.M., and Grubensky, M.J., 2002, The Orocopia Schist in southwest Arizona: Early Tertiary oceanic rocks trapped or transported far inland, *in* Barth, A.P., ed., Contributions to Crustal Evolution of the Southwestern United States: Geological Society of America Special Paper 365, p. 99–128, https://doi.org/10.1130/0-8137-2365-5.99.

Henderson, L.J., Gordon, R.G., and Engebretson, D.C., 1984, Mesozoic aseismic ridges on the Farallon Plate and southward migration of shallow subduction during the Laramide Orogeny: Tectonics, v. 3, p. 121–132, https://doi.org/10.1029/TC003i002p00121.

Hildreth, W., and Moorbath, S., 1988, Crustal contributions to arc magmatism in the Andes of Central Chile: Contributions to Mineralogy and Petrology, v. 98, p. 455–489, https://doi.org/10.1007/BF00372365.

Hollis, J.A., Clarke, G.L., Klepeis, K.A., Daczko, N.R., and Ireland, T.R., 2004, The regional significance of Cretaceous magmatism and metamorphism in Fiordland, New Zealand, from U-Pb zircon geochronology: Journal of Metamorphic Geology, v. 22, p. 607–627, https://doi.org/10.1111/j.1525-1314.2004.00537.x.

Hollister, L., and Andronicos, C., 2006, Formation of new continental crust in Western British Columbia during transpression and transtension: Earth and Planetary Science Letters, v. 249, p. 29–38, https://doi.org/10.1016/j.epsl.2006.06.042.

Hsu, K.J., 1955, Granulites and Mylonites of the Region about Cucamonga and San Antonio Canyons, San Gabriel Mountains: Berkeley, California, University of California Press, 351 p.

Irel, T.R., and Gibson, G.M., 1998, SHRIMP monazite and zircon geochronology of high-grade metamorphism in New Zealand: Journal of Metamorphic Geology, v. 16, p. 149–167, https://doi.org/10.1111/j.1525-1314.1998.00112.x.

Jacobson, C.E., Grove, M., Pedrick, J.N., Barth, A.P., Marsaglia, K.M., Gehrels, G.E., and Nourse, J.A., 2011, Late Cretaceous–early Cenozoic tectonic evolution of the southern California margin inferred from provenance of trench and forearc sediments: Geological Society of America Bulletin, v. 123, p. 485–506, https://doi.org/10.1130/B30238.1.

Johnston, S.M., Kylander-Clark, A.R.C., and Chapman, A.D., 2018, Detrital zircon geochronology and evolution of the Nacimiento block late Mesozoic forearc basin, central California coast, *in* Ingersoll, R.V., Lawton, T.F., and Graham, S.A., eds., Tectonics, Sedimentary Basins, and Provenance: A Celebration of the Career of William R. Dickinson: Geological Society of America Special Paper 540, p. 383–408, https://doi.org/10.1130/2018.2540(17).

Johnston, S.M., Singleton, J.S., Chapman, A.D., and Murray, G., 2019, Geologic map and structural development of the northernmost Sur-Nacimiento fault zone, central California coast: Geosphere, v. 15, p. 171–187, https://doi.org/10.1130/GES02015.1.

Jongens, R., Turnbull, I.M., and Allibone, A.H., 2023, Lithostratigraphy of Paleozoic metasediments in southern Fiordland, New Zealand: New Zealand Journal of Geology and Geophysics, v. 66, p. 428–455, https://doi.org/10.1080/00288306.2022.2157845.

Kapp, J.D., Miller, C.F., and Miller, J.S., 2002, Ireteba pluton, Eldorado Mountains, Nevada: Late, deep-source, peraluminous magmatism in the Cordilleran interior: The Journal of Geology, v. 110, p. 649–669, https://doi.org/10.1086/342864.

Kemp, A.I.S., Hawkesworth, C.J., Foster, G.L., Paterson, B.A., Woodhead, J.D., Hergt, J.M., Gray, C.M., and Whitehouse, M.J., 2007, Magmatic and crustal differentiation history of granitic rocks from Hf-O isotopes in zircon: Science, v. 315, p. 980–983, https://doi.org/10.1126/science.1136154.

Kidder, S., Ducea, M., Gehrels, G., Patchett, P.J., and Vervoort, J., 2003, Tectonic and magmatic development of the Salinian Coast Ridge Belt, California: Tectonics, v. 22, https://doi.org/10.1029/2002TC001409.

Kimbrough, D.L., Smith, D.P., Mahoney, J.B., Moore, T.E., Grove, M., Gastil, R.G., Ortega-Rivera, A., and Fanning, C.M., 2001, Forearc-basin sedimentary response to rapid Late Cretaceous batholith emplacement in the Peninsular Ranges of southern and Baja California: Geology, v. 29, p. 491–494, https://doi.org/10.1130/0091-7613(2001)029<0491:FBSRTR>2.0.CO;2.

Kirsch, M., Paterson, S.R., Wobbe, F., Ardila, A.M.M., Clausen, B.L., and Alasino, P.H., 2016, Temporal histories of Cordilleran continental arcs: Testing models for magmatic episodicity: The American Mineralogist, v. 101, p. 2133–2154, https://doi.org/10.2138/am-2016-5718.

Klein, B.Z., and Jagoutz, O., 2021, Construction of a transcrustal magma system: Building the Bear Valley Intrusive Suite, southern Sierra Nevada, California: Earth and Planetary Science Letters, v. 553, https://doi.org/10.1016/j.epsl.2020.116624.

Klein, B.Z., Jagoutz, O., and Ramezani, J., 2021, High-precision geochronology requires that ultrafast mantle-derived magmatic fluxes built the transcrustal Bear Valley Intrusive Suite, Sierra Nevada, California, USA: Geology, v. 49, p. 106–110, https://doi.org/10.1130/G47952.1.

Klemetti, E.W., Lackey, J.S., and Starnes, J., 2014, Magmatic lulls in the Sierra Nevada captured in zircon from rhyolite of the Mineral King pendant, California: Geosphere, v. 10, p. 66–79, https://doi.org/10.1130/GES00920.1.

Klepeis, K., Schwartz, J., Miranda, E., Robles, F., Baskin, J., and Mora-Klepeis, G., 2023, Magma-deformation interactions in Southern California during Late Cretaceous onset of the Laramide orogeny, San Gabriel Mountains, California: Geological Society of America Abstracts with Programs, v. 55, no. 6, https://doi.org/10.1130/abs/2023AM-394141.

Klepeis, K.A., Schwartz, J.J., Miranda, E., Lindquist, P., Jongens, R., Turnbull, R., and Stowell, H., 2022, The initiation and growth of transpressional shear zones through continental arc lithosphere, southwest New Zealand: Tectonics, v. 41, https://doi.org/10.1029/2021TC007097.

Kylander-Clark, A.R.C., Hacker, B.R., and Cottle, J.M., 2013, Laser-ablation split-stream ICP petrochronology: Chemical Geology, v. 345, p. 99–112, https://doi.org/10.1016/j.chemgeo.2013.02.019.

Lackey, J.S., Valley, J.W., and Hinke, H.J., 2006, Deciphering the source and contamination history of peraluminous magmas using $\delta^{18}O$ of accessory minerals: Examples from garnet-bearing plutons of the Sierra Nevada batholith: Contributions to Mineralogy and Petrology, v. 151, p. 20–44, https://doi.org/10.1007/s00410-005-0043-6.

Lackey, J.S., Cecil, M.R., Windham, C.J., Frazer, R.E., Bindeman, I.N., and Gehrels, G.E., 2012, The Fine Gold Intrusive Suite: The roles of basement terranes and magma source development in the Early Cretaceous Sierra Nevada batholith: Geosphere, v. 8, p. 292–313, https://doi.org/10.1130/GES00745.1.

Liu, L., Gurnis, M., Seton, M., Saleeby, J., Müller, R.D., and Jackson, J.M., 2010, The role of oceanic plateau subduction in the Laramide orogeny: Nature Geoscience, v. 3, p. 353–357, https://doi.org/10.1038/ngeo829.

Livaccari, R.F., Burke, K., and Şengör, A.M.C., 1981, Was the Laramide orogeny related to subduction of an oceanic plateau?: Nature, v. 289, p. 276–278, https://doi.org/10.1038/289276a0.

Martínez Ardila, A.M., Paterson, S.R., Memeti, V., Parada, M.A., and Molina, P.G., 2019, Mantle driven creta-

ceous flare-ups in Cordilleran arcs: Lithos, v. 326–327, p. 19–27, https://doi.org/10.1016/j.lithos.2018.12.007.

Mattinson, J.M., 2010, Analysis of the relative decay constants of ^{235}U and ^{238}U by multi-step CA-TIMS measurements of closed-system natural zircon samples: Chemical Geology, v. 275, p. 186–198, https://doi.org/10.1016/j.chemgeo.2010.05.007.

Matzel, J.E.P., Bowring, S.A., and Miller, R.B., 2004, Protolith age of the Swakane Gneiss, North Cascades, Washington: Evidence of rapid underthrusting of sediments beneath an arc: Tectonics, v. 23, 18 p., https://doi.org/10.1029/2003TC001577.

Maxson, J., and Tikoff, B., 1996, Hit-and-run collision model for the Laramide orogeny, western United States: Geology, v. 24, p. 968–972, https://doi.org/10.1130/0091-7613(1996)024<0968:HARCMF>2.3.CO;2.

May, D.J., 1989, Late Cretaceous intra-arc thrusting in southern California: Tectonics, v. 8, p. 1159–1173, https://doi.org/10.1029/TC008i006p01159.

May, D.J., and Walker, N.W., 1989, Late Cretaceous juxtaposition of metamorphic terranes in the southeastern San Gabriel Mountains, California: Geological Society of America Bulletin, v. 101, p. 1246–1267, https://doi.org/10.1130/0016-7606(1989)101<1246:LCJOMT>2.3.CO;2.

McPhillips, D., and Scharer, K.M., 2018, Quantifying uncertainty in cumulative surface slip along the Cucamonga fault, a crustal thrust fault in Southern California: Journal of Geophysical Research: Solid Earth, v. 123, p. 9063–9083, https://doi.org/10.1029/2018JB016301.

Miller, C.F., and Barton, M.D., 1990, Phanerozoic plutonism in the Cordilleran Interior, U.S.A., *in* Kay, S.M., and Rapela, C.W., eds., Plutonism from Antarctica to Alaska: Geological Society of America Special Paper 241, p. 213–231, https://doi.org/10.1130/SPE241-p213.

Miller, C.F., and Bradfish, L.J., 1980, An inner Cordilleran belt of muscovite-bearing plutons: Geology, v. 8, p. 412, https://doi.org/10.1130/0091-7613(1980)8<412:AICBOM>2.0.CO;2.

Miller, J.S., Glazner, A.F., and Crowe, D.E., 1996, Muscovite-garnet granites in the Mojave Desert: Relation to crustal structure of the Cretaceous arc: Geology, v. 24, p. 335, https://doi.org/10.1130/0091-7613(1996)024<0335:MGGITM>2.3.CO;2.

Miller, R.B., and Paterson, S.R., 2001, Influence of lithological heterogeneity, mechanical anisotropy, and magmatism on the rheology of an arc, North Cascades, Washington: Tectonophysics, v. 342, p. 351–370, https://doi.org/10.1016/S0040-1951(01)00170-6.

Miller, R.B., and Snoke, A.W., 2009, The utility of crustal cross sections in the analysis of orogenic processes in contrasting tectonic settings, *in* Miller, R.B., and Snoke, A.W., eds., Crustal Cross Sections from the Western North American Cordillera and Elsewhere: Implications for Tectonic and Petrologic Processes: Geological Society of America Special Paper 456, p. 1–38, https://doi.org/10.1130/2009.2456(01).

Miller, R.B., Paterson, S., and Matzel, J., 2009, Plutonism at different crustal levels: Insights from the ~5–40 km (paleodepth) North Cascades crustal section, Washington, *in* Miller, R.B., and Snoke, A.W., eds., Crustal Cross Sections from the Western North American Cordillera and Elsewhere: Implications for Tectonic and Petrologic Processes: Geological Society of America Special Paper 456, p. 125–149, https://doi.org/10.1130/2009.2456(05).

Morton, D.M., and Matti, J.C., 1987, The Cucamonga fault zone: Geologic setting and Quaternary history, *in* Morton, D.M., and Yerkes, R.F., eds., Recent Transverse Faulting in the Transverse Ranges: U.S. Geological Survey Professional Paper 1339, p. 179–203.

Morton, D.M., and Miller, F.K., 2003, Preliminary geologic map of the San Bernardino 30′ × 60′ quadrangle, California: U.S. Geological Survey Open-File Report 03-293, p. 118, https://pubs.usgs.gov/of/2003/of03-293/ (accessed June 2024).

Morton, D.M., Matti, J.C., Koukladas, C., and Cossette, P.M., 2001, Geologic map of the Cucamonga Peak 7.5′ quadrangle, San Bernardino County, California: U.S. Geological Survey Open-File Report 01-311, https://pubs.usgs.gov/of/2001/0311/ (accessed June 2024).

Müntener, O., Kelemen, P.B., and Grove, T.L., 2001, The role of H_2O during crystallization of primitive arc magmas under uppermost mantle conditions and genesis of igneous pyroxenites: An experimental study: Contributions to Mineralogy and Petrology, v. 141, p. 643–658, https://doi.org/10.1007/s004100100266.

Needy, S.K., Anderson, J.L., Wooden, J.L., Fleck, R.J., Barth, A.P., Paterson, S.R., Memeti, V., and Pignotta, G.S., 2009, Mesozoic magmatism in an upper- to middle-crustal section through the Cordilleran continental margin arc, eastern Transverse Ranges, California, *in* Miller, R.B., and Snoke, A.W., eds., Crustal Cross Sections from the Western North American Cordillera and Elsewhere: Implications for Tectonic and Petrologic Processes: Geological Society of America Special Paper 456, p. 187–218, https://doi.org/10.1130/2009.2456(07).

Nourse, J., and Thompson, M.A., 2022, Newly recognized Permo-Triassic intrusions in the Claremont Wilderness Block, San Gabriel Mountains, California: Geological Society of America Abstracts with Programs, v. 54, no. 2, https://doi.org/10.1130/abs/2022CD-374085.

Nourse, J.A., Swanson, B.J., Lusk, A.D., Barth, N.C., Schwartz, J.J., and Vermillion, K.B., 2020, Recent advancements in geochronology, geologic mapping, and landslide characterization in basement rocks of the San Gabriel Mountains block, *in* Heermance, R.V., and Schwartz, J.J., eds., From the Islands to the Mountains: A 2020 View of Geologic Excursions in Southern California: Geological Society of America Field Guide 59, p. 21–93, https://doi.org/10.1130/2020.0059(02).

Otamendi, J.E., Cristofolini, E.A., Morosini, A., Armas, P., Tibaldi, A.M., and Camilletti, G.C., 2020, The geodynamic history of the Famatinian arc, Argentina: A record of exposed geology over the type section (latitudes 27°–33° south): Journal of South American Earth Sciences, v. 100, https://doi.org/10.1016/j.jsames.2020.102558.

Paterson, S., Clausen, B., Memeti, V., and Schwartz, J.J., 2017, Arc magmatism, tectonism, and tempos in Mesozoic arc crustal sections of the Peninsular and Transverse Ranges, southern California, USA, *in* Kraatz, B., Lackey, J.S., and Fryxell, J., eds., Field Excursions in Southern California: Field Guides to the 2016 GSA Cordilleran Section Meeting: Geological Society of America Field Guide 45, p. 81–186, https://doi.org/10.1130/2017.0045(04).

Paterson, S.R., and Ducea, M.N., 2015, Arc magmatic tempos: Gathering the evidence: Elements, v. 11, p. 91–98, https://doi.org/10.2113/gselements.11.2.91.

Paterson, S.R., Okaya, D., Memeti, V., Economos, R., and Miller, R.B., 2011, Magma addition and flux calculations of incrementally constructed magma chambers in continental margin arcs: Combined field, geochronologic, and thermal modeling studies: Geosphere, v. 7, p. 1439–1468, https://doi.org/10.1130/GES00696.1.

Patiño Douce, A.E., 1999, What do experiments tell us about the relative contributions of crust and mantle to the origin of granitic magmas?, *in* Castro, A., et al., eds., Understanding Granites: Integrating New and Classical Techniques: Geological Society, London, Special Publication 168, p. 55–75, https://doi.org/10.1144/GSL.SP.1999.168.01.05.

Patiño Douce, A.E., Humphreys, E.D., and Dana Johnston, A., 1990, Anatexis and metamorphism in tectonically thickened continental crust exemplified by the Sevier hinterland, western North America: Earth and Planetary Science Letters, v. 97, p. 290–315, https://doi.org/10.1016/0012-821X(90)90048-3.

Paton, C., Woodhead, J.D., Hellstrom, J.C., Hergt, J.M., Greig, A., and Maas, R., 2010, Improved laser ablation U-Pb zircon geochronology through robust downhole fractionation correction: Geochemistry, Geophysics, Geosystems, v. 11, https://doi.org/10.1029/2009GC002618.

Paton, C., Hellstrom, J., Paul, B., Woodhead, J., and Hergt, J., 2011, Iolite: Freeware for the visualisation and processing of mass spectrometric data: Journal of Analytical Atomic Spectrometry, v. 26, p. 2508–2518, https://doi.org/10.1039/c1ja10172b.

Pearson, D.M., MacLeod, D.R., Ducea, M.N., Gehrels, G.E., and Jonathan Patchett, P., 2017, Sediment underthrusting within a continental magmatic arc: Coast Mountains batholith, British Columbia: Tectonics, v. 36, p. 2022–2043, https://doi.org/10.1002/2017TC004594.

Petford, N., and Atherton, M., 1996, Na-rich partial melts from newly underplated basaltic crust: The Cordillera Blanca Batholith, Peru: Journal of Petrology, v. 37, p. 1491–1521, https://doi.org/10.1093/petrology/37.6.1491.

Petford, N., and Gallagher, K., 2001, Partial melting of mafic (amphibolitic) lower crust by periodic influx of basaltic magma: Earth and Planetary Science Letters, v. 193, p. 483–499, https://doi.org/10.1016/S0012-821X(01)00481-2.

Powell, R.E., 1993, Balanced palinspastic reconstruction of pre-late Cenozoic paleogeology, southern California: Geologic and kinematic constraints on evolution of the San Andreas fault system, *in* Powell, R.E., et al., eds., The San Andreas Fault System: Displacement, Palinspastic Reconstruction, and Geologic Evolution: Geological Society of America Memoir 178, p. 1–106, https://doi.org/10.1130/MEM178-p1.

Premo, W.R., Morton, D.M., Wooden, J.L., and Fanning, C.M., 2014, U-Pb zircon geochronology of plutonism in the northern Peninsular Ranges batholith, southern California: Implications for the Late Cretaceous tectonic evolution of southern California, *in* Morton, D.M., and Miller, F.K., eds., Peninsular Ranges Batholith, Baja California and Southern California: Geological Society of America Special Paper 211, p. 145–180, https://doi.org/10.1130/2014.1211(04).

Rapp, R.P., and Watson, E.B., 1995, Dehydration melting of metabasalt at 8–32 kbar: Implications for continental growth and crust-mantle recycling: Journal of Petrology, v. 36, p. 891–931, https://doi.org/10.1093/petrology/36.4.891.

Ratschbacher, B.C., Keller, C.B., Schoene, B., Paterson, S.R., Anderson, J.L., Okaya, D., Putirka, K., and Lippoldt, R., 2018, A new workflow to assess emplacement duration and melt residence time of compositionally diverse magmas emplaced in a sub-volcanic reservoir: Journal of Petrology, v. 59, p. 1787–1809, https://doi.org/10.1093/petrology/egy079.

Rezeau, H., Klein, B.Z., and Jagoutz, O., 2021, Mixing dry and wet magmas in the lower crust of a continental arc: New petrological insights from the Bear Valley Intrusive Suite, southern Sierra Nevada, California: Contributions to Mineralogy and Petrology, v. 176, p. 73, https://doi.org/10.1007/s00410-021-01832-2.

Riggs, N.R., Reynolds, S.J., Lindner, P.J., Howell, E.R., Barth, A.P., Parker, W.G., and Walker, J.D., 2013, The Early Mesozoic Cordilleran arc and Late Triassic paleotopography: The detrital record in Upper Triassic sedimentary successions on and off the Colorado Plateau: Geosphere, v. 9, p. 602–613, https://doi.org/10.1130/GES00860.1.

Ringwood, M.F., Schwartz, J.J., Turnbull, R.E., and Tulloch, A.J., 2021, Phanerozoic record of mantle-dominated arc magmatic surges in the Zealandia Cordillera: Geology, v. 49, p. 1230–1234, https://doi.org/10.1130/G48916.1.

Rudnick, R.L., 1995, Making continental crust: Nature, v. 378, p. 571–578, https://doi.org/10.1038/378571a0.

Saleeby, J., 2011, Geochemical mapping of the Kings-Kaweah ophiolite belt, California—Evidence for progressive mélange formation in a large offset transform-subduction initiation environment, *in* Wakabayashi, J., and Dilek, Y., eds., Mélanges: Processes of Formation and Societal Significance, Geological Society of America Special Paper 480, p. 31–73, https://doi.org/10.1130/2011.2480(02).

Saleeby, J., and Dunne, G., 2015, Temporal and tectonic relations of early Mesozoic arc magmatism, southern Sierra Nevada, California, *in* Anderson, T.H., Didenko, A.N., Johnson, C.L., Khanchuk, A.I., and MacDonald, J.H., Jr., eds., Late Jurassic Margin of Laurasia—A Record of Faulting Accommodating Plate Rotation: Geological Society of America Special Paper 513, p. 223–268, https://doi.org/10.1130/2015.2513(05).

Saleeby, J., and Sharp, W., 1980, Chronology of the structural and petrologic development of the southwest Sierra Nevada foothills, California: Geological Society of America Bulletin, v. 91, p. 1416–1535, https://doi.org/10.1130/GSAB-P2-91-1416.

Saleeby, J., Ducea, M., and Clemens-Knott, D., 2003, Production and loss of high-density batholithic root, southern Sierra Nevada, California: Tectonics, v. 22, https://doi.org/10.1029/2002TC001374.

Saleeby, J.B., 1982, Polygenetic ophiolite belt of the California Sierra Nevada: Geochronological and tectonostratigraphic development: Journal of Geophysical Research: Solid Earth, v. 87, p. 1803–1824, https://doi.org/10.1029/JB087iB03p01803.

Saleeby, J.B., 1990, Progress in tectonic and petrogenetic studies in an exposed cross-section of young (∼100 Ma) continental crust, southern Sierra Nevada, California, *in* Salisbury, M.H., and Fountain, D.M., eds., Exposed Cross-Sections of the Continental Crust, Dordrecht, Netherlands, Springer, p. 137–158, https://doi.org/10.1007/978-94-009-0675-4_6.

Saleeby, J.B., and Busby, C., 1993, Paleogeographic and tectonic setting of axial and western metamorphic framework rocks of the southern Sierra Nevada, California, *in* Dunne, G., and McDougall, K., eds., Mesozoic Paleogeography of the Western United States—II, Los Angeles, Pacific Section, Society of Economic Paleontologists and Mineralogists Book 71, p. 197–225.

Samperton, K.M., Bell, E.A., Barboni, M., Brenhin Keller, C., and Schoene, B., 2017, Zircon age-temperature-compositional spectra in plutonic rocks: Geology, v. 45, p. 983–986, https://doi.org/10.1130/G38645.1.

Sams, D.B., and Saleeby, J.B., 1988, Geology and petrotectonic significance of crystalline rocks of the southernmost Sierra Nevada, California, *in* Ernst, W.G., ed., Metamorphism and Crustal Evolution of the Western United States: Englewood Cliffs, New Jersey, Prentice-Hall, p. 865–893.

Sauer, K.B., Gordon, S.M., Miller, R.B., Vervoort, J.D., and Fisher, C.M., 2017a, Evolution of the Jura-Cretaceous North American Cordilleran margin: Insights from detrital-zircon U-Pb and Hf isotopes of sedimentary units of the North Cascades Range, Washington: Geosphere, v. 13, p. 2094–2118, https://doi.org/10.1130/GES01501.1.

Sauer, K.B., Gordon, S.M., Miller, R.B., Vervoort, J.D., and Fisher, C.M., 2017b, Transfer of metasupracrustal rocks to midcrustal depths in the North Cascades continental magmatic arc, Skagit Gneiss Complex, Washington: Tectonics, v. 36, p. 3254–3276, https://doi.org/10.1002/2017TC004728.

Sauer, K.B., Gordon, S.M., Miller, R.B., Vervoort, J.D., and Fisher, C.M., 2018, Provenance and metamorphism of the Swakane Gneiss: Implications for incorporation of sediment into the deep levels of the North Cascades continental magmatic arc, Washington: Lithosphere, v. 10, p. 460–477, https://doi.org/10.1130/L712.1.

Sauer, K.B., Gordon, S.M., Miller, R.B., Jacobson, C.E., Grove, M., Vervoort, J.D., and Fisher, C.M., 2019, Deep-crustal metasedimentary rocks support Late Cretaceous "Mojave-BC" translation: Geology, v. 47, p. 99–102, https://doi.org/10.1130/G45554.1.

Saul, L.R., 1986, Mollusks of latest Cretaceous and Paleocene age, Lake Nacimiento, California, *in* Grove, K., and Graham, S., eds., Geology of Upper Cretaceous and Lower Tertiary Rocks near Lake Nacimiento, California, Los Angeles, California: Pacific Section, Society of Economic Paleontologists and Mineralogists, v. 49, p. 25–31.

Saylor, J.E., and Sundell, K.E., 2016, Quantifying comparison of large detrital geochronology data sets: Geosphere, v. 12, p. 203–220, https://doi.org/10.1130/GES01237.1.

Schiller, D., and Finger, F., 2019, Application of Ti-in-zircon thermometry to granite studies: Problems and possible solutions: Contributions to Mineralogy and Petrology, v. 174, p. 51, https://doi.org/10.1007/s00410-019-1585-3.

Schwartz, J.J., Stowell, H.H., Klepeis, K.A., Tulloch, A.J., Kylander-Clark, A.R.C., Hacker, B.R., and Coble, M.A., 2016, Thermochronology of extensional orogenic collapse in the deep crust of Zealandia: Geosphere, v. 12, p. 647–677, https://doi.org/10.1130/GES01232.1.

Schwartz, J.J., Klepeis, K.A., Sadorski, J.F., Stowell, H.H., Tulloch, A.J., and Coble, M.A., 2017, The tempo of continental arc construction in the Mesozoic Median Batholith, Fiordland, New Zealand: Lithosphere, v. 9, p. 343–365, https://doi.org/10.1130/L610.1.

Schwartz, J.J., Andico, S., Turnbull, R.E., Klepeis, K.A., Tulloch, A.J., Kitajima, K., and Valley, J.W., 2021, Stable and transient isotopic trends in the crustal evolution of Zealandia Cordillera: The American Mineralogist, v. 106, p. 1369–1387, https://doi.org/10.2138/am-2021-7626.

Schwartz, J.J., Lackey, J.S., Miranda, E.A., Klepeis, K.A., Mora-Klepeis, G., Robles, F., and Bixler, J.D., 2023, Magmatic surge requires two-stage model for the Laramide orogeny: Nature Communications, v. 14, p. 3841, https://doi.org/10.1038/s41467-023-39473-7.

Seiders, V.M., 1986, Structural geology of Upper Cretaceous and lower Tertiary rocks near the Nacimiento Fault, northwest of Lake Nacimiento, California, *in* Grove, K., and Graham, S., eds., Geology of Upper Cretaceous and Lower Tertiary Rocks near Lake Nacimiento, California: Pacific Section, Society of Economic Paleontologists and Mineralogists, v. 49, p. 33–39.

Sharman, G.R., Graham, S.A., Grove, M., Kimbrough, D.L., and Wright, J.E., 2015, Detrital zircon provenance of the late Cretaceous–Eocene California forearc: Influence of Laramide low-angle subduction on sediment dispersal and paleogeography: Geological Society of America Bulletin, v. 127, p. 38–60, https://doi.org/10.1130/B31065.1.

Sharman, G.R., Sharman, J.P., and Sylvester, Z., 2018, detritalPy: A Python-based toolset for visualizing and analysing detrital geo-thermochronologic data: The Depositional Record: A Journal of Biological, Physical and Geochemical Sedimentary Processes, v. 4, p. 202–215, https://doi.org/10.1002/dep2.45.

Singleton, J.S., and Cloos, M., 2013, Kinematic analysis of mélange fabrics in the Franciscan complex near San Simeon, California: Evidence for sinistral slip on the Nacimiento fault zone?: Lithosphere, v. 5, p. 179–188, https://doi.org/10.1130/L259.1.

Sliter, W.V., 1986, Maastrichtian foraminifers from near Lake Nacimiento, California: Their paleoenvironmental interpretation and regional correlation, *in* Grove, K., and Graham, S., eds., Geology of Upper Cretaceous and Lower Tertiary Rocks near Lake Nacimiento, California: Pacific Section, Society of Economic Paleontologists and Mineralogists, v. 49, p. 17–24.

Stacey, J.S., and Kramers, J.D., 1975, Approximation of terrestrial lead isotope evolution by a two-stage model: Earth and Planetary Science Letters, v. 26, p. 207–221, https://doi.org/10.1016/0012-821X(75)90088-6.

Stern, T., Bateman, P.C., Morgan, B.A., Newell, M.F., and Peck, D.L., 1981, Isotopic U-Pb ages of zircon from the granitoids of the central Sierra Nevada, California: U.S. Geological Survey Professional Paper 1185, 17 p., https://doi.org/10.3133/pp1185.

Stewart, J., 2005, Eolian deposits in the Neoproterozoic Big Bear Group, San Bernardino Mountains, California, USA: Earth-Science Reviews, v. 73, p. 47–62, https://doi.org/10.1016/j.earscirev.2005.07.012.

Stone, P., Barth, A.P., and Wooden, J.L., Fohey-Breting, Vasquez, J.A., and Priest, S.S., 2013, Geochronologic and geochemical data from Mesozoic rocks in the Black Mountain area northeast of Victorville, San Bernardino County, California: U.S. Geological Survey Open-File Report 2013-1146, 31 p., https://doi.org/10.3133/ofr20131146.

Strickland, E.D., Singleton, J.S., and Haxel, G.B., 2018, Orocopia Schist in the northern Plomosa Mountains, west-central Arizona: A Laramide subduction complex exhumed in a Miocene metamorphic core complex: Lithosphere, v. 10, p. 723–742, https://doi.org/10.1130/L742.1.

Taylor, S.R., and McLennan, S.M., 1985, The Continental Crust: Its Composition and Evolution: An Examination of the Geochemical Record Preserved in Sedimentary Rocks: Blackwell Scientific Publications, 312 p.

Tera, F., and Wasserburg, G.J., 1972, U-Th-Pb systematics in three Apollo 14 basalts and the problem of initial Pb in lunar rocks: Earth and Planetary Science Letters, v. 14, p. 281–304, https://doi.org/10.1016/0012-821X(72)90128-8.

Tibaldi, A.M., Otamendi, J.E., Cristofolini, E.A., Baliani, I., Walker, B.A., and Bergantz, G.W., 2013, Reconstruction of the Early Ordovician Famatinian arc through thermobarometry in lower and middle crustal exposures, Sierra de Valle Fértil, Argentina: Tectonophysics, v. 589, p. 151–166, https://doi.org/10.1016/j.tecto.2012.12.032.

Tikoff, B., Housen, B.A., Maxson, J.A., Nelson, E.M., Trevino, S., and Shipley, T.F., 2023, Hit-and-run model for Cretaceous–Paleogene tectonism along the western margin of Laurentia, *in* Whitmeyer, S.J., Williams, M.L., Kellett, D.A., and Tikoff, B., eds., Laurentia: Turning Points in the Evolution of a Continent: Geological Society of America Memoir 220, p. 659–705, https://doi.org/10.1130/2022.1220(32).

Ulmer, P., Kaegi, R., and Müntener, O., 2018, Experimentally derived intermediate to silica-rich arc magmas by fractional and equilibrium crystallization at 1·0 GPa: An evaluation of phase relationships, compositions, liquid lines of descent and oxygen fugacity: Journal of Petrology, v. 59, p. 11–58, https://doi.org/10.1093/petrology/egy017.

Vermeesch, P., 2013, Multi-sample comparison of detrital age distributions: Chemical Geology, v. 341, p. 140–146, https://doi.org/10.1016/j.chemgeo.2013.01.010.

Vermeesch, P., 2018, IsoplotR: A free and open toolbox for geochronology: Geoscience Frontiers, v. 9, p. 1479–1493, https://doi.org/10.1016/j.gsf.2018.04.001.

Walker, B.A., Bergantz, G.W., Otamendi, J.E., Ducea, M.N., and Cristofolini, E.A., 2015, A MASH zone revealed: The mafic complex of the Sierra Valle Fértil: Journal of Petrology, v. 56, p. 1863–1896, https://doi.org/10.1093/petrology/egv057.

Wooden, J.L., Barth, A.P., and Mueller, P.A., 2013, Crustal growth and tectonic evolution of the Mojave crustal province: Insights from hafnium isotope systematics in zircons: Lithosphere, v. 5, p. 17–28, https://doi.org/10.1130/L218.1.

Wright, J.E., and Wooden, J.L., 1991, New Sr, Nd, and Pb isotopic data from plutons in the northern Great Basin: Implications for crustal structure and granite petrogenesis in the hinterland of the Sevier thrust belt: Geology, v. 19, p. 457, https://doi.org/10.1130/0091-7613(1991)019<0457:NSNAPI>2.3.CO;2.

Yang, J., Cao, W., Gordon, S.M., and Chu, X., 2020, Does underthrusting crust feed magmatic flare-ups in continental arcs?: Geochemistry, Geophysics, Geosystems, v. 21, https://doi.org/10.1029/2020GC009152.

Science Editor: Mihai Ducea
Associate Editor: Jay Chapman

Manuscript Received 18 March 2024
Revised Manuscript Received 15 June 2024
Manuscript Accepted 9 July 2024